# DEVELOPMENT OF EUDRAGIT ELECTROSPUN FIBERS FUNCTIONALIZED BY CINNAMON LEAF OIL COMPLEXATION WITH CYCLODEXTRINS FOR WOUND HEALING APPLICATION

WOUND HEALING APPLICATION
$\mathbf{b}\mathbf{y}$
·
MELIKE COKOL CAKMAK
Submitted to the Graduate School of Engineering and Natural Sciences in partial fulfillment
of the requirements for the degree of Doctor of Philosophy
Sabancı University
Submici Chiversity
December 2021

# DEVELOPMENT OF EUDRAGIT ELECTROSPUN FIBERS FUNCTIONALIZED BY CINNAMON LEAF OIL COMPLEXATION WITH CYCLODEXTRINS FOR WOUND HEALING APPLICATION

APPROVED BY:		
	Prof. Dr. Selim Cetiner (Thesis Supervisor)	
	Assoc. Prof. Dr. Meral Yuce	
	Assoc. Prof. Dr. Meltem Sezen (	Ozkoc
	Assoc. Prof. Dr. Ali Zarrabi	
	Asst. Prof. Dr. Dilek Tekdal	

Date of Approval: 17.12.2021

© Melike Cokol Cakmak 2021

All Rights Reserved

# DEVELOPMENT OF EUDRAGIT ELECTROSPUN FIBERS FUNCTIONALIZED BY CINNAMON LEAF OIL COMPLEXATION WITH CYCLODEXTRINS FOR WOUND HEALING APPLICATION

Melike Cokol Cakmak

Molecular Biology, Genetics and Bioengineering, PhD Thesis, 2021

Thesis Supervisor: Prof. Dr. Selim Cetiner

Thesis Co-supervisor: Assoc. Prof. Dr. Feray Bakan Misirlioglu

#### **Abstract**

Essential oils are powerful agents which have natural antimicrobial activity. However, its poor water solubility and high volatility make its usage limited. There are different methods to overcome this challenge. Among the most interesting of them is their encapsulation inside nanomaterials which not only could improve their water solubility but also extend the shelf life of essential oils. The aim of this thesis was to reach to a high-performance encapsulated oil via utilizing inclusion complexes and electrospinning methods, simultaneously, to benefit from the advantages of both methods. To reach this aim, Eudragit electrospun fibers were functionalized by cinnamon leaf oil complexation with cyclodextrins. For this, firstly, cinnamon leaf oil was molecularly encapsulated within  $\beta$ -cyclodextrin and sulfobutyl ether  $\beta$ -cyclodextrin sodium via freeze-drying method. Solubilizing and complexing ability of β-CD and SBE-β-CD were confirmed via phase solubility assay. Encapsulated amount of CEO was determined using UV-Vis spectrometry. The formation of inclusion complexes was characterized by several analyses includes DLS, SEM, FTIR, TGA, DSC, and <sup>1</sup>H-NMR spectroscopy. Then, the antibacterial activity of CEO/β-CD-IC and CEO/SBE-β-CD-IC were assessed against both gram-negative bacteria (E. coli) and gram-positive bacteria (S. aureus). In the second part, CEO/βCD-IC loaded Eudragit S100 fiber and CEO/SBE-βCD-IC loaded Eudragit S100 fiber were produced using the electrospinning method, and the physicochemical properties, wetting ability, and water uptake capacity of the electrospun fibers were characterized. The antibacterial activity of these fibers was determined against E. coli and S. aureus by the colony counting method. Also, the cytotoxic effect of these fibers was tested on the L929 fibroblast cell line. The amount of oil inside the fibers and their release profile at different pH were determined by UV-Vis spectrometry. According to the results of this study, CEO/βCD-IC loaded Eudragit S100 **fiber** was found to be a good candidate for wound healing applications especially for treatment of diabetic ulcer because of its high-water uptake, a balanced hydrophilic outer surface, nontoxic property, high antibacterial activity, and controlled drug release ability at pH 5.5.

**Keywords:** Cinnamon leaf oil, cyclodextrin, electrospinning, controlled release, wound dressing

## YARA ÖRTÜSÜ UYGULAMASI İÇİN TARÇIN YAPRAK YAĞI YAĞI VE SİKLODEKSTRİN KOMPLEKSİYONLARI İLE FONKSİYONELLEŞTİRİLEN EUDRAGIT ELEKTROSPUN LİFLERİNİN GELİŞTİRİLMESİ

#### Melike Cokol Cakmak

Moleküler Biyoloji, Genetik and Biyomühendislik, Doktora Tezi, 2021

Tez Danışmanı: Prof. Dr. Selim Çetiner

Tez Eş Danışmanı: Doç.Dr. Feray Bakan Mısırlıoğlu

#### Özet

Esansiyel yağlar, doğal antimikrobiyal aktiviteye sahip güçlü ajanlardır. Ancak suda çözünürlüğünün düşük olması ve uçuculuğunun yüksek olması kullanımını sınırlı kılmaktadır. Bu zorluğun üstesinden gelmek için farklı yöntemler vardır. Bunların en ilginçleri arasında, sadece suda çözünürlüklerini iyileştirmekle kalmayıp aynı zamanda esansiyel yağların raf ömrünü de uzatabilen nanomalzemeler içinde kapsüllenmeleri yer almaktadır. Bu tezin amacı, inklüzyon kompleksleri ve elektro-eğirme yöntemlerini aynı anda kullanarak, her iki yöntemin de avantajlarından yararlanarak yüksek performanslı enkapsüle edilmiş yağa ulaşmaktır. Bu amaca ulaşmak için, Eudragit elektrospun lifleri, siklodekstrinler ile tarçın yaprağı yağı kompleksleştirmesi ile fonksiyonelleştirilmiştir. Bunun için, ilk olarak, tarçın yaprağı yağı, dondurarak kurutma yöntemi ile β-siklodekstrin ve sülfobütil eter β-siklodekstrin sodyum içerisinde moleküler olarak kapsüllendi. β-CD ve SBE-β-CD' nin çözündürme ve kompleks oluşturma yeteneği, faz çözünürlük testi ile doğrulandı. Enkapsüle edilen CEO miktarı UV-Vis spektrometrisi kullanılarak belirlendi. İnklüzyon komplekslerinin oluşumu, DLS, SEM, FTIR, TGA, DSC ve <sup>1</sup>H-NMR spektroskopisini içeren çeşitli analizlerle karakterize edildi. Ardından, ilk kez, CEO/β-CD-IC ve CEO/SBE-β-CD-IC' nin antibakteriyel aktivitesi hem gram negatif bakteri (E. coli) hem de gram pozitif bakteri (S. aureus)' a karşı değerlendirildi. İkinci olarak, CEO/β-CD-IC ve CEO/SBE-β-CD-IC yüklü Eudragit elektrospun lifleri ilk kez elektro-eğirme yöntemiyle üretildi ve karşılaştırıldı. Elektrospun liflerin fiziko-kimyasal özellikleri, ıslatma kabiliyeti ve su alma kapasitesi karakterize edildi. Bu liflerin antibakteriyel aktivitesi, koloni sayma yöntemiyle E. coli ve S. aureus' a karşı belirlendi. Ayrıca bu liflerin sitotoksik etkisi L929 fibroblast hücre hattı üzerinde test edildi. UV-Vis spektrometresi ile lif içerisindeki yağ miktarı ve farklı pH' daki ilaç salım profili belirlendi. CEO/\(\beta\)CD-IC y\(\text{ukl\tilde{u}}\) Eudragit S100 fiberin, yüksek su alımı, dengeli hidrofilik dış yüzeyi, toksik olmayan özelliği, yüksek antibakteriyel aktivitesi ve pH 5.5'da kontrollü ilaç salımı nedeniyle yara iyileştirme uygulamaları için özellikle diyabetik ülser tedavisinde iyi bir aday olduğu bulundu.

**Anahtar Kelimeler:** Tarçın yaprağı yağı, siklodekstrin, elektro-eğirme, kontrollü salım, yara örtüsü

#### Acknowledgments

I would like to appreciate my advisor Prof. Dr. Selim Cetiner for supporting me to study in this project in my doctorate and my co-advisor Assoc. Prof. Dr. Feray Bakan for helping me at every stage of my thesis from the beginning to the end and supporting me in overcoming all kinds of problems in my doctorate and my life.

I am grateful to Assoc. Prof. Dr. Ali Zarrabi, who gave me very useful feedback with his knowledge and experience that I could ask questions to him without hesitation and Assoc. Prof. Dr. Meltem Sezen who motivated me when I gave up.

I would like to special thank Atefeh Zarepour. I was able to consult her for all my questions in my thesis and ask her without considering the time. I would like also to thank Eda Ciftci Dede and Golnaz Naseri Azari for their contributions in the laboratory processes, and Tuce Fidan and Busra Tugba Camic who provided support in SEM images.

I would like to thank my lab friends Sezgin Mengi and Nihal Oztalan Erol, who were with me in all parts of my doctorate and listen to me tirelessly. I special thanks to Asst. Prof. Dr. Dilek Tekdal who was my lab colleague and now my esteemed jury.

I'm also thankful to my friends Umran Yazar, Sebahat Torlak, Cahide Tepeli, Hilal Topcu, Ebru Resmen, Fatih Resmen and Sumeyra Vural Korkmaz who make my life more enjoyable.

I would like to express my deepest gratitude and respect to my mother Mukerrem Cokol and my father Cevat Cokol, who raised me with great effort and helped me reach these days, and to my dear brothers Mustafa Cokol and Murat Cokol, who have never given up their moral and financial support throughout my life. I would also special thank Murat Cokol who tried to teach me everything he knew and always encouraged me even when I failed. We did good work together during my doctorate. He will always be my role model in my life.

I would like to express my endless thanks to my dear husband Yusuf Cakmak for his patience. He was always with me throughout this difficult and stressful process and supported me throughout my doctorate.

# CHAPTER 1: Inclusion Complexes of $\beta$ -Cyclodextrin and its Sulfobutyl Ether Derivative with Cinnamon Leaf Oil: Preparation, Characterization and Antibacterial Activity

#### TABLE OF CONTENTS

1. Introduction	1
1.1 Essential Oils	1
1.1.1 General Properties of Essential Oils	1
1.1.2 Chemical Properties of Essential Oils	2
1.1.3 Antibacterial Mechanisims of Essential Oils	3
1.1.4 Cinnamon Leaf Essential oil	4
1.2. Microencapsulation	6
1.3. Molecular encapsulation	6
1.3.1. History of Cyclodextrin	7
1.3.2. Molecular Structure of Cyclodextrin	8
1.3.3. Modified Cyclodextrin	10
1.3.4. Inclusion Complex of Cyclodextin	12
1.4. Physicochemical Characterization Analysis of Inclusion Complexes	13
1.4.1. Phase solubility assay	14
1.4.2. Morphological Analysis	15
1.4.3. Size and Surface Charge Analysis	15
1.4.4. Functional Analyis.	16
1.4.5. Thermal Analysis	16
1.4.6. Molecular Analysis	17
1.5. Studies on inclusion complexes	17
1.6. Aim of the study	21
2. Materials and Methods	21
2.1. Materials	21
2.2. Methods	22
2.2.1. Phase Solubility Assay	22
2.2.2. Preparation of the Cinnamon oil/β-CD and Cinnamon oil/SBE-β-CD In	nclusion
Complexes	22
2.2.3. Preparation of the Cinnamon oil/β-CD and Cinnamon oil/SBE-β-CD	Physical
Mixtures	24
2.2.4. Determination of Yield, Loading Efficiency and Encapsulation Efficiency	24

2.2.5. Inclusion complexes characterization.	26
2.2.5.1. Scanning Electron Microscopy (SEM)	26
2.2.5.2. Dynamic Light Scattering (DLS)	26
2.2.5.3. Fourier Transform Infrared Spectroscopy (FTIR)	26
2.2.5.4. Thermogravimetric Analysis (TGA)	26
2.2.5.5. Differential Scanning Calorimetry (DSC)	27
2.2.5.6. <sup>1</sup> H-NMR Spectroscopy	27
2.2.6. Antibacterial activity of essential oil	27
2.2.6.1. Microorganism	27
2.2.6.2. Media Preparation	27
2.2.6.3. Agar disk diffusion test	27
2.2.6.4. MIC determination by serial dilution dose-response experiment	28
2.2.7. Antibacterial activity of inclusion complexes	29
3. Results and Discussion	29
3. Results and Discussion	
	29
3.1. Phase Solubility Assay	29
<ul><li>3.1. Phase Solubility Assay</li><li>3.2. Determination of Yield, Loading Efficiency and Encapsulation Efficiency</li></ul>	29 32
<ul><li>3.1. Phase Solubility Assay</li><li>3.2. Determination of Yield, Loading Efficiency and Encapsulation Efficiency</li><li>3.3. Scanning Electron Microscopy (SEM) Analysis</li></ul>	29 32 34
<ul> <li>3.1. Phase Solubility Assay</li> <li>3.2. Determination of Yield, Loading Efficiency and Encapsulation Efficiency</li> <li>3.3. Scanning Electron Microscopy (SEM) Analysis</li> <li>3.4. Dynamic Light Scattering (DLS)</li> </ul>	29 32 34 36
<ul> <li>3.1. Phase Solubility Assay</li> <li>3.2. Determination of Yield, Loading Efficiency and Encapsulation Efficiency</li> <li>3.3. Scanning Electron Microscopy (SEM) Analysis</li> <li>3.4. Dynamic Light Scattering (DLS)</li> <li>3.5. Fourier Transform Infrared Spectroscopy (FTIR)</li> </ul>	29 32 34 36 38
<ul> <li>3.1. Phase Solubility Assay</li> <li>3.2. Determination of Yield, Loading Efficiency and Encapsulation Efficiency</li> <li>3.3. Scanning Electron Microscopy (SEM) Analysis</li> <li>3.4. Dynamic Light Scattering (DLS)</li> <li>3.5. Fourier Transform Infrared Spectroscopy (FTIR)</li> <li>3.6. Thermogravimetric Analysis (TGA)</li> </ul>	29 32 36 38 41
<ul> <li>3.1. Phase Solubility Assay</li> <li>3.2. Determination of Yield, Loading Efficiency and Encapsulation Efficiency</li> <li>3.3. Scanning Electron Microscopy (SEM) Analysis</li> <li>3.4. Dynamic Light Scattering (DLS)</li> <li>3.5. Fourier Transform Infrared Spectroscopy (FTIR)</li> <li>3.6. Thermogravimetric Analysis (TGA)</li> <li>3.7. Differential Scanning Calorimetry (DSC)</li> </ul>	29 34 36 38 41 45
<ul> <li>3.1. Phase Solubility Assay</li></ul>	29 32 36 38 41 45 45
3.1. Phase Solubility Assay	29 32 36 38 41 45 45 50
3.1. Phase Solubility Assay	293234363841455050

## CHAPTER 2: Eudragit Electrospun Fibers Functionalized by Cinnamon Leaf oil Complexation with Cyclodextrins for Wound Dressing Application

### TABLE OF CONTENTS

1. Introduction5	5
1.1. Wounds5	55
1.1.1. Wound Healing5	57
1.1.2. The Importance of pH in Wound Healing5	58
1.2. Wound dressing6	60
1.2.1 Nanofibers based wound dressing6	51
1.3. Electrospinning6	53
1.4. Studies on electrospun fibers with cyclodextrin inclusion complexes	<b>5</b> 5
1.5. Aim of the study	71
2. Materials and Methods	72
2.1. Materials	2
2.2. Methods	/2
2.2.1. Preparation of Eudragit polymeric solution with and without inclusion	n
complexes	12
2.2.2. Production of pristine and Cinnamon leaf oil/Cyclodextrin-Inclusion Complex loaded	ed
Eudragit S100 fiber by electrospinning	72
2.2.3. Encapsulation efficiency of Cinnamon leaf oil/Cyclodextrin-Inclusion Complex loaded	ed
Eudragit S100 electrospun fiber	13
2.2.4. Morphology and diameter distribution of electrospun	74
2.2.5. Functional and thermal properties of electrospun fiber	74
2.2.6. Wettability of electrospun fibers	14
2.2.7. Water uptake of electrospun fibers	74
2.2.8. Antibacterial activity of electrospun fibers	74
2.2.9. Drug release assay	15
2.2.10. Cell Viability assay	75
3. Results and Discussion	<b>6</b>
3.1. Morphology and diameter distribution of electrospun fibers	76
3.2. Encapsulation efficiency of Cinnamon leaf oil/Cyclodextrin-Inclusion Complex loade	ed
Eudragit S100 electrospun fiber	30
3.3. Functional and thermal properties of electrospun fibers	31

5. References	93
4. Conclusion	92
3.8. Cell viability assay	90
3.7. Drug release assay	87
3.6. Antibacterial activity of electrospun fibers	86
3.5. Water uptake of electrospun fibers	85
3.4. Wettability of electrospun fibers	84

### **List of Figures**

Figure 1. Chemical structures of some compounds in essential oils
Figure 2. Antibacterial mechanisms of essential oils
<b>Figure 3</b> . GC-MS chromatogram showing chemical compositions of cinnamon leaf oil
<b>Figure 4.</b> The molecular and functional structure scheme of cyclodextrins9
<b>Figure 5.</b> Chemical structure and schematic representation of natural cyclodextrin10
<b>Figure 6.</b> Schematic representation of inclusion complex formation
<b>Figure 7.</b> (a) Different the cyclodextrin–guest ratio for the inclusion complex and (b) phase solubility diagram
<b>Figure 8.</b> Preparation process of inclusion complexes in 1:1 M ratio (a) and appearance of the complexes (b)
<b>Figure 9.</b> Agar disk diffusion test for evaluation of antibacterial activity28
Figure 10. Serial dilution dose-response experiment
Figure 11. UV-Vis absorption spectra of increasing concentrations of cinnamon leaf oil diluted in ddH <sub>2</sub> O (a) and calibration curve of pure cinnamon leaf essential oil in ddH <sub>2</sub> O at 280 nm (b)
<b>Figure 13.</b> (a) Calibration curve of pure cinnamon leaf essential oil in hexane at 281 nm and (b) Yield, loading efficiency and encapsulation efficiency of cinnamon leaf oil included in SBE-β-CD and β-CD after freeze-drying
<b>Figure 14.</b> SEM images of βCD (a-b), CEO/βCD-PM (c-d) and CEO/βCD-IC (e-f)35
<b>Figure 15.</b> SEM images of SBE-βCD (a-b), CEO/SBE-βCD-PM (c-d) and CEO/SBE-βCD-IC (e-f)
<b>Figure 16.</b> Particle size distribution of (a) CEO/βCD-IC and (b) CEO/SBE-βCD-IC37

<b>Figure 17.</b> FTIR spectrum for β-CD, CEO, CEO/β-CD PM and CEO/β-CD IC40
<b>Figure 18.</b> FTIR spectrum for SBE-β-CD, CEO, CEO/SBE-β-CD PM and CEO/SBE-β-CD IC
<b>Figure 19.</b> Thermogravimetric analysis (a) and DTG (b) of βCD, CEO, CEO/βCD-PM and CEO/βCD-IC43
<b>Figure 20.</b> Thermogravimetric analysis (a) and DTG (b) of SBE-βCD, CEO, CEO/ SBE-βCD-PM and CEO/ SBE-βCD-IC
<b>Figure 21.</b> DSC thermograms of (a) βCD, CEO, CEO/βCD-PM and CEO/SBE-βCD-IC, and (b) SBE-βCD, CEO, CEO/SBE-βCD-PM and CEO/SBE-βCD-IC47
<b>Figure 22.</b> <sup>1</sup> H NMR photographs of β-CD, CEO and CEO/β-CD-IC48
<b>Figure 23.</b> <sup>1</sup> H NMR photographs of SBE-β-CD, CEO and CEO/SBE-β-CD-IC49
<b>Figure 24.</b> Inhibition zones of different essential oils against <i>E. coli</i> (a) and <i>S. aureus</i> (b). A: cinnamon leaf oil, B: clove oil, C: St. John's worth oil, D: coriander oil, E: ampicillin antibiotic
<b>Figure 25.</b> Bacterial growth curve of (A) <i>Escherichia coli</i> and (B) <i>Staphylococcus aureus</i> in LB liquid medium in the presence of essential oil with different concentrations51
<b>Figure 26.</b> Images of plates showing bacterial growth of <i>E. coli</i> and <i>S. aureus</i> in term of colonies in the presence of inclusion complexes
Figure 27. Stages of wound healing
Figure 28. Changes of pH on acute wounds (a) and chronic wounds (b) on healing59
<b>Figure 29.</b> Microbial growth in different pH range
<b>Figure 30.</b> The use of nanofibers in different fields of biomedicine
<b>Figure 31.</b> Experimental setup for solution preparation and electrospinning process fibers with and without inclusion complexes
<b>Figure 32.</b> Schematic representation of obtaining electrospun fibers with cyclodextrin inclusion complexes in different ways (A) cyclodextrin/drug blended polymeric fiber, (B) polycyclodextrin/drug fiber and (C) polymer free-cyclodextrin/drug fiber

Figure 33. Experimental setup for solution preparation and electrospinning process fibers v	with
and without inclusion complexes.	73
<b>Figure 34.</b> SEM micrographs of pristine Eudragit S100 fiber at different concentrations 2.	
(a) and 12 % (b) at magnification 500 X	77
Figure 35. SEM micrographs of (a) pristine Eudragit S100 fiber, (b) CEO/βCD-IC loa	ıded
Eudragit S100 fiber and (c) CEO/SBE- $\beta$ CD-IC loaded Eudragit S100 fiber at 500X	78
<b>Figure 36.</b> Fiber diameter distribution of the (a) pristine Eudragit S100 fiber, (b) CEO/βCD	)-IC
loaded Eudragit S100 fiber and (c) CEO/SBE- $\beta$ CD-IC loaded Eudragit S100 fiber	80
Figure 37. FTIR spectra of pristine fiber, CEO/βCD-IC loaded Eudragit S100 fiber (a)	and
CEO/SBE-βCD-IC loaded Eudragit S100 fiber (b)	82
<b>Figure 38.</b> TGA of pristine fiber, CEO/βCD-IC loaded Eudragit S100 fiber (a) and CEO/S	BE-
βCD-IC loaded Eudragit S100 fiber (b)	83
Figure 39. The appearance of water on the surface of Eudragit S100 fiber (a) and contact an	ngle
of obtained electrospun fibers (b)	85
Figure 40. Water uptake percentage for Eudragit S100 fiber, CEO/βCD-IC loaded Eudr	agit
S100 fiber and CEO/SBE-βCD-IC loaded Eudragit S100 fiber	86
Figure 41. UV light exposure on obtained fibers	87
Figure 42. Images of plates showing bacterial growth of E. coli and S. aureus in term	n of
colonies in the presence of inclusion complexes loaded fibers	87
Figure 43. Calibration curve of pure cinnamon leaf essential oil in PBS at 280 nm	88
Figure 44. Effect of pH on the release of cinnamon leaf oil from CEO/βCD-IC loaded Eudr	agit
S100 fiber	89
Figure 45. Time dependent release profiles of CEO/βCD-IC loaded Eudragit S100 fiber	and
CEO/SBE-βCD-IC loaded Eudragit S100 fiber at pH 5.5 and pH 7.4	90
Figure 46. In vitro cytotoxicity test of Eudragit fiber with and without inclusion comple	xes,
and equivalent amount of CEO in the fibers against L929 cell line	91
Figure 47. In vitro cytotoxicity test of pristine Eudragit fiber, CEO/βCD-IC loaded Eudr	agit
\$100 fiber and equivalent amount of CEO in the fibers against L929 cell line	92

### **List of Tables**

Table 1. The mechanism of action of cinnamon leaf essential oil to different
microorganisims6
Table 2. Physicochemical properties of cyclodextrins properties of β-CD and its derivatives.
Table 3. Literature research on essential oil loaded cyclodextrin inclusion
complex18
<b>Table 4.</b> The phase solubility diagram parameters of the inclusion complex formed between CEO-SBE-β-CD and CEO-β-CD
<b>Table 5.</b> Regions of the Infrared Spectrum
<b>Table 6.</b> <sup>1</sup> H NMR chemical shifts (δ) of β-CD and CEO/β-CD-IC48
<b>Table 7.</b> <sup>1</sup> H NMR chemical shifts (δ) of SBE-β-CD and CEO/SBE-β-CD-IC49
Table 8. Classification of wound.   55
Table 9. Literature research on electrospun fibers with cyclodextrin inclusion
complexes

#### **List of Abbreviations**

B. cereus Bacillus cereus

 $\beta$ -CD  $\beta$ -cyclodextrin

CEO Cinnamon leaf essential oil

ddH<sub>2</sub>O Double distilled water

DI-water Deionized water

DMEM-HG Dulbecco's modified Eagle's medium-high glucose

DMSO-d<sub>6</sub> Deuterated dimethylsulfoxide

DPBS Dulbecco's Phosphate-Buffered Saline

EO Essential oil

E. coli Escherichia coli

FBS Fetal Bovine Serum

IC Inclusion Complex

LB agar Luria-Bertani agar

LB broth Luria Bertani broth

L. monocytogenes Listeria monocytogenes

MIC Minimum Inhibitory Concentration

OD Optical Density

P. aeruginosa Pseudomonas aeruginosa

PDI Polydispersity indices

S. aureus Staphylococcus aureus

SBE-β-CD Sulfobutyl ether β-cyclodextrin sodium

S. dysenteriae Shigella dysenteriae

S. typhimurium Salmonella typhimurium

# CHAPTER 1: Inclusion Complexes of β-Cyclodextrin and its Sulfobutyl Ether Derivative with Cinnamon Leaf Oil: Preparation, Characterization and Antibacterial Activity

#### 1. Introduction

#### 1.1 Essential Oils

#### 1.1.1. General Properties of Essential Oils

Plant essential oils, which can also be called aromatic oil or ethereal oil, are among the important components of plant chemistry. They can be defined as colorless or light yellow hydrophobic and concentrated volatile aroma compounds that are usually liquid at room temperature <sup>1</sup>. The composition and amounts of essential oils vary depending on the type of plant, the part of the plant, the geographical location where plant is grown, climate and the extraction method <sup>2,3</sup>. They are obtained from various aromatic plants that grow in the geography between the warm tropical countries and the temperate Mediterranean region countries <sup>4</sup>. Turkey has a very rich flora, especially in terms of plants containing essential oil.

Essential oils are secreted by glandular trichomes and specialized secretory tissues on the woody structures, rhizomes (e.g., ginger), leaves and stems (e.g., oregano basil, cinnamon, eucalyptus, wintergreen, parsley), fruits (e.g., lime, grapefruit), flowers (e.g., orange, lavender, clove), barks (e.g., cinnamon), roots (e.g., valerian) of the plant <sup>1,5</sup>. These secreted oils have many benefits on plants. They can be listed as <sup>1,6</sup>;

- Helping pollination: The plant can communicate with its environment with the volatile compounds it synthesizes. In this way, it can attract the attention of a bee and carry the pollen to the female species.
- Preventing water loss: If they are located on the outer surface of the plant (leaves, flowers, etc.), they can reduce the water loss of the plant <sup>7</sup>.
- Protecting plants against enemies: The volatile compounds it produces against a harmful species can show repellent properties.
- Tissue healing: In case of injury to the plant, essential oils with antibacterial and antifungal properties can prevent the plant from getting infected.

Medicinal and aromatic plants have been used for the treatment of diseases since ancient times <sup>8</sup>. It is known that the volatile compounds in plant essential oils have inhibitory effects on the development, spread and toxin formation of microorganisms such as bacteria, molds and yeasts <sup>9–11</sup>. In addition, the phenolic compounds contained in essential oils can be used as antioxidant,

antimicrobial, anticancer, anti-obesity, antidiabetic and antimutagenic agents in the perfumery, cosmetics and the food industry <sup>12–14</sup>. Methods for obtaining essential oils from plant sources are distillation method, extraction method and mechanical extraction (pressing) method <sup>15</sup>. Mechanical extraction (pressing) and steam distillation are mostly preferred for products to be produced as an alternative to bactericidal, fungicidal, food additives and pharmaceutical synthetic chemical compounds; solvent extraction or supercritical carbon dioxide extraction method is preferred in the production of essences to be produced for the perfumery industry <sup>4</sup>.

#### 1.1.2. Chemical Properties of Essential Oils

Although they are defined as oils because they are insoluble in water and dissolved in organic solvents, they are different from fixed oils. They contain different chemical compounds in their structure. The chemical components of essential oils mainly include terpenoids (mostly monoterpenes; minor amounts of sesquiterpenes and diterpenes), acids, alcohols, aldehydes, ketones, acyclic esters, lactones, less frequently nitrogenous and sulfurous compounds, coumarins and their oxygen-bound derivatives (phenylpropanoids) <sup>16–18</sup>. The chemical structures of some compounds in essential oils are given in **Figure 1**.

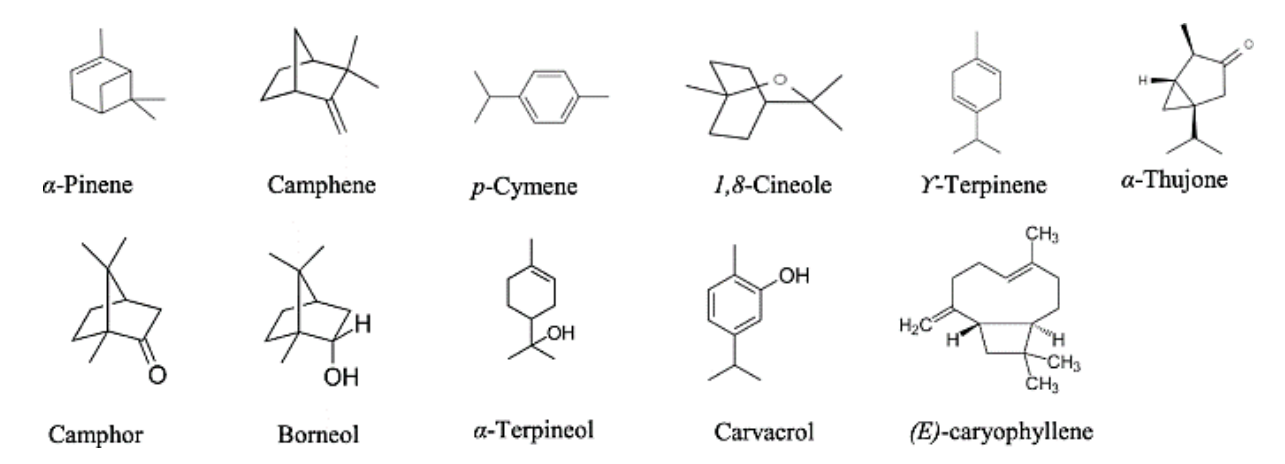


**Figure 1.** Chemical structures of some compounds in essential oils <sup>19</sup>.

Essential oils can be grouped according to their chemical composition, aromatic properties, pharmacological and therapeutic effects. Terpenic substances constitute the majority of essential oils <sup>20</sup>. They are found in essential oils as monoterpene, sesquiterpene and diterpene. Oxygenated derivatives formed by the oxidation of terpenes give essential oils their distinctive smell, taste and therapeutic properties <sup>21,22</sup>. For this reason, when classifying essential oils, the oxygen compounds found in essential oils are taken as a basis.

Essential oils obtained from fennel, anise, ceylon cinnamon, thyme and clove are examples. Essential oils, which are also grouped according to their pharmacological and therapeutic effects, are generally for therapeutic purposes and their importance has increased with the increasing importance of alternative medicine. According to their pharmacological effects, essential oils are grouped as such antitussive, antirheumatic, anti-inflammatory, diuretic disinfectant.

#### 1.1.3. Antibacterial Mechanisms of Essential Oils

Because of their chemical components, they have antimicrobial properties against bacteria. The mechanism of action of essential oils secreted by plants has been the subject of studies for many years. As a result of the studies, many antibacterial action mechanisms have been identified. Functional groups and composition in essential oils determine the activity on bacteria <sup>23</sup>. It has been reported that the most effective of these is the effect of bacteria on disrupting the integrity of the membrane structure <sup>24</sup>. The phenolic components in plant essential oils affect the cell membrane easily, causing an increase in permeability and a weakening of the integrity of the cell membrane <sup>25</sup>. As a result of this interaction, the ions in the structures of the cells and their components disappear over time, leading to cell death <sup>26</sup>.

Another important mechanism of action of essential oils is that terpenes impart hydrophobic properties to essential oils. With these properties, they can easily pass-through cell walls and cell membranes. Hydrophobic and lipophilic nature of essential oil components interact with fatty acid of cell membrane, damage the cytoplasmic membrane, increase the permeability, disturb the protein membrane, inhibits ATP synthase and cause the cell death <sup>27–29</sup>. In addition, other mechanisms may be affected by these effects of plant essential oils. These features can be counted as causing toxic effects, inhibiting the cell defense system and causing deterioration of cell DNA and RNA structures <sup>30</sup>.

It is known that gram-positive bacteria are more susceptible to EOs as compared to gram-negative bacteria. The outer membrane of gram-negative bacteria prevents the diffusion of hydrophobic compounds from within the cell, however, these hydrophobic compounds in essential oils easily pass through the cell membrane with lipoteichoic acid lipophilic ends in gram-positive bacteria. <sup>31</sup>.

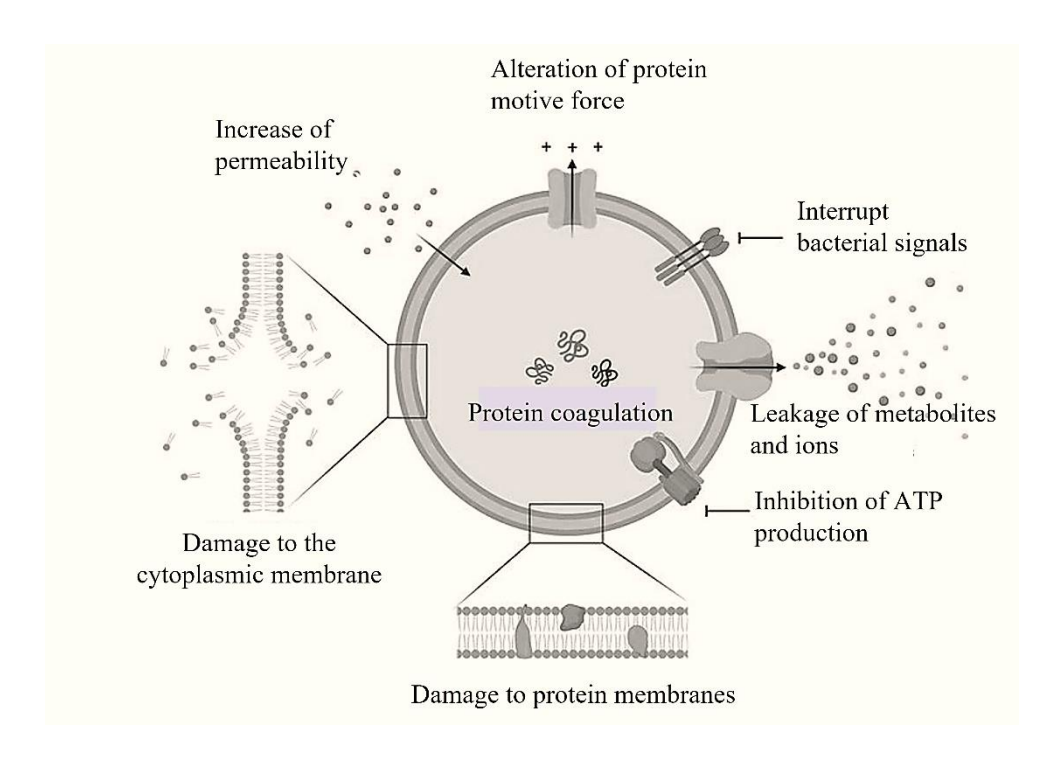


**Figure 2.** Antibacterial mechanisms of essential oils. There are five major modes of action: (1) coagulation of cytoplasm, (2) inhibition of ATP synthase, (3) alteration in ion transport, (4) degradation of the cell wall, and (5) bacterial membrane destruction <sup>32</sup>.

#### 1.1.4. Cinnamon Leaf Essential Oil

Cinnamon oil is obtained from the leaves and bark of the *Cinnamonum zeylanicum* Blume plant. This oil is very rich in monoterpenoids and phenyl propanoids. However, the major chemical components in cinnamon oil vary depending on where they are obtained. The compounds in the structure of these oils can be examined in detail using gas chromatography (GC) and mass spectrometry (MS). Swetha et al and Jeong et. al compared the cinnamon bark oil and leaf oil with gas chromatography and reported that cinnamaldehyde is the predominant component in cinnamon bark oil while eugenol is major component in cinnamon leaf oil <sup>33,34</sup>. GC-MS chromatogram of cinnamon leaf oil is depicted in **Figure 3**.

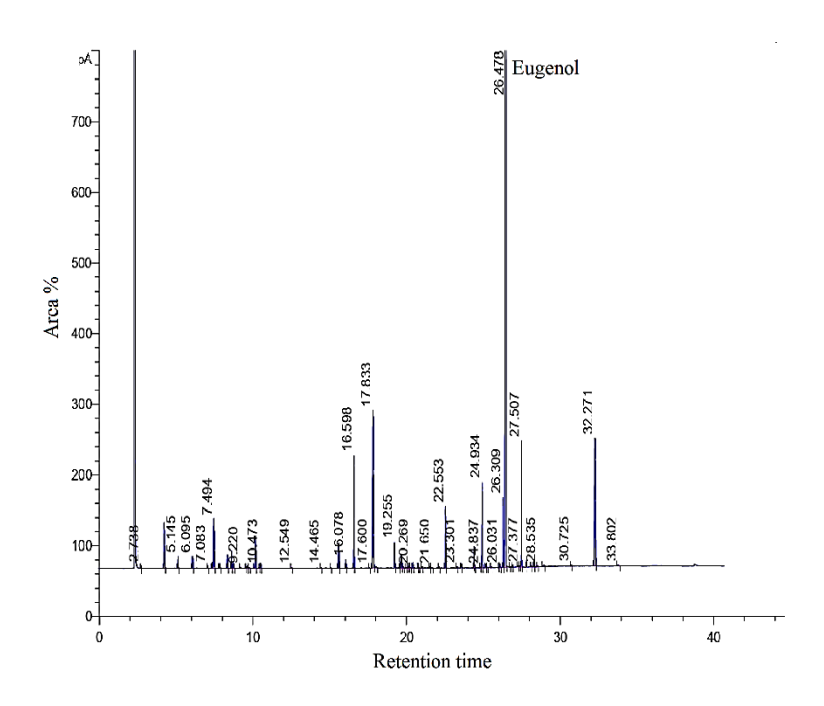


**Figure 3.** GC-MS chromatogram showing chemical compositions of cinnamon leaf oil <sup>33</sup>.

Cinnamon oils are classified by the US Food and Drug Administration (FDA) as GRAS 'Generally safe-harmless' <sup>35–37</sup> and known that they have anti-inflammatory, antioxidant, mosquito repellent, antispasmodic, antidiarrhea, antiparasitic and antimicrobial effect <sup>38–41</sup> Several disorders as respiratory, immune, lymphatic, nervous, cardiovascular, digestive, urinary and reproductive system complaints can be treated with this herb <sup>41</sup>. Farahpour et al. also found that *Cinnamon verum* essential oil can be used for topical application because of owing to characteristic antioxidant properties give oil to accelerate healing of the wound <sup>35</sup>. In another study, suppressing lipid peroxidation and inhibiting hepatic 3-hydroxy-3-methylglutaryl reductase activity by hepatic antioxidant enzyme activity of cinnamon essential oil accelerate healing wound site of rats <sup>42</sup>. Eugenol would exert inflammatory effects to a cyclooxygenase-2 antagonist that helps accelerate wound healing <sup>43,44</sup>. Zainol et. al produced a nano cream including cinnamon leaf essential oil for wound healing <sup>41</sup>, the undiluted oil can cause irritation when it comes into direct contact with the skin <sup>45</sup>.

Studies on cinnamon show that eugenol in cinnamon inhibit the growth and toxin production of some mold species <sup>46,47</sup>. They have antifungal effect against Fusarium species (e.g., *Fusarium avenaceum*, *Fusarium oxysporum*), Penicillium species (e.g., *Penicillium glabrum*, *Penicillium expansum*, *Penicillium italicum*) and Aspergillus species (e.g., *Aspergillus niger*) <sup>48</sup>. It has also antibacterial effective on Gram (-) and Gram (+) bacteria as *Staphylococcus aureus*, *Staphylococcus epidermidis*, *Streptococcus pyogenes*, *Streptococcus pneumoniae*,

Helicobacter pylori, Bacillus cereus and Escherichia coli <sup>49,50</sup>. Oliveira et al. reported that eugenol-loaded cellulose paper showed a very good inhibitory effect against Escherichia coli microorganism, but Staphylococcus aureus was more resistant <sup>51</sup>. In another study, eugenol showed a stronger effect than antibiotics against the growth of E. coli and K. pneumoniae <sup>52</sup>. Although the information about the mechanism of action is limited, it is suggested that this is related to the lipophilic properties and chemical structures of the oils. **Table 1** shows the mechanism of action of cinnamon leaf essential oil against gram positive and gram-negative bacteria.

**Table 1.** The mechanism of action of cinnamon leaf essential oil to different microorganisms. S.aureus: Staphylococcus aureus; B. cereus: Bacilllus cereus; E. coli: Escherichia coli; K. pneumoniae: Klebsiella pneumoniae; C. freundii: Citrobacter freundii

Essential oil	Major Components	Microorganisms	Mechanism	References
	HO	Gram + bacteria:		
		S. aureus, B. cereus		
	Eugenol		Inhibition of	
	(% 86.02)		ATP synthase	
		Gram - bacteria:		53–56
<b>~</b>	CH₃		Disruption of	33–30
Cinnamon	H <sub>2</sub> C H CH <sub>3</sub>	E. coli,	the cell	
Cinnamomum	ĊH₃	K. pneumoniae,	membrane	
zeylanicum	Caryophyllene	C. freundii, Proteus		
	(% 5.70)	spp		

#### 1.2. Microencapsulation

Beside the antimicrobial potential, essential oils have some limitations as being volatile. They are sensitive to heat, light, moisture and oxygen <sup>53</sup>. Encapsulation is one of the most efficient processes to increase the shelf life of essential oils and to preserve their bioactive properties. Microencapsulation can be defined as the confinement of solid, liquid or gaseous food components, enzymes, cells and other similar substances by wrapping them with protein or carbohydrate-derived coating material <sup>57,58</sup>. It is used in many areas of food, including stabilization of the encapsulated material, controlled release, oxidation control, color, odor

masking and taste <sup>59</sup>. The main purpose is to protect the material to be encapsulated against deterioration caused by the external environment and to release certain substances in its composition <sup>60</sup>. Microencapsulation applications have gained importance for many reasons, these are <sup>61</sup>: reducing the interaction of the encapsulated material with environmental conditions (water, oxygen, light); reducing the evaporation of the material to the external environment; facilitating the usability of the material (preventing agglomeration, converting from liquid form to solid form, etc.); providing controlled release to the environment under desired conditions; making the taste and odor of the substance; ensuring homogeneous distribution in the environment.

Microencapsulation can be achieved by rotational suspension separation, spray drying, extrusion coating, coacervation, fluidized-bed coating, centrifugal extrusion, liposome entrapment and **inclusion complexation** <sup>58</sup>. Although there are many components that can be used as coating material in microencapsulation, it is possible to collect them under the headings of proteins and carbohydrates. Among the proteins, coating materials such as milk proteins, whey proteins and soy proteins have been widely used <sup>62</sup>. Carbohydrates such as hydrolyzed starch, modified starch, gums, **cyclodextrins** and maltodextrins are used in the microencapsulation of essential oils <sup>63,64</sup>.

#### 1.3. Molecular encapsulation

Studies have shown that the inclusion complex formation method with cyclodextrins is more cheaper, simpler and effective than other methods in protecting volatile and sensitive components <sup>65</sup>. The most important advantage of this method is that encapsulation can be achieved at the molecular level <sup>66</sup>.

#### 1.3.1. History of Cyclodextrin

The history of cyclodextrins can be divided into three main stages as follows: (a) period of discovery: 1891-1930; (b) period of exploration: 1935-1970 and (c) period of industrial use: 1970- onwards <sup>67</sup>. Cyclodextrins were first discovered by Villers in 1891. He obtained crystalline substance from *Bacillus amylobacter* growth on starch medium and named this substance "cellulosine" because of its similarity to cellulose <sup>68</sup>. A monograph by Thoma and Stewart in 1965 was followed by Caesar in 1968. Later, new methods were developed for the preparation of cyclodextrins on a larger scale, and their chemical and physical properties were investigated. The first pharmaceutical product (prostaglandin E2:βCD) using cyclodextrins were launched in Japan in 1976 <sup>67</sup>.

Cyclodextrins are widely used for the encapsulation of many compounds (antimicrobials, antioxidant compounds, etc.) due to their non-toxicity and acceptable price for industrial purposes <sup>69–71</sup>. They have become one of the most studied host molecules, as they are approved by the FDA and listed as GRAS <sup>72</sup>. Their use in pharmaceutical technology is increasing day by day and there are many patents on this subject. In recent years, cyclodextrin production factories have been established in countries such as the United States, Germany, Japan, Hungary and France, and their production amounts are increasing from year to year <sup>73</sup>.

#### 1.3.2. Molecular Structure of Cyclodextrins

Cyclodextrins are natural oligosaccharides includes glucopyranose units that is linked via  $\alpha$ -1,4-glycosidic bond <sup>74</sup>. They are obtained by a simple fermentation of starch. First of all, cyclodextrin glycosyltransferase (CGTase) enzyme is produced from *Bacillus macerans*, *Klebsiella pneumonia* or *Alcalophile bacillus* microorganisms <sup>75</sup>. As a result of the breakdown of hydrolyzed starch with this enzyme, cyclodextrins are formed.

Cyclodextrins have the appearance of a truncated cone with a central cavity because of chair conformation of the glucopyranose unit in them <sup>76</sup>. Ethereal oxygens and skeletal carbons of the glucose residues are lined in central cavity of the cyclodextrin. The cyclodextrin cavity has a **hydrophobic** character due to secondary C-H bonds <sup>76</sup>. Due to the rotation of the C6 carbon atom with respect to the C2 and C3 hydroxyl groups, the cyclodextrin space narrows towards the bottom. The hydroxyls attached to C2 are directed towards the inner cavity, while the hydroxyls attached to C3 are directed outwards from the inner cavity. As a result of the presence of hydrogen bonds between the secondary hydroxyl groups on the C2 and C3 atoms and the alignment of the space with glycosidic oxygen bridges, the space acquires a hydrophobic feature. Hydroxyl groups from sugar residues are orientated at narrow and wider edge of the shape and provided the cyclodextrin to have hydrophilic surface <sup>76</sup>. The hydroxyl groups in the structures are responsible for the solubility of this compound in water. There are two protons H3 and H5 on the inner surface of the cavity and three protons H1, H2 and H4 on the outer surface of the cyclodextrins. The H3 proton is closer to the wide rim, while the H5 proton is closer to the narrow part <sup>77</sup>. As the guest molecule enters the cyclodextrin cavity, a chemical shift occurs in the H3 and H5 protons and indicates that an inclusion complex occurred <sup>78</sup>. Molecular and functional structure scheme of cyclodextrin is shown in **Figure 4**.

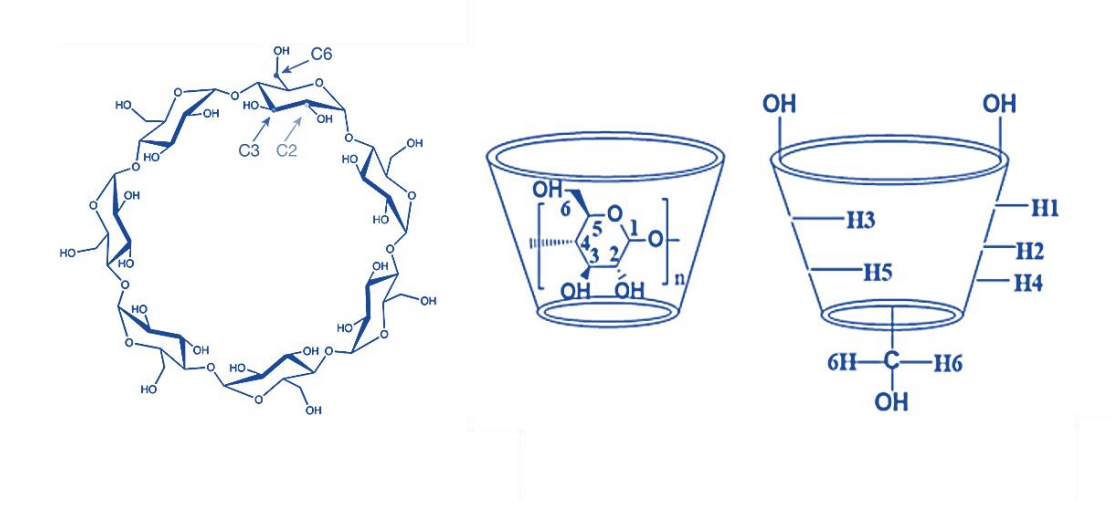


**Figure 4.** The molecular and functional structure scheme of cyclodextrins <sup>79,80</sup>.

Cyclodextrins are named according to the number of  $\alpha$ -1,4-D(+)-glycosidic-linked glucopyranose units in the molecule <sup>81</sup>. The structures of  $\alpha$ -cyclodextrin (6 units),  $\beta$ -cyclodextrin (7 units) and  $\gamma$ -cyclodextrin (8 units) are given in **Figure 5** <sup>69</sup>. This property is useful for solubilizing and stabilizing highly hydrophobic molecules in solvents such as water. Hydroxyl groups in the outer structure of the rings of cyclodextrins are responsible for the solubility of this compound in water.

Although the cavity height is same for all types of natural cyclodextrin, the volume and the diameter cavity vary  $^{82}$ . The type of cyclodextrin used depends on which guest molecule fit better in host of cyclodextrins  $^{82}$ . Depending on the diameters of the hydrophobic space inside the cyclodextrin of 4.7-5.3 A° ( $\alpha$ -CD), 6.0-6.5 A° ( $\beta$ -CD) and 7.5-8.3 A° ( $\gamma$ -CD), cyclodextrins form inclusion complex (guest-host structure) with aromatic compounds. Small cavities in  $\alpha$ -cyclodextrin are not acceptable in many molecules. Larger cavities in  $\gamma$ -cyclodextrin are not suitable for small molecules because of weak hydrophobic charges with cavity not facilitating complexation.  $\beta$ -CD is more preferable with its lower cost price  $^{83}$ . Also,  $\beta$ -CD is the most suitable cyclodextrin for encapsulating aromatic substances that can bond with aromatic substances in liquid media. It also provide better stability with increasing dissolution rate and solubility  $^{84}$ .

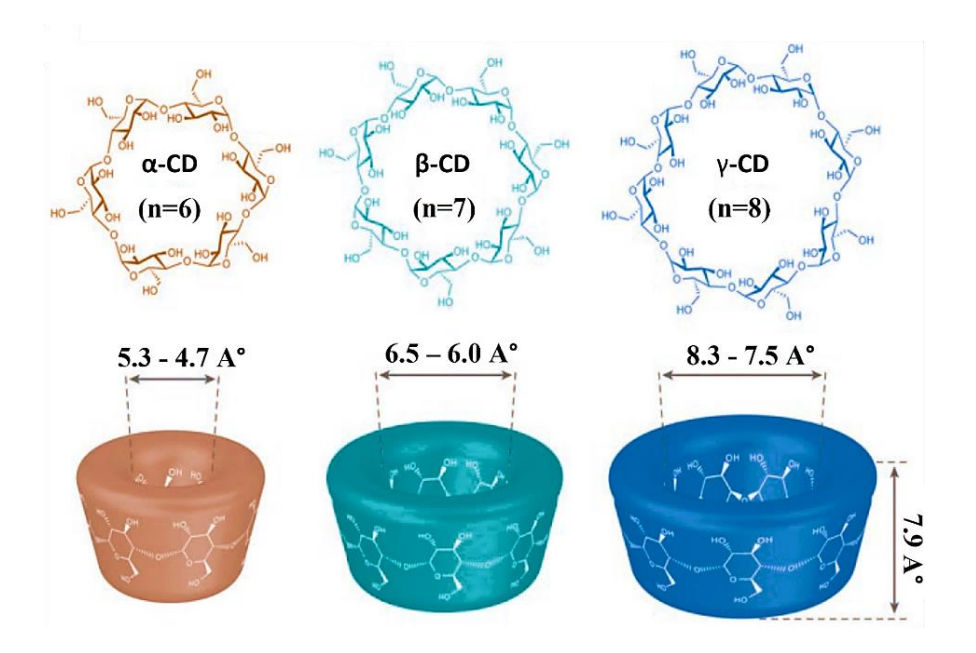


**Figure 5.** Chemical structure and schematic representation of natural cyclodextrin. Figure adopted from Lee et al. <sup>85</sup>.

#### 1.3.3. Modified Cyclodextrins

There are 14 secondary hydroxyl groups in the wide rim and 7 primary hydroxyl groups in the narrow rim of  $\beta$ -cyclodextrins <sup>86</sup>. All these hydroxyl groups are possible to make structural modifications and many guests can be placed in the molecular ring. The low solubility of  $\beta$ -cyclodextrin in water may be due to hydrogen bonds that may occur between the hydroxyl groups in the cyclodextrin molecule. Therefore, hydrogen bonding is prevented by the attachment of the aliphatic structures to the primary and secondary hydroxyl groups of C2, C3 and C6, and as a result, the physicochemical properties of  $\beta$ -cyclodextrin change significantly. The physicochemical properties and functional groups of various modified cyclodextrins are compared in **Table 2**. Among the reasons why cyclodextrins are modified that <sup>87–89</sup>:

- Enhancing the water solubility of  $\beta$ -cyclodextrin and their inclusion complexes
- Eliminating hemolysis and nephrotoxicity, which are most important side effects of natural cyclodextrins after administration.
- Changing drug release characteristics (extended, controlled, or delayed release)
- Increasing the interaction of cyclodextrins with the guest molecule and as a result forming more durable inclusion complexes
- Binding some groups to the cyclodextrin molecule and synthesizing new derivatives

**Table 2.** Physicochemical properties of cyclodextrins properties of  $\beta$ -CD and its derivatives <sup>90</sup>

Cylodextrin	Substitution degree	Molecular structure	Water solubility (mg/ml)	Molecular Weight (Da)
β-CD	-	OH OH OH OH	<2	1135
HP-β-CD	0.65	$\begin{bmatrix} RO & & \\ OR & \\ OR & \end{bmatrix}_{7} R = H \text{ or } * C$	CH <sub>3</sub> >600	1400
SBE-β-CD	0.9	$\begin{array}{c} \text{OR} & \text{R = -H} \\ \text{OR} & \text{-CH}_2\text{CH}_2\text{CH} \\ \text{OR} & \text{7} \end{array}$	<sub>2</sub> CH <sub>2</sub> SO <sub>3</sub> Na >500	2163
М-β-СD	1.8	R = H  or	*-cH <sub>3</sub> >500	1312

The cyclodextrin derivatives that are frequently used in the pharmaceutical field and formulation of drug delivery systems are categorized to three types:

- 1. **Hydroxypropyl cyclodextrins** (HP-β-CD) are statistically substituted derivatives. As the reaction continues, the reactivity of the hydroxyl groups changes. This results in various products with different degrees of substitution. The solubility of these cyclodextrins is endothermic. Therefore, the solubility does not decrease with the increase in temperature. The degree of substitution of hydroxypropyl cyclodextrins is proportional to their inclusion capacity <sup>91</sup>. Commercial preparations using hydroxypropyl cyclodextrins include tablets, eye drops, and are marketed under the trade names Encapsin® and Molecusol® <sup>92</sup>.
- 2. **Sulfobutylether-β-cyclodextrins** (SBE-β-CD) are very well soluble in water, are good solubilizers for drugs when they form inclusion complexes with many poorly soluble drugs. Its superiority to hydroxypropyl cyclodextrins is its high complexation capacity

- <sup>93</sup>. It is safer than other CD derivatives because it can form a complex with cholesterol and other membrane lipids at a ratio of 1:2 <sup>94</sup>.
- 3. **Methylated cyclodextrins** (M-β-CD) are obtained by methylation from C2 secondary or C6 primary hydroxyl groups (dimethyl cyclodextrin) or C2, C3 and C6 (trimethyl cyclodextrin) hydroxyl groups. The most important disadvantage of methylated cyclodextrins is that decreasing their solubility with the increase in temperature. This disadvantage causes strong binding of the drug and a strong hemolytic effect <sup>95</sup>.

Hydroxypropyl cyclodextrins and sulfobutylether- $\beta$ -cyclodextrin are the most widely used derivatives in the pharmaceutical industry because of having low toxicity, high solubility, and are suitable for oral and parental (genetic) applications  $^{71}$ .

#### 1.3.4. Inclusion Complex of Cyclodextrins

Inclusion complexes are compounds formed by a host molecule holding a guest molecule in its cavity without forming any covalent bonds. The guest molecule is inserted into the host cavity without significantly affecting the host structure. It is a characteristic feature that the size and shape of the existing cavity remain unchanged despite slight deformation. The guest molecule partially or completely enters the cavity of the cyclodextrins <sup>96</sup>.

An aqueous solution is required for these complexation reactions to occur <sup>97</sup>. Schematic representation of inclusion complex formation is given in **Figure 6**. In this respect, it is very important to understand the mechanism of interactions between host-guest structures and water. Incorporation of a guest molecule into the cyclodextrin cavity occurs as the water molecules in the cavity are replaced by the guest molecule. Inclusion complex process is a preferred interaction between the apolar guest molecule and the hydrophobic space. <u>Hydrophobic interaction and Van der Waals interaction are the main driving force for forming inclusion complexes</u> <sup>98</sup>. The complex formation consists of the following basic steps <sup>99</sup>:

- 1. The water molecules reach an energy level corresponding to the gaseous state by leaving the cyclodextrin space.
- 2. It results in a decrease in the number of hydrogen bonds and Van der Waals interactions and an increase in the freedom of water molecules' rotational degrees.
- 3. As a result of relaxation, cyclodextrin's conformation energy decreases, especially in  $\alpha$  and  $\beta$  cyclodextrin. The apolar guest molecule becomes the ideal gas by trapping the hydrate shell.

- 4. The guest molecule, which is assumed to be an ideal gas, settles in the cyclodextrin space and the stabilized by sometimes hydrogen bonds and Van der Waals interactions.
- 5. Thus, the displaced water molecules undergo a phase change from gaseous to liquid.
- 6. Water molecules surround the exposed part of the guest molecule and fuse with the hydrate shell of the cyclodextrin molecule.

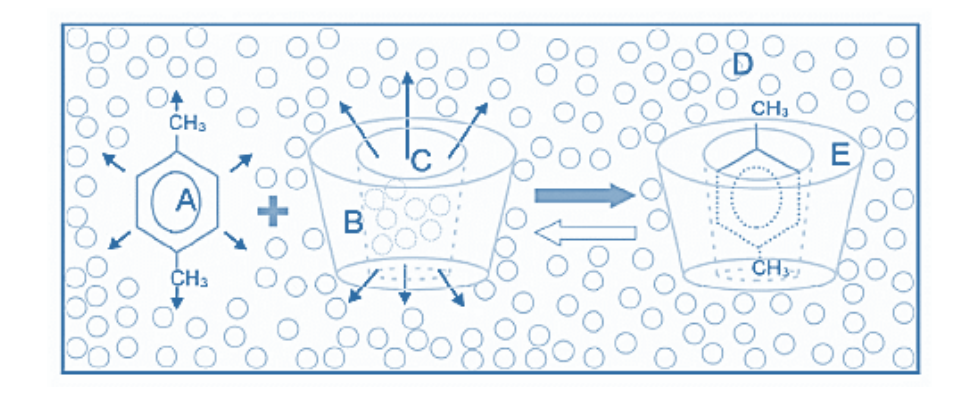


**Figure 6.** Schematic representation of inclusion complex formation. A, B,C, D and E refers to drug, cyclodextrin molecule, cavity of cyclodextrin, water molecules and inclusion complex, respectively <sup>67</sup>.

The factors affecting the formation can be listed as solution dynamics, temperature, and use of solvents. The solubility of the guest molecule, the heating of the complex to a certain temperature, the selection of the solvent used to increase the solubility of the guest and cyclodextrin are factors that increase the complex yield. In addition, organic solvents such as ethanol and diethyl ether increase the solubility of the guest molecule and can be easily removed by evaporation at the same time <sup>100</sup>.

#### 1.4. Physicochemical Characterization Analysis of Inclusion Complexes

Inclusion complexes between the cyclodextrin and the guest molecule may not form in all cases. In many cases, the resulting products consist of un-complexed guest molecules and cyclodextrins that could not have a guest in its cavity. For this reason, the interaction between the guest molecule and the cyclodextrin is investigated using physicochemical and thermodynamic techniques. Determination of guest molecule content in the resulting product and determination whether guest molecules are partially or completely incorporated into the cyclodextrin cavity are provided by some techniques. The "Higuchi Connor phase solubility assay" is used to determine the complex stoichiometry and stability constant. Scanning Electron Microscopy (SEM), Dynamic Light Scattering (DLS), Fourier Transform Infrared Spectroscopy (FTIR), Thermogravimetric analysis (TGA), Differential Scanning Calorimetry

(DSC) and Nuclear Magnetic Resonance Spectroscopy (NMR) are the examples of characterization methods.

#### 1.4.1. Phase solubility assay

In the formation of inclusion complex, there is a physical interaction between the guest and the host molecule. This interaction is carried out within the framework of a chemical equilibrium. The stability constant of the equilibrium complex reaction is related to the reaction formation rate constant and the dissociation rate constant of the complex. The stability constant  $(K_c)$  gives information about the stability of the guest molecule in the complex.

An inclusion complex is formed when 1 unit guest molecule partially or completely enters 1 unit of cyclodextrin molecule and is called 1:1 stoichiometrically. However, the guest molecule may be too large to fit in the cyclodextrin cavity or much smaller than the cavity. In this case, a guest-host complex with a molar ratio of 2:1, 1:2 can be formed (**Figure 7a**) <sup>101</sup>. In 2:1 inclusion complex is with the placement of a guest molecule on both sides of a cyclodextrin molecule. In 1:2 inclusion complexes, there is a separate cyclodextrin entry to both ends of the guest molecule. With the help of the phase solubility assay developed by Higuchi and Connors, both the type of inclusion complex formed and the stability constant value are determined <sup>83,102</sup>.

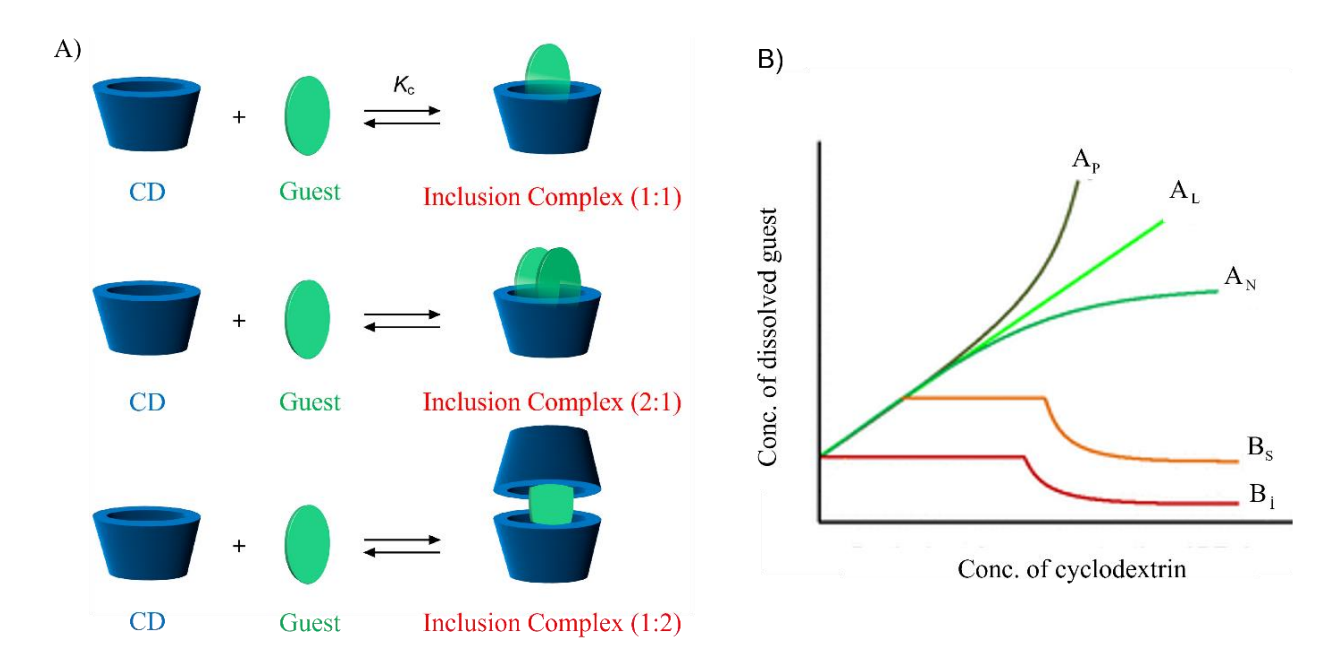


**Figure 7.** (a) Different the cyclodextrin—guest ratio for the inclusion complex and (b) phase solubility diagram. Figure adopted from Topuz et al. <sup>101</sup> and Williams et al. <sup>103</sup>.

The equilibrium stability constants of the inclusion complexes formed in a 1:1 molar ratio can be calculated from the phase solubility diagram. Different curve profiles appear in this diagram (**Figure 7b**). These profiles are divided into two groups as A type for soluble inclusion complexes and B type for insoluble inclusion complexes  $^{104}$ . Type B curves are divided into two subgroups. The Bs group represents poorly soluble inclusion complexes, while the  $B_i$  group represents insoluble inclusion complexes. Type A curves are divided into subgroups called  $A_L$  (linear increase in drug solubility due to cyclodextrin solubility),  $A_P$  (positive deviation from isotherm) and  $A_N$  (negative deviation from isotherm). When AL type curves are obtained, it shows that a 1:1 stoichiometric inclusion complex is formed  $^{105}$ . The type of inclusion complex shown by the  $A_P$  type curves forms a complex with the guest molecule at a higher stoichiometric ratio than the host molecule. The  $A_N$  type of graph is difficult to interpret; It cannot be predicted whether it forms any complex. It is thought that this situation may be caused by the change in dielectric constant seen in the solvent.

#### 1.4.2. Morphological Analysis

The guest molecule, the cyclodextrin and the changes in the crystal structures of the formed complexes can be characterized by SEM. Obtained SEM images give important information such as morphology, shape, and size of the applied sample. However, this method is insufficient to analyze the inclusion complex. Results should be supported by other characterization techniques.

#### 1.4.3. Size and Surface Charge Analysis

Particle size and polydispersity index (PDI) of inclusion complexes can be determined by DLS method using Malvern Zetasizer. DLS is based on measuring the intensity and variation of light scattered from small particles in a dilute solution. Measurements made with the DLS technique are considered an important analysis since they represent the movement of a particle in a liquid. It is based on the detection of vibrations caused by laser light beaming into particles. The change in the intensity of the scattered light depends on the motion of the particle and accordingly the size of the particle, the viscosity of the medium and the temperature. Zeta potential is a measure of the push-pull or electrostatic value between particles <sup>106</sup>. Zeta potential measurement provides detailed information on dissipation mechanisms and is the key to electrostatic dissipation control. The surface charge (zeta potential, mV) of inclusion complexes can be measured using the Zeta sizer system.

#### 1.4.4. Functional Analysis

FTIR analysis is a vibrational spectroscopy technique based on the measurement of the excitation of molecules to vibrational and rotational energy levels by absorption of IR light (0.78–1000 µm wavelength), and molecular bond characterization can be performed with this method. With the FTIR-ATR unit, a decrease in the wavelength of the absorption bands is created and this allows spectral analyzes of the substances. Since the formation of inclusion complexes will cause changes in the cyclodextrin bands, the change can be followed by the FTIR-ATR system. It is widely used in the characterization of solid-state complexes. The characteristic bands of cyclodextrin rarely change after complex formation. But the size of the bands belonging to the guest molecule varies. The disappearance or reduction of the bands of the guest molecule shows that the free molecules in the environment form complexes with the cyclodextrin molecules <sup>99</sup>.

#### 1.4.5. Thermal Analysis

It is based on the measurement of temperature and properties of the system, such as weight, heat of reaction, or volume change.

DTG is used to determine the thermal and gravimetric changes that occur in a material with an increase in temperature. Weight changes (such as water loss, organic matter removal) occurring within the material can be detected by thermogravimetry (TG), and temperature changes resulting from exothermic or endothermic reactions can be detected by differential thermal analysis (DTA). When the temperature is increased, the mass of the complexing product is measured continuously and then these measurements are plotted. The graphed information (thermogram) provides quantitative data about the complex. With these methods, it is determined whether the cyclodextrin shows some change before its thermal decomposition at 252–400 °C <sup>107</sup>.

Complexation causes endothermic peaks to disappear, new peaks to appear, and peak broadening indicating a change in melting, boiling, or sublimation points. A powerful qualitative analytical technique, DSC, is used to investigate changes in thermal behavior of cyclodextrin complexes. In this analysis, it is examined whether there is an endothermic peak at the melting point temperature of the mixture <sup>108</sup>.

#### 1.4.6. Molecular Analysis

The interaction between cyclodextrin and active substances that form a complex can be detected by NMR spectroscopy, as it will cause the signal of the material to change in the magnetic field. NMR spectroscopy provides information about the structure of the molecule by using the specific magnetic properties of the atomic nuclei. Beside the quantitative and qualitative information, this method provides information about which part of the guest molecule forms a complex. The direction of entry of the essential oil into the cyclodextrin cavity and the interactions between molecules can be analyzed by  $^1$ H-NMR methods. If there is a change in the NMR spectrum of the essential oil and the essential oil/cyclodextrin inclusion complex, it means that there is an interaction between them. Changes occur in the magnetic field where the guest molecules used with cyclodextrin form complexes. Chemical shift changes ( $\Delta\delta$ ) were calculated according to  $^1\Delta\delta = \delta$  (complex)  $^-\delta$  (free)'. The values of chemical shifts occurring in cyclodextrins, essential oils and inclusion complexes were shown in ppm.

#### 1.5. Studies on inclusion complexes

The importance of the inclusion complex is improving the physicochemical properties of the hydrophobic guest molecule entrapped by the cyclodextrin. These properties include stabilization of the guest molecule, increasing water solubility of hydrophobic structures protection from heat or UV light, masking of undesirable tastes and odors and physical state change control. Inclusion complexes are also preferred due to their controlled release feature. Long-term use is ensured by encapsulating volatile components with cyclodextrins. These advantages enable inclusion complexes to be used frequently in industries such as, food, packaging, cosmetics, environment, pharmaceutical and textile <sup>109</sup>.

Some studies on inclusion complexes formed with various oils or their major component and their application areas are shown in **Table 3**. Although there are many studies on the inclusion complex of cinnamon bark oil with cyclodextrins, **studies with cinnamon leaf oil are limited**. When a comprehensive literature was searched, only two studies were found with cinnamon leaf oil.

Lin et al.  $^{110}$  formed inclusion complexes with  $\beta$ -CD and cinnamon leaf oil using the ultrasonic wave method. Complexes were characterized using FTIR and Raman. Encapsulation efficiency of the complexes was calculated. Then, CEO/ $\beta$ -CD proteoliposomes were produced and antibacterial effect of these proteoliposomes was investigated against *Bacillus cereus* bacteria.

These liposomes were inserted into the fibers prepared using the PEO polymer. The antibacterial application of CEO/ $\beta$ -CD proteoliposomes nanofibers on beef was investigated.

Zavala et al.  $^{111}$  studied the molecular encapsulation of cinnamon leaf and garlic oil in  $\beta$ -CD molecule. İnclusion complexes were prepared according to the precipitation method. Gas chromatography analysis, moisture sorption—desorption isotherm, and infrared spectroscopy were used in characterization studies. The antifungal activity of complexed oils was tested against *Alternaria alternata*. As a result, it was stated that cinnamon oil formed a complex with  $\beta$ -cyclodextrin, and these complexes showed strong antifungal activity.

**Table 3.** Literature research on essential oil loaded cyclodextrin inclusion complex. HP-  $\beta$ -CD: 2-hydroxypropyl- $\beta$ -cyclodextrin, HP- $\gamma$ -CD: hydroxypropyl- $\gamma$ -cyclodextrin,  $\beta$ -CD:  $\beta$ -cyclodextrin, M $\beta$ CD: Methyl- $\beta$ -cyclodextrin, RAMEB: Randomly methylated  $\beta$ -cyclodextrin, CRYSMEB: Low 2-O-methylated- $\beta$ -CD, SBE- $\beta$ -CD: Sulfobutylether- $\beta$ -CD.

Cyclodextrins	Essential oil	Their constituents	Applications	References
HP- β-CD	-	Cuminaldehyde	Antibacterial	112
HP- β-CD	-	1,8-cineole	Larvicidal	113
RAMEB	Lemon balm,	Borneol, citral, linalool,	Antimicrobial	114
	peppermint,	menthol and thymol	Antioxidant	
	lavender and			
	thyme			
β-CD	Lippia gracilis	-	Larvicidal	115
β-CD	Oregano	Carvacrol	Antiparasitic	116
HР-β-CD,	-	Thymol	Antioxidant	117
HP-γ-CD and				
M-β-CD				
β-CD	Tea tree	-	Antibacterial	118
			packaging	
β-CD	-	Allyl isothiocyanate	Antimicrobial	119
β-CD	Eucalyptus	-	Antimicrobial	120

				121
$\alpha$ -CD, $\beta$ -CD,	-	Nerolidol	-	121
γ-CD, HP-β-				
CD,				
RAMEB,				
CRYSMEB				
and SBE-β-				
CD				
β-CD	Lippia grata		Antioxidant	122
			Anti-hyperalgesic	
β-CD	Hyptis	-	Antibacterial	123
	martiusii			
HP- β-CD	-	Anethole	Larvicidal	124
НР-βСD,	-	Limonene	Gastroprotective	125
MβCD, and				
HРγCD				
НРВСО,	-	Vanillin	Antioxidant	126
HPγCD and				
MβCD				
β-СD	Xiangfu Siwu	-	Pharmaceutical	127
	decoction			
β-CD	-	2-nonanone	Fungistatic	128
β-CD	Cymbopogon	-	Pharmacological	129
	winterianus			
β-CD	-	Carvacrol	Pharmacological	130
			Cancer pain	
α-CD, β-CD,	Peppermint	Menthol, menthone,	Controlled release	131
γ-CD, HP-β-		pulegone and eucalyptol		
CD,				
RAMEB,				
CRYSMEB				
	Black pepper	-	Antibacterial	132

β-CD	Citronella oil	Citronellal or citronellol	Mosquito repellent	133
β-CD	Clove, mexican oregano	-	Antimicrobial	134
HP-β-CD	Guava leaf	-	Antioxidant, Antimicrobial	135
HP-β-CD	Cinnamon bark		Antimicrobial food packaging  Controlled release	136
HP-β-CD	Cinnamon bark	-	Antimicrobial	137
β-CD	Cinnamon bark	-	Antimicrobial packaging	138
β-СD	Cinnamon bark	1	Insect-resistance packaging	139
β-CD	Cinnamon bark	=	Controlled release	140
β-СD	Cinnamon bark	-	Antimicrobial packaging	141
β-CD	Cinnamon leaf	-	Antibacterial packaging	110
			Controlled release	
β-CD	Cinnamon leaf, garlic	-	Antimicrobial	111
β-CD	-	Thymol, trans-anethole and eugenol	Larvicidal	142

НР-β-СD,	-	Eugenol	Antioxidant	143
HP-γ-CD and				
M-β-CD				
HP-β-CD	Clove	Eugenol		144
β-CD	-	Carvacrol, trans-	Antimicrobial	70
		cinnamaldehyde and		
		eugenol		
β-CD	Cinnamon	Trans-cinnamaldehyde,	Antimicrobial	145
	bark, clove	eugenol		
	bud			

#### 1.6. Aim of the study

The aim of this study was to develop inclusion complexes of cinnamon leaf oil with  $\beta$ -cyclodextrin and for the first time, its sulfobutyl ether derivative by freeze drying method to improve cinnamon leaf oil physicochemical properties, stability, solubility, and thermal behavior. To reach this aim, the formation of complexes was characterized by several analysis includes SEM, FTIR, TGA, DSC and  $^{1}$ H-NMR spectroscopy. Then, for the first time, the antibacterial activity of inclusion complexes of cinnamon leaf oil/ $\beta$ -CD and cinnamon leaf oil/SBE- $\beta$ -CD were assessed against both gram negative (*E. coli*) and gram positive (*S. aureus*).

#### 2. Materials and Methods

#### 2.1. Materials

The cinnamon leaf oil was purchased from Tisserand Institute. Model bacteria, *S. aureus* (ATCC® 29213<sup>TM</sup>) and *E. coli* (ATCC® 25922<sup>TM</sup>), were gifted from Assoc. Prof. Dr. Meral Yuce from SUNUM (Sabanci University Nanotechnology Research and Application Center). β-cyclodextrin (≥97% purity, average M<sub>W</sub> = 1135 Da), DMSO-d6, LB broth and LB agar were obtained from Sigma-Aldrich; Betadex sulfobutyl ether sodium (average M<sub>W</sub> = 1451 Da) was obtained from USP company. Double distilled water and DPBS (w/o: Ca and Mg - PAN-Biotech) were used throughout the study. Other solvents and chemicals were analytical reagent grade.

#### 2.2. Methods

## 2.2.1. Phase Solubility Assay

Phase solubility studies were performed as mentioned by Higuchi and Connors to estimate the molar ratio and the apparent stability constants of the two inclusion complexes. Solubility studies were carried out by adding excess amounts of oil separately in quantities exceeding its aqueous solubility containing increasing concentrations of CDs. For this, solutions of  $\beta$ -CDs (0-10 mM in 2 ml water) were irradiated in a microwave oven at 700 W for 30 s at 10 s intervals to reach 70 °C. This process increases the aqueous solubility of  $\beta$ -CDs and facilitates complexation. An excess of essential CEO (17 mM) was added to each  $\beta$ -CD solutions, which were again irradiated for 30 s at 10 s intervals to reach 70 °C. For, SBE- $\beta$ -CD, different concentrations (0-10 mM) were dissolved in 2 ml of water. After SBE- $\beta$ -CD solution was vortexed for 2 min, an excess of essential CEO (17 mM) was added. The mixtures were sonicated in an ultrasonic bath for 10 min at room temperature.

All samples were rotated on a laboratory shaker at 250 rpm for 18 hr in darkness. After equilibrium was reached, the samples vortexed and filtered through a  $0.45 \,\mu m$  PTFE membrane. The amount of CEO was analyzed at 280 nm by UV-Vis Spectroscopy. For standard curve preparation, several concentrations (3–107 ug/mL) of cinnamon leaf oil were prepared in ddH<sub>2</sub>O and the absorbance of each concentration was measured at 280 nm. The absorbance at 280 nm was plotted against cinnamon leaf oil concentrations to establish a standard curve.

# 2.2.2. Preparation of the Cinnamon oil/ $\beta$ -CD and Cinnamon oil/SBE- $\beta$ -CD Inclusion Complexes

Encapsulation of cinnamon leaf essential oil was carried out through inclusion complex formation with  $\beta$ -Cyclodextrin and Sulfobutyl ether  $\beta$ -cyclodextrin sodium. The inclusion complexes were prepared at a molar ratio 1:1 according to method proposed by Torres-Alvarez et al. with some modifications <sup>146</sup>.

## Complex #1: CEO/β-CD-IC

For  $\beta$ -CD inclusion complex, 100 mg of  $\beta$ -CD were dissolved in 15 mL of ethanol and DI water (1:2 v/v). The solution was magnetically stirred at  $55 \pm 2^{\circ}$ C about 15 minutes, until the complete dissolution of  $\beta$ -CD. 27.2 mg of CEO was dissolved in ethanol (10% w/v) and then added dropwise to the warm  $\beta$ -CD solution using continuous stirring. After turning of heater, the mixture was left in a sealed container under stirring (250 rpm/21 h) at room temperature

(~25°C) and protected from the light. The resulting solution containing inclusion complex, uncomplexed cyclodextrin and un-complexed oil was frozen at -80°C. Then, it was lyophilized at -99°C for approximately 72 hr and the pressure was held at around 0.001 Pa. For purification, 50 ml DI water was added to freeze products for separating the oil. It was centrifugated at 4°C at 4500 rpm for 30 min. Centrifugation divided samples into two phases: (i) the supernatant phase, containing CEO/β-CD-IC, dissolved but un-complexed CD and probable residual oil (ii) precipitate: excess of un-complexed oil and un-dissolved β-CD. Supernatant was filtered with 0.45 μm PTFE filter to help complex for passing through filter. After freezing at -80°C, it was lyophilized at -99°C for approximately 72 hr and the pressure was held at around 0.001 Pa. The freeze-dried powders labelled as CEO/SBE-β-CD-IC were weighted and left in a refrigerator (-20°C) prior to analysis.

### Complex #2: CEO/SBE-β-CD-IC

For SBE-β-CD inclusion complex, 100 mg of SBE-β-CD were dissolved in 15 mL of ethanol and DI water (1:2 v/v). Because SBE-β-CD is freely soluble in the solution, it was magnetically stirred at RT about 5 minutes without heating. 21.2 mg of CEO was dissolved in ethanol (10%) w/v) and then added dropwise to SBE-β-CD solution using continuous stirring. The mixture was left in a sealed container under stirring (250 rpm/21 h) at room temperature (~25°C) and protected from the light. The resulting solution containing inclusion complex, un-complexed cyclodextrin, and un-complexed oil was frozen at -80°C. Then, it was lyophilized at -99°C for approximately 72 hr and the pressure was held at around 0.001 Pa. For purification, 50 ml DI water was added to freeze products for separating the oil. It was centrifugated at 4°C at 4500 rpm for 30 min. Centrifugation divided samples into two phases: (i) the supernatant phase, containing CEO/SBE-β-CD-IC, dissolved but un-complexed SBE-β-CD and probable residual oil (ii) precipitate: excess of un-complexed oil. Supernatant was filtered with 0.45 μm PTFE filter to help complex for passing through filter. After freezing at -80°C, it was lyophilized at -99°C for approximately 72 hr and the pressure was held at around 0.001 Pa. The freeze-dried powders labelled as CEO/SBE-β-CD-IC were weighted and left in a refrigerator (-20°C) prior to analysis. Preparation process of inclusion complexes was presented in **Figure 8**.

The yield of powders was calculated using the following equation:

Yield (%) = 
$$\frac{\text{Total weight of obtained inclusion complexes (mg)}}{\text{Initial CDs weight (mg)} + \text{initial CEO weight (mg)}} \times 100$$

## 2.2.3. Preparation of the Cinnamon oil/β-CD and Cinnamon oil/SBE-β-CD Physical Mixtures

The physical mixtures were prepared in the same molar ratio, 1:1. For this, cyclodextrins and cinnamon leaf oil were mixed and homogenized for 15 minutes using a mortar and pestle without freezing them  $^{147}$ . The physical mixtures were labelled as CEO/ $\beta$ -CD-PM and CEO/SBE- $\beta$ CD-PM, foiled and left in a refrigerator (-20°C).

## 2.2.4. Determination of Yield, Loading Efficiency and Encapsulation Efficiency

Total CEO content in the inclusion complexes was determined by solvent extraction method <sup>148,149</sup>. Briefly, inclusion complex (2 mg) was weighted into falcon tube and resuspended with 1 ml of DI water followed by addition and mixture with 9 ml hexane. They were vortexed at the highest speed for 1 minute. CEO was extracted from CD cavities with hexane by heating the samples in a glass tube at 45°C in a water bath in heater shaker with intermittent mixing during 2 hr. Since evaporation was observed above 45 °C, the maximum temperature was selected as 45 °C. After the heating period, the solution was kept cooling to room temperature and centrifuged at 4,000 rpm for 20 minutes to separate hexane from the aqueous phase. After centrifuging, it was resulted with a 2-phase solution and upper hexane layer containing the oil was collected by pasteur pipette. The amount of CEO present in the hexane was quantified by measuring absorbance with spectrophotometer at 281 nm using hexane as reference, in polystyrene cuvettes. The content of CEO was calculated by means of a standard curve for CEO in hexane ( $\geq 95\%$ ), at various concentrations (0.75–54ug/mL). The absorbance of each concentration was measured was plotted against cinnamon leaf oil concentrations to establish a standard curve. The concentration was calculated by using a calibration curve. The percentage of EE and LE were determined using the following equations:

$$EE (\%) = \frac{\text{weight of entrapped CEO (mg)}}{\text{initial CEO weight (mg)}} \times 100$$

LE (%) = 
$$\frac{\text{Weight of entrapped CEO (mg)}}{\text{Weight of obtained inclusion complexes (mg)}} \times 100$$

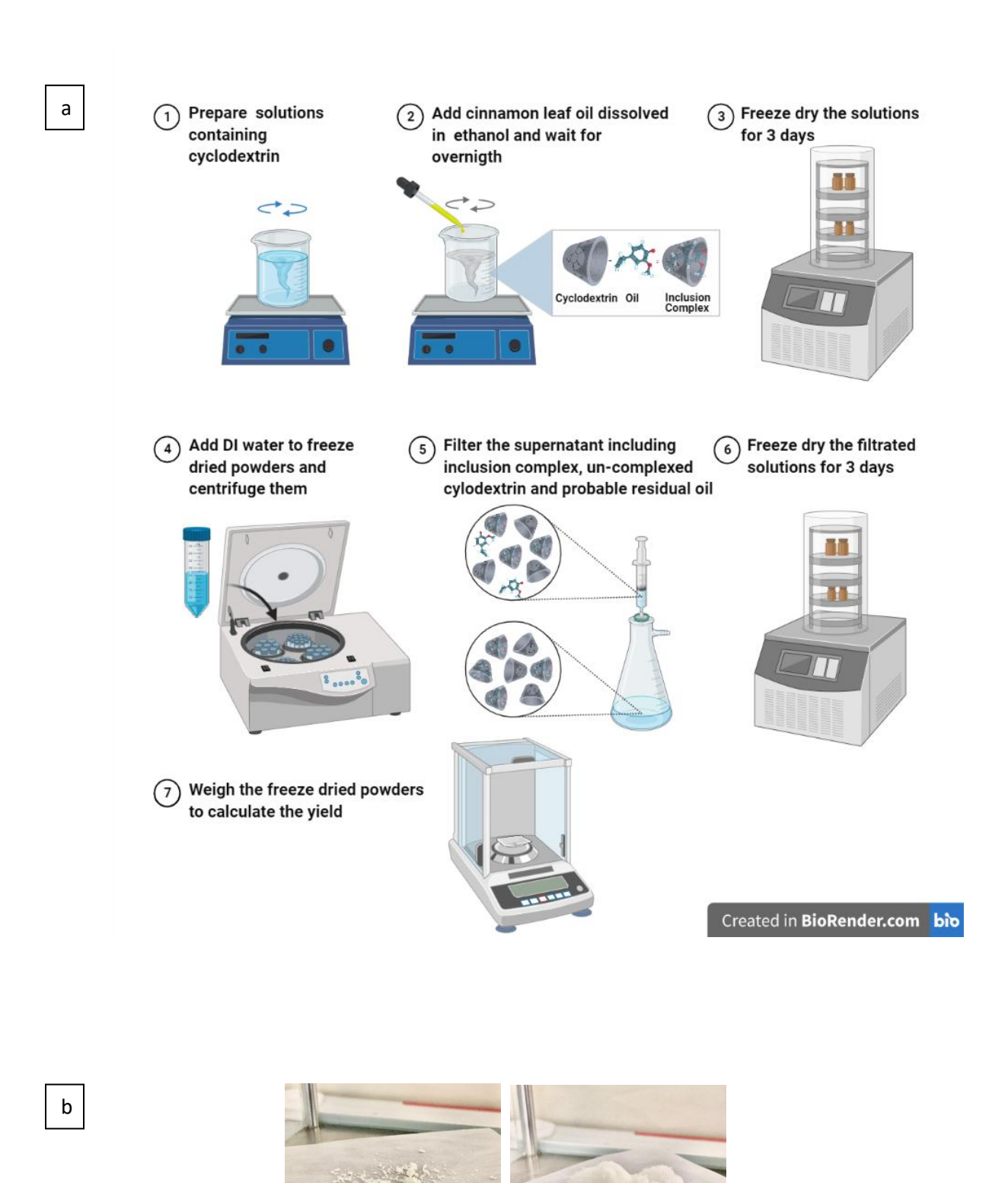


**Figure 8.** Preparation process of inclusion complexes in 1:1 M ratio (a) and appearance of the complexes (b).

CEO/SBE-β-CD IC

CEO/β-CD IC

#### 2.2.5. Inclusion complexes characterization

The complexes of cinnamon oil were formed with two different cyclodextrin,  $\beta$ CD and SBE- $\beta$ CD. Pure cyclodextrins, cinnamon oil, freeze dried formulation and physical mixtures were analyzed by SEM, DLS, ATR-FTIR, TGA, DSC and  $^{1}$ H-NMR Spectroscopy to determine if inclusion complexes were formed.

#### 2.2.5.1. Scanning Electron Microscopy

The particle morphology of the samples was evaluated by JIB 4601F FIB-SEM MultiBeam system using a (3-5 kV) acceleration voltage and a magnification ranging 4000-10.000 X. The samples were coated in vacuum with a thin layer of gold/palladium for improving surface conductivity.

#### 2.2.5.2. Dynamic Light Scattering

The mean particle size (Z-Average), size distribution (PDI) and zeta-potential determinations were performed by DLS method, using the Malvern Zetasizer. Samples (1 mg) were sonicated for 10 minutes following dispersed in DPBS (3 ml). The same procedure was applied in Hepes buffer in folded capillary cell DTS1070 for zeta potential measurement. All the measurements were carried out at  $25 \pm 1$  °C

#### 2.2.5.3. Fourier Transform Infrared Spectroscopy

To confirm the functionalization of host-guest inclusion complexes, samples were obtained on a Bruker Equinox 55 IR Spectrometer equipped with an attenuated total reflectance (ATR) crystal. Samples were scanned 64 times over a range of 4000–600 cm<sup>-1</sup> with a resolution of 4 cm<sup>-1</sup>.

## 2.2.5.4. Thermogravimetric Analysis

Thermal properties of  $\beta$ -CD, SBE- $\beta$ -CD, CEO, inclusion complexes and physical mixtures were analyzed using thermogravimetric analyzer (TGA, Shimadzu DTG-60H) using approximately 2 mg of the sample in aluminum crucibles The experiment was performed at a heating rate of 5 °C/min in a dynamic high purity nitrogen flow of 100 ml/min. The temperature of the furnace was programmed to rise from 25 to 500 °C.

## 2.2.5.5. Differential Scanning Calorimetry

Samples each of DSC curves for  $\beta$ -CD, SBE- $\beta$ -CD, CEO, inclusion complexes and physical mixtures in the weight range of 2-3 mg, were scanned at a rate of  $10^{\circ}$ C/min on a DSC Q2000 between  $25^{\circ}$ C and  $300^{\circ}$ C under an inert atmosphere of nitrogen (50 ml/min). Results were characterized by a clear overlap of individual thermograms.

## 2.2.5.6. <sup>1</sup>H-NMR Spectroscopy

The  $^1$ H-NMR analysis of  $\beta$ CD, CEO, CEO/ $\beta$ CD-IC, SBE- $\beta$ CD and CEO/SBE- $\beta$ CD-IC were performed at 500 MHz. For this, 5 mg of samples were dissolved in 600 ul of deuterated DMSO- $d_6$  and sonicated for 2 minutes. In this study, samples were prepared using DMSO- $d_6$  to obtain the appropriate solubility due to the very low solubility of oil in water. MestRenova Program was used to analyze data.

## 2.2.6. Antibacterial activity of essential oil

## 2.2.6.1. Microorganism

Strains of gram-negative bacteria *E. coli* and gram-positive bacteria *S. aureus* were used as microorganism. The bacteria were cultured overnight in 5 mL of LB medium at 37 °C for 18 hr.

## 2.2.6.2. Media Preparation

LB broth: 20 grams of LB broth was dissolved in 1 L of distillated water. It was autoclaved at 121°C for 15 min and stored at RT.

LB agar: 20 grams of LB broth and 15 grams of agar were dissolved in 1 L of distillated water. It was autoclaved at  $121^{\circ}C$  for 15 min. LB agar poured to plates and stored at  $4^{\circ}C$ .

#### 2.2.6.3. Agar disk diffusion test

For quantitative method, agar disk diffusion test was used with checking the diameter of inhibition zone to determine the cinnamon leaf oil activity against E. coli and S. aureus (**Figure 9**). For comparison, clove oil, coriander oil and St. John's wort oil was tested. For this process, 200 ul of bacterial suspensions ( $OD_{600}$ : 0.1) were spreaded on sterile LB agar media and 6 mm sterile diameter disk were put on the agar surface. 10 ul of pure essential oils were added to each disk. Ampicillin (15 mg/ml) antibiotic solution was used as a positive control to assess the susceptibility of tested strains. These plates were sealed with parafilm and incubated overnight

at 37 °C. After the incubation period, the inhibition zone diameter (IZD) where bacteria did not grow was measured in mm using a ruler for each disc. The images of plates were taken with Bio-Rad Gel Imaging.

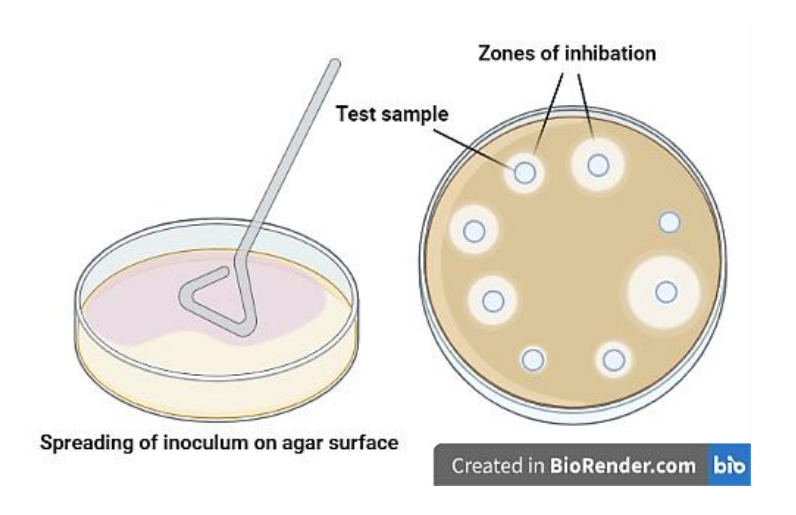
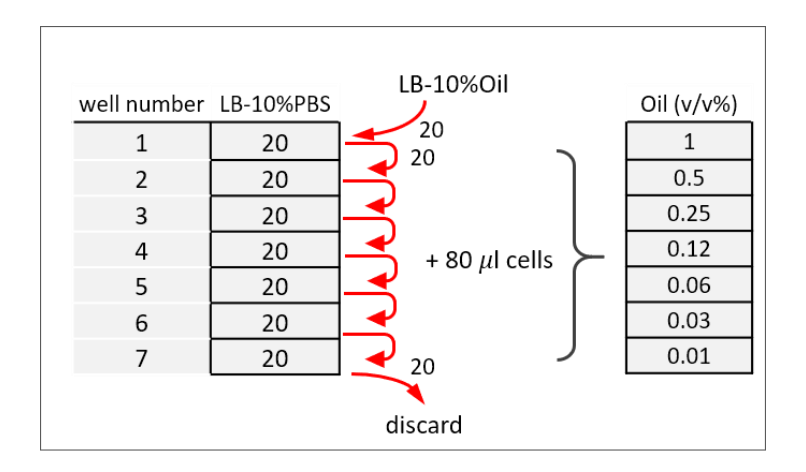


Figure 9. Agar disk diffusion test for evaluation of antibacterial activity

## 2.2.6.4. MIC determination by serial dilution dose-response experiment

For quantitative method, the study was performed according to the method by 'Miniaturized Checkboard Assays to Measure Antibiotic Interaction' with using spectrophotometric measurements <sup>150</sup>.

MIC of cinnamon leaf oil against *Escherichia coli* (gram negative) and *Staphylococcus aureus* (gram positive) bacteria were determined in LB growth media by using a cell growth assay in 96- well culture plates. Cinnamon leaf oil was directly used in the original solution (100%, v/v). The oil was subjected to serial dilution to reach an effective concentration. For this, oil was two-fold serially diluted and then spiked with 80 ul inoculum (OD<sub>600</sub>:0.1) of *E. coli* and *S. aureus* (**Figure 10**). An automated plate reader (Tecan) was used to quantitatively measure the turbidity in all wells. This microplate reader keeps the temperature at 37°C and provides air flow by shaking the plates in every 15 minutes <sup>151</sup>. The plate was sealed and incubated at 37 °C for 18 hours. The concentration at which there is no increase in turbidity (no cell growth) was identified as the MIC for that drug. The MIC determined by this method corresponds to the concentration at which the essential oil is bacteriostatic (prevent cell proliferation).



**Figure 10.** Serial dilution dose-response experiment. Preparation of serial dilution dose-response for oil and corresponding final concentrations of the oil <sup>150</sup>

## 2.2.7. Antibacterial activity of inclusion complexes

The antibacterial activities of CEO/β-CD-IC and CEO/SBE-β-CD-IC against *E. coli* and *S. aureus* bacteria were measured according to method proposed by Cui et al. with some modifications <sup>112</sup>. For this, the bacterial strains were grown in LB broth medium for 18 h on a 200-rpm shaker at 37 °C. 10 ul of adjusted cultures (OD<sub>600</sub>=0.1) of bacterium were added separately in tubes containing 1 mL of PBS. UV irradiation was applied on inclusion complexes for 10 minutes. UV-sterilized inclusion complexes (15 and 30 mg) were added to the culture and incubated at 37 °C for 24 h. 0.1 ml of the above culture containing PBS, bacteria and inclusion complexes was spread on a LB agar plate. It was incubated again at 37 °C for 24 hr. Same amount of essential oil that was in CDs was used as a positive control and CDs alone were used as a negative control. The images of plates were taken with Bio-Rad Gel Imaging System. The colonies are counted and the percentage of antibacterial activity of inclusion complexes were measured determined using the equation <sup>152</sup>:

% Antibacterial activity = (population number of control bacteria - population number of experimental bacteria) / population number of control bacteria x100

#### 3. Results and Discussion

#### 3.1. Phase Solubility Assay

The UV-Vis spectrum of cinnamon leaf displays absorption bands at 270-290 nm which regards the electronic shift of  $n-\pi$  type for C-O group that binds with eugenol aromatic ring <sup>153</sup>. Considering the information, spectroscopic analysis used to observe the key band of cinnamon

leaf oil. A wavelength of 280-282 nm was adopted as the reference wavelength for eugenol, and the intensity of this characteristic peak was used to determine the CEO concentrations in the complexes <sup>154</sup>.

The concentration of the CEO was measured spectrophotometrically by using the UV-VIS spectrometer. For standard curve preparation, several concentrations (13–215 ug/mL) of cinnamon leaf oil were prepared in ddH<sub>2</sub>O and the absorbance of each concentration was measured at 280 nm. The absorbance at 280 nm was plotted against cinnamon leaf oil concentrations to establish a standard curve (**Figure 11**).

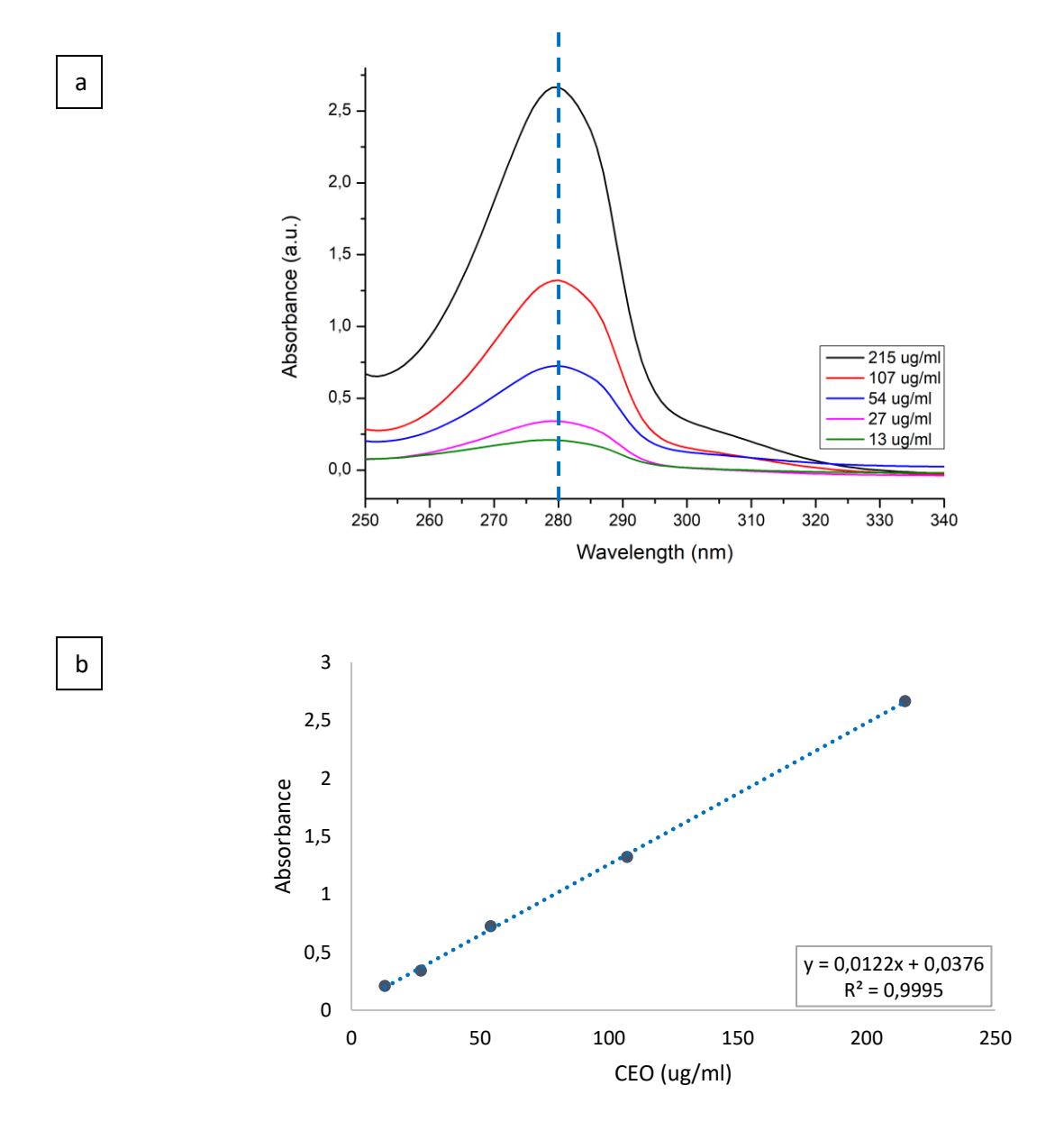


**Figure 11.** UV-Vis absorption spectra of increasing concentrations of cinnamon leaf oil diluted in ddH<sub>2</sub>O (a) and calibration curve of pure cinnamon leaf essential oil in ddH<sub>2</sub>O at 280 nm (b).

Phase solubility diagram of CEO/SBE- $\beta$ -CD-IC and CEO/ $\beta$ -CD-IC could be classified as  $A_L$  type, as the solubility of the CEO almost linearly increased with increasing concentration of CD (0 M-10 mM) (**Figure 12**). The increase in solubility in the system is due to molecular interactions between CEO and  $\beta$ -CDs to form complex. Because the straight line had a slope less than unity, it was assumed that increase in solubility was observed due to formation of 1:1 complex.

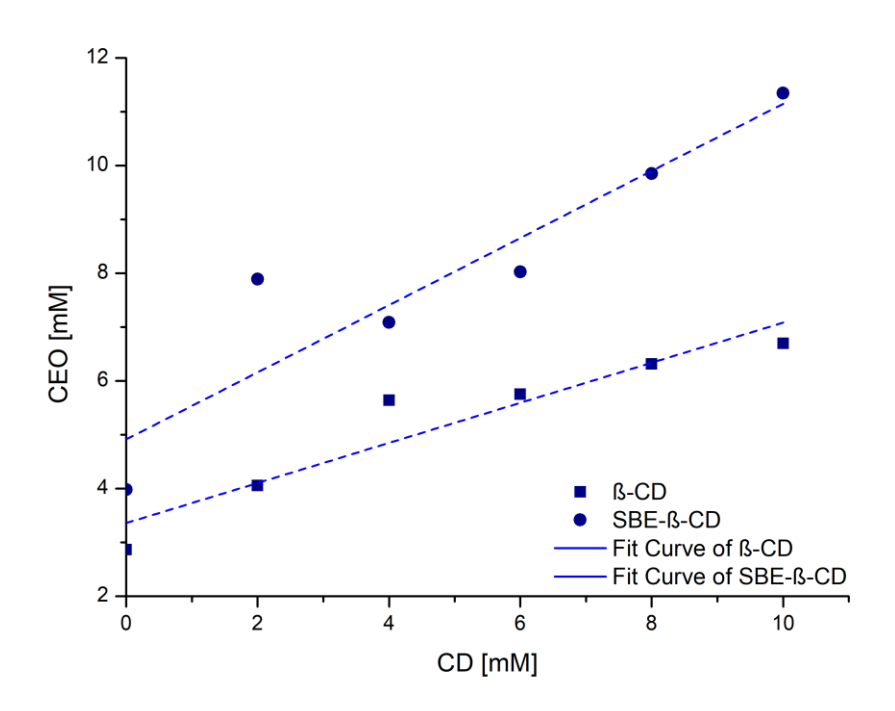


**Figure 12.** The solubility phase diagrams for the CEO/β-CD-IC and CEO/SBE-β-CD-IC

The stability constants ( $K_{1:1}$ ) of CEO with each CD were calculated using Equation ( $K_{1:1}$  = Slope/Intercept (1 - Slope)) and given in **Table 4**. The  $K_{1:1}$  value was 176.5 M<sup>-1</sup> for  $\beta$ CD. The value falling within the range of 50- 2000 M <sup>-1</sup> <sup>155</sup>, is to be adequate for the formation of inclusion complex, which may contribute to improve dissolution of poorly water soluble drugs. However, the  $K_{1:1}$  value for CEO/SBE- $\beta$ -CD-IC complex was found to be 337.08 M<sup>-1</sup> which is 1.9-fold higher than  $\beta$ CD. SBE- $\beta$ -CD showed superior solubilizing and complexing ability. The different complexation constants found for different CD molecules indicated that the derivative group on CDs appear to play an important role in the incorporation of CEO into CD cavity since much higher complexation constants were obtained with SBE- $\beta$ CD <sup>156</sup>.

**Table 4.** The phase solubility diagram parameters of the inclusion complex formed between CEO-SBE-β-CD and CEO-β-CD

Molar		Molar			Stability	
concentration	Absorbance,	concentration	Slope	Intercept	constant,	Phase
SBE-β-CD,	A	of CEO,			$K_{1:1}[M^{-1}]$	diagram
[mM]		M=A/e, [mM]				
0	0,526982	3,9828				
2	1,007253	7,8916				
4	0,908728	7,0897	0,62357	4,91433	337,08	A <sub>L</sub> type
6	1,024079	8,0285	-			
8	1,247967	9,8506	-			
10	1,432151	11,3496	-			
		Molar				
Molar	Absorbance,	concentration	Slope	Intercept	Stability	Phase
concentration	A	of CEO,			constant,	diagram
β-CD, [mM]		M=A/e, [mM]			$K_{1:1}[M^{-1}]$	
0	0,389824	2,8666				
2	0,535903	4,0554	-			
4	0,730515	5,6393	0,37235	3,36051	176,5	A <sub>L</sub> type
6	0,744905	5,7564	1			
8	0,813619	6,3157	1			
10	0,860829	6,6999	1			

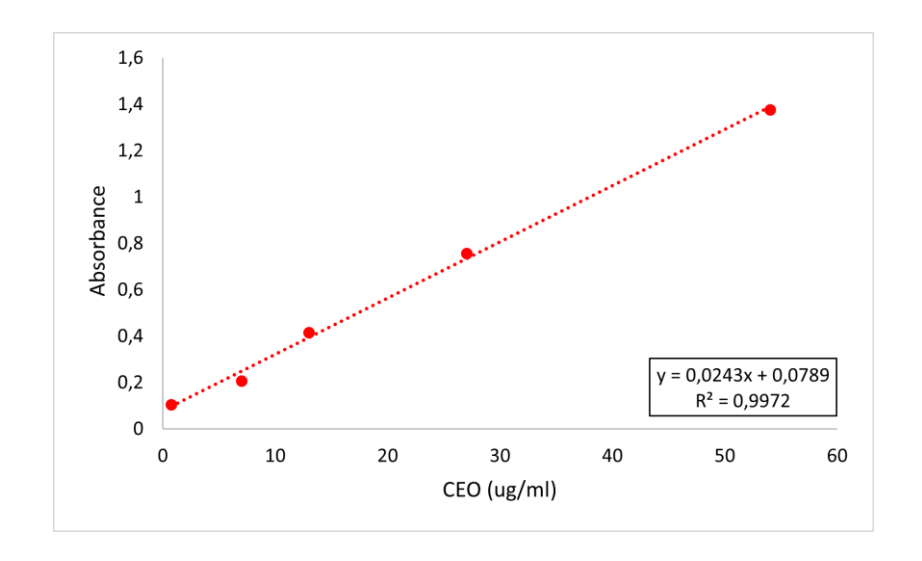
## 3.2. Determination of Yield, Loading Efficiency and Encapsulation Efficiency

Determination of the encapsulation efficiency (EE) of the CEO/ $\beta$ -CD-IC and CEO/SBE- $\beta$ -CD-IC is of great importance, as it provides a direct estimation concerning the effectiveness of the CEO encapsulation, as well as evidence concerning the available CEO quantity in the ICs, which along with its release profile directly affect the way that the ICs are going to be used in several applications. The % encapsulation efficiency, loading efficiency and yield of CEO in the CEO/ $\beta$ -CD-IC and CEO/SBE- $\beta$ -CD-IC were determined directly, using UV-Vis Spectroscopy, by quantification of the encapsulated CEO. The CEO of encapsulated in the

cyclodextrins was measured using the solvent extraction method modified from the reported literatures <sup>157</sup> <sup>158</sup> <sup>149</sup>.

Although same molar ratio of cyclodextrin were used to encapsulate essential oil, different percentage of yield, loading efficiency and encapsulation efficiency was observed (Figure 13). The included oil content in the powder is the highest value when SBE-β-CD is used as an encapsulant. It is probably related with chemical structure ( $R = H \beta$ -CD and R = (CH<sub>2</sub>)<sub>4</sub>SO<sub>3</sub>SBE-β-CD) <sup>159</sup>. Encapsulation efficiency and loading efficiency after freeze-drying were 18 % and 11 % for CEO/β-CD-IC and 23 % and 5 % for CEO/SBE-β-CD-IC. It has also showed high yield with CEO/SBE-β-CD-IC (77%) when compare with CEO/β-CD-IC (35 %). However, results were significantly lower than the ones reported in the literature for the main cinnamon EO component, eugenol <sup>160</sup>. This was expected as the EOs constitute complex mixtures of different compounds that present high affinities for CD molecules, competing against each other for IC formation with the  $\beta$ -CD <sup>135</sup>. Similar observation has been reported for other authors in the literature showing that obtained encapsulation efficiency for the formed β-CD-oregano EO ICs was 22.60 %. Rakmai et al. also found that guava leaf oil encapsulation efficiency was 52.5%, while it reached 91.8% for limonene, the major pure compound of guava leaf oil <sup>135</sup>. In the case of yarrow oil and carvacrol (yarrow oil major component), there efficiency was 45.05 and 86.59%, respectively <sup>161</sup>. Black pepper exhibit similar behavior with efficiency of 50.55 and 85.30, respectively, for essential oil and its main component (β-caryophyllene) <sup>132</sup>. Nevertheless, the obtained inclusion efficiencies were reproducible and, interestingly, much higher than the range of the theoretical maximum loading for  $\beta$ -CD with other EOs (8%–12%)  $^{162}$ , suggesting an efficient encapsulation of the cinnamon leaf EO in β-CD.





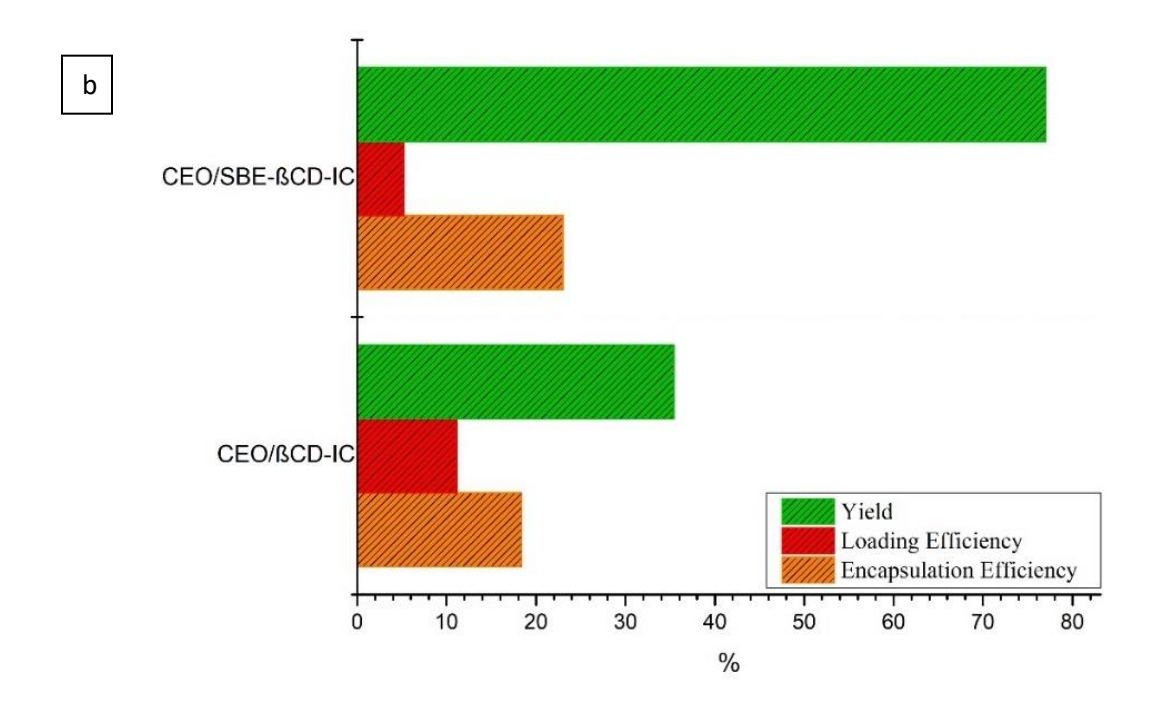


**Figure 13.** (a) Calibration curve of pure cinnamon leaf essential oil in hexane at 281 nm and (b) Yield, loading efficiency and encapsulation efficiency of cinnamon leaf oil included in SBE- $\beta$ -CD and  $\beta$ -CD after freeze-drying.

#### 3.3. Scanning Electron Microscopy Analysis

SEM images of  $\beta$ CD, CEO/ $\beta$ -CD-PM and CEO/ $\beta$ -CD-IC are reported in **Figure 14**.  $\beta$ CD is defined by blocky particles with different sizes of rectangular-shaped crystals <sup>163</sup> (**Figure 14a-b**). In case of the physical mixture, it can easily be seen that the CEO adheres onto the surface the  $\beta$ CD (**Figure 14c-d**). In contrast to physical mixture, organized blocky particle with rhomboid shaped crystals were observed in freeze-dried CEO/ $\beta$ -CD-IC (**Figure 14e-f**). No visible fractures, cracks or pores were shown on the complex form. These results are supported by several studies performed on inclusion complex between  $\beta$ CD and other guest molecules <sup>164</sup>

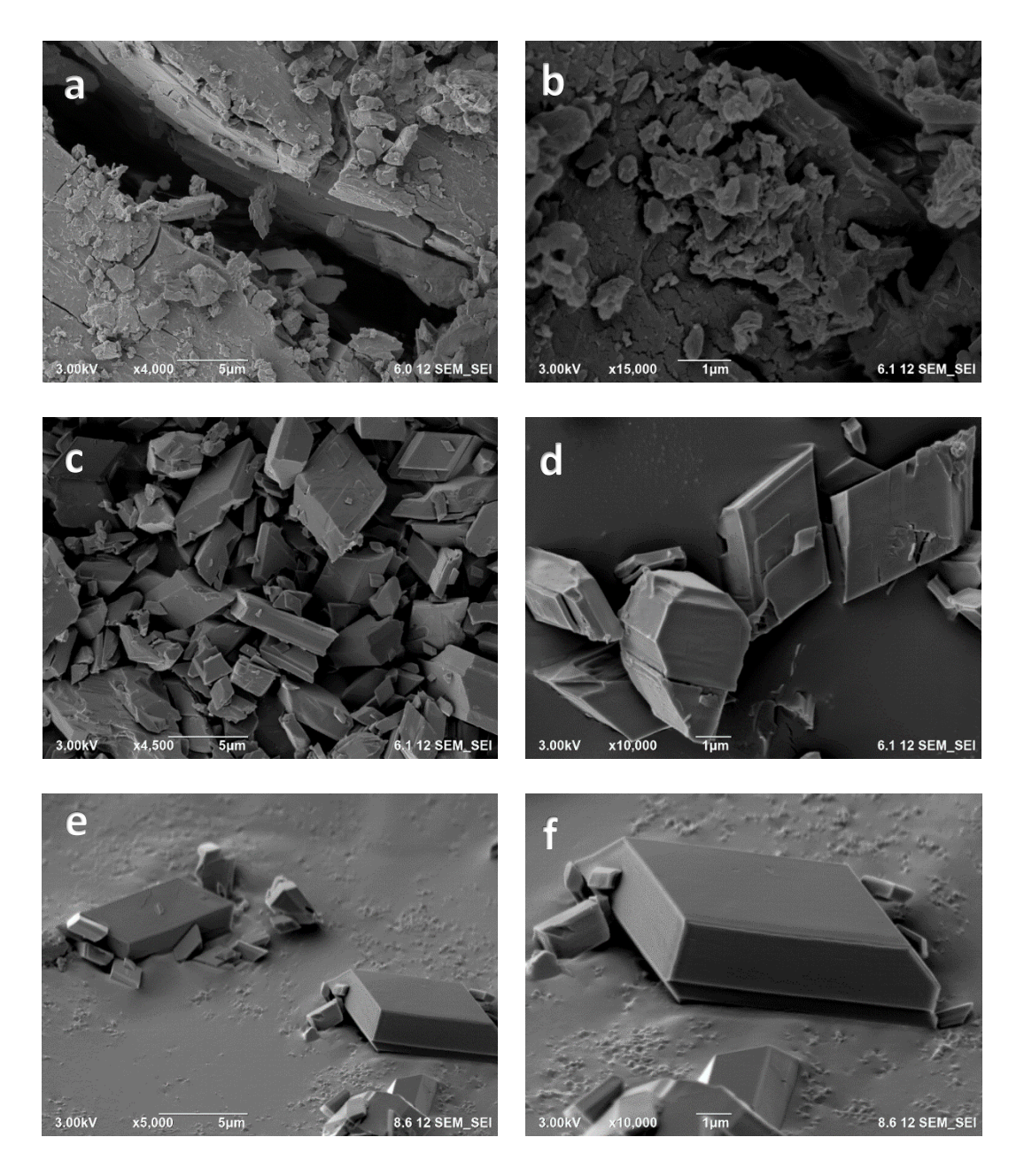


**Figure 14.** SEM images of β-CD (a-b), CEO/β-CD-PM (c-d) and CEO/β-CD-IC (e-f).

SEM images of SBE-β-CD, CEO/SBE-β-CD-PM and CEO/SBE-β-CD-IC are reported in **Figure 15**. SBE-βCD is represented by amorphous shrink spherical particles  $^{165}$  (**Figure 15a-b**). Both individual CEO and SBE-β-CD could be distinguished in CEO/SBE-β-CD-PM (**Figure 15c-d**). CEO adhered on the surface of SBE-βCD particles in the physical mixture. On the other hand, characteristic CEO and SBE-β-CD morphologies couldn't be identified in freeze-dried CEO/SBE-β-CD-IC. SBE-β-CD had lost their original shapes and aggregated with each other. The drastic change occurred because of possible interaction between CEO and SBE-β-CD (**Figure 15e-f**). Results of CEO/β-CD-IC and CEO/SBE-β-CD-IC proved that the cinnamon oil is encapsulated into both β-CD and SBE-β-CD.

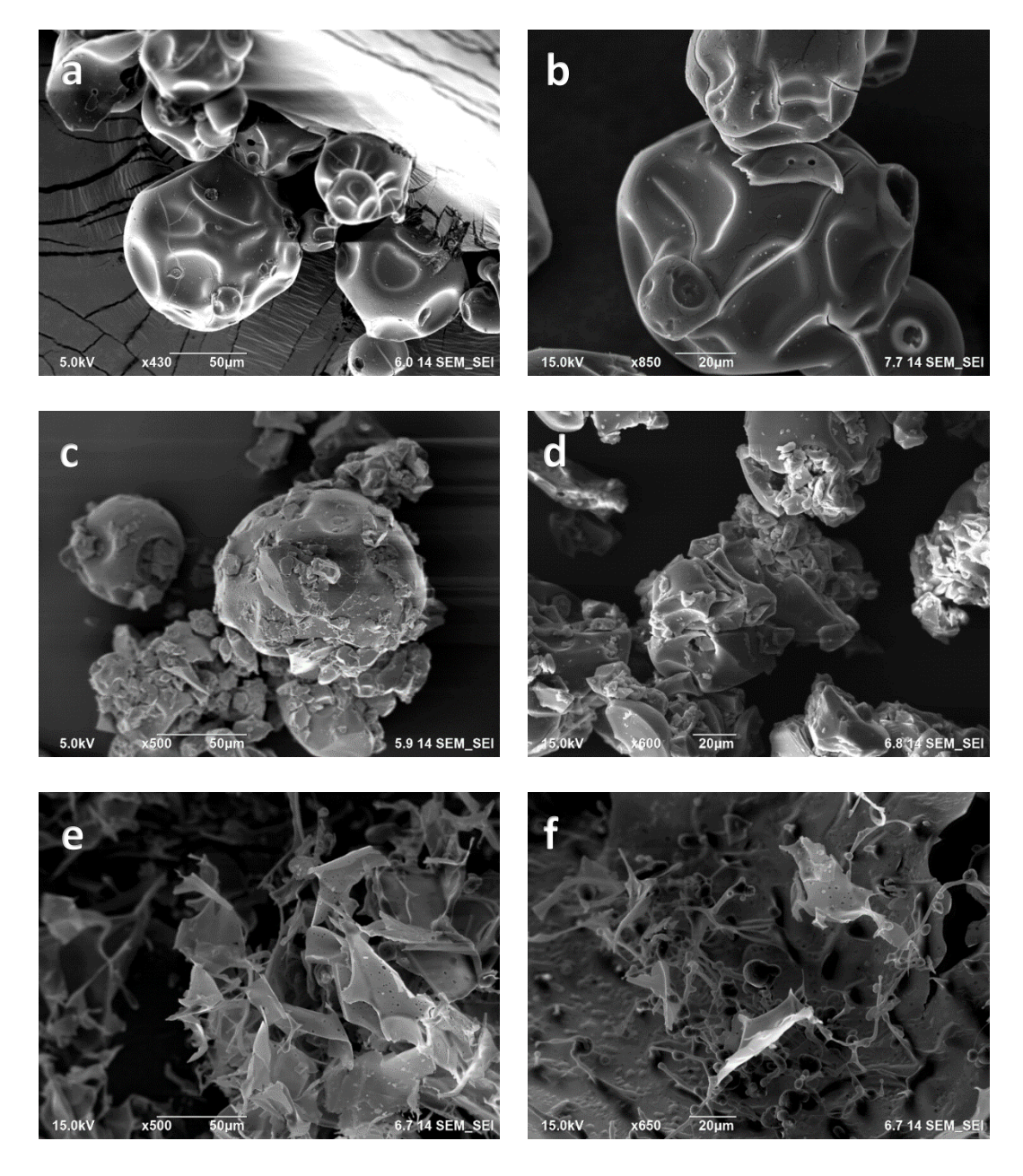


**Figure 15.** SEM images of SBE- $\beta$ -CD (a-b), CEO/SBE- $\beta$ -CD-PM (c-d) and CEO/SBE- $\beta$ -CD-IC (e-f).

## 3.4. Dynamic Light Scattering

Particle size of drug delivery systems is very important. According to particle size, drug delivery systems accumulate in different tissues and organs  $^{166}$ . The particle size of a good drug delivery system should be large enough not to leak through the blood vessel and small enough not to be noticed by the mononuclear phagocytic system  $^{167}$ . Particle size and distribution are important in the characterization of formulations as they affect drug loading, drug release and stability. The particle sizes of the prepared CEO/ $\beta$ -CD-IC and CEO/SBE- $\beta$ -CD-IC were determined by dynamic light scattering technique using the dispersions in pH 7.4 phosphate

buffer. In the study, the mean particle size (Z-Ave) was measured as 885.8 nm for CEO/β-CD-IC and 345 nm for CEO/SBE-β-CD-IC. Considering the results, it is understood that these inclusion complexes are at nano level. Accordingly, particle diameter size obtained in our study showed results consistent with the literature. Hill et al. encapsulated eugenol with βCD in their study and found the particle size 860 nm <sup>145</sup>. Also, they have worked with clove bud extracts which has same major component, eugenol, and found the particle size 1398 nm. Inclusion complexes in our study also displayed a monodispersed suspension and homogenous particle sizes, with a low PDI value. Polydispersity indices (PDI) of CEO/β-CD-IC and CEO/SBE-β-CD-IC was measured as 0.314 and 0.836, respectively. This moderate homogeneity of the IC population was also being perceived through their size distribution graph (Figure 16a-b). Zeta potential is an extremely important concept for the stability of nanoparticle suspensions due to electrostatic repulsion between charged particles. It also gives an idea of whether the active substance is encapsulated inside or on the surface of the nanoparticle. Studies in the literature have shown that nanoparticles with a zeta potential in the range of  $\pm$  30 mV are stable in suspension <sup>167</sup>. When the zeta potential value decreases, the loaded nanoparticle suspension cannot maintain its stable state. As a result of the zeta potential analysis, the zeta potential values of inclusion complexes were determined to be close to -30 mV. It was found -19.7 mV for CEO/β-CD-IC and -18 mV for CEO/SBE-β-CD-IC which means that these complexes are quite stable. Accordingly, it was determined that the preparation method was effective on the zeta potential of nanoparticles. These negative zeta potential causes prevents agglomeration of nanoparticles, stabilizes the suspensions of nanoparticles and causes an increase in dispersion in water <sup>168</sup>.

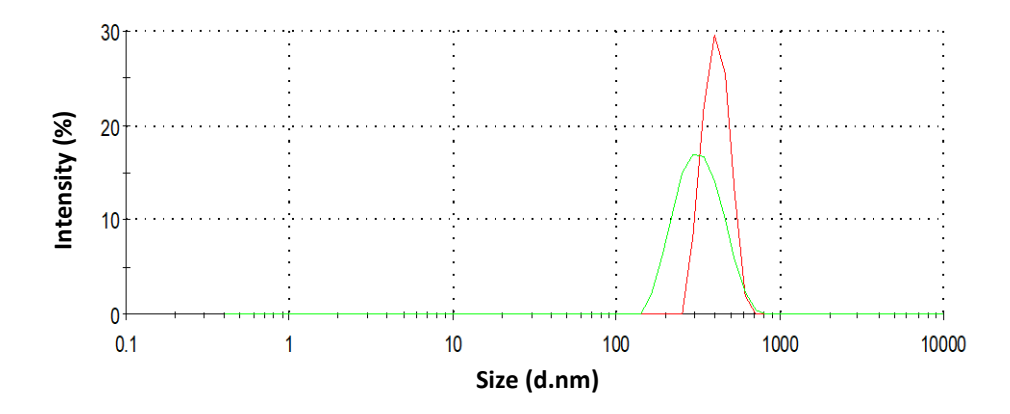


**Figure 16.** Particle size distribution of (a) CEO/ $\beta$ CD-IC (red line) and (b) CEO/SBE- $\beta$ CD-IC (green line).

## 3.5. Fourier Transform Infrared Spectroscopy

Complex formation was confirmed by the absence of characteristic peaks of cinnamon leaf oil in the inclusion complexes in the analysis of FT-IR spectra, and the appearance of original peaks that were not previously seen in both pure cyclodextrins and cinnamon leaf oil <sup>169</sup>. Infrared characteristic peaks of CEO and inclusion complexes were determined by using **Table** 5. The infrared characterization curves of the samples are illustrated in **Figure 17** and **Figure 18**.

**Table 5.** Regions of the Infrared Spectrum <sup>170</sup>.

Region (cm <sup>-1</sup> )	Group	<b>Possible Compounds</b>	
3700-3100	-OH	Alcohol, aldehyde, carboxylic acids	
	-NH	Amides, amines	
	≡С-Н	Alkynes	
3100-3000	=С-Н	Aromatic compounds	
	-CH2 or -CH=CH-	Alkenes or unsaturated rings	
3000-2800	СН, -СН2-, -СН3	Aliphatic groups	
2800-2600	-СНО	Aldehydes	
2700-2400	-РОН	Phosphorus compounds	
	-SH	Mercaptans and thiols Phosphine	
	-PH		
2400-2000	-C≡N	Nitriles	
	-N=N+=N-	Azides	
	-C≡C-	Alkynes	
1870-1650	C=O	Acid halides, aldehydes, amides,	
		amino acids, anhydrides, carboxylic	
		acids, esters, ketones, lactams,	
		lactones, quinines	
1650-1550	C=C, C=N, NH	Unsaturated aliphatics, aromatics,	
		unsaturated heterocycles, amides,	
		amines, amino acids	
1550-1300	NO2 Nitro compound		
	CH3 and CH2	Alkanes, alkenes, etc	

1300-1000	C-O-C and C-OH	Ethers, alcohols, sugars	
	S=O, P=O, C-F	Sulphur, phosphorus, and fluorine	
		compounds	
1100-800	Si-O and P-O	Organosilicon and phosphorus	
		compounds	
1000-650	=C-H	Alkenes and aromatic compounds	
	-NH	Aliphatic amines	
800-400	C-halogen	Halogen compounds	
	Aromatic rings	Aromatic compounds	

The ATR-FTIR spectrum of pure CEO exhibited characteristic peaks at 1637 cm<sup>-1</sup> and 1674 cm<sup>-1</sup> assigned to the CC stretching vibration. The stretching vibration of the C–O groups and C–O–C ring are respectively evident at 1264 cm<sup>-1</sup> and 1231 cm<sup>-1</sup>. CEO had C=O stretching vibrations at 1674 cm<sup>-1</sup> and 1719 cm<sup>-1</sup>. The ATR-FTIR spectra of β-CD show characteristic peaks at 3268 and 2924 cm<sup>-1</sup> caused by the O-H and C-H stretching of vibration. Besides that, peaks at 1204, 1151 and 1076 cm<sup>-1</sup> indicate the presence of C-O-C stretching glucose units of β-CD. The infrared characteristic peaks of cinnamon oil (1637 cm<sup>-1</sup>) and β-CD (1076 cm<sup>-1</sup>) can be found in the curve, indicating that physical mixture is just a simple mixture of β-CD and CEO.

In the case of inclusion complex between  $\beta$ -CD and CEO, all the sharp peaks belonging to the  $\beta$ -CD exist and only a few characteristics of CEO peaks are visible. The spectrum of the inclusion complex looks almost like the pure  $\beta$ CD indicating a formation of an inclusion complex. The shifts to all  $\beta$ -CD related peaks were shifted to a higher or lower wavelength such as at 1076 to 1077 cm<sup>-1</sup>, 1204 to 1205 cm<sup>-1</sup>, 2924 to 2922 cm<sup>-1</sup> and 3268 to 3272 cm<sup>-1</sup>. Cinnamon oil in inclusion complex had the intensity of the peak at 1604 and 1637 cm<sup>-1</sup> for C=C stretching vibration, indicating that these part of the carbon–carbon double bond are likely to be inserted into the cone-shaped cavity of  $\beta$ -CD. The broader OH stretching band of the inclusion complex in the frequency 3272 cm<sup>-1</sup> again corresponds to the multiple OH functional groups of  $\beta$ -CD molecules. These data confirm the presence of CEO and  $\beta$ -CD in the CEO/ $\beta$ -CD inclusion complex and suggest that CEO was efficiently encapsulated into the hydrophobic cavity of  $\beta$ -CD.

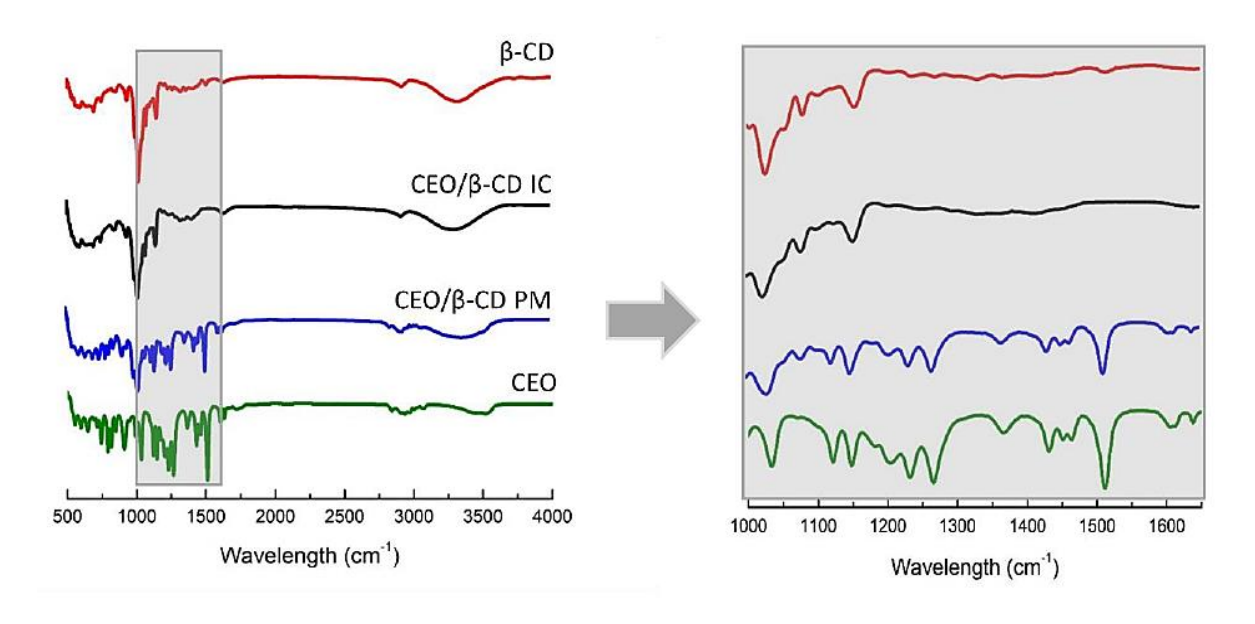


**Figure 17.** FTIR spectrum for  $\beta$ -CD, CEO, CEO/ $\beta$ -CD-PM and CEO/ $\beta$ -CD-IC

The ATR-FTIR spectra of SBE- $\beta$ -CD show characteristic intense bands at 3700-3100 cm<sup>-1</sup> caused by the O-H stretching vibration <sup>171</sup>. The band at 3000–2800 cm<sup>-1</sup> associated to the vibration of the CH groups. In this experiment, for pure SBE- $\beta$ CD, there was a C–H stretching vibration peak at 2934 cm<sup>-1</sup>. A prominent band with a transmittance peak at ~1648 cm<sup>-1</sup> owing to H-O-H bending of water molecules attached to CD <sup>171</sup>. The band at 1161 cm<sup>-1</sup> and 1044 cm<sup>-1</sup> respectively ascribed to C–O–C stretching vibration and sulfoxide stretch <sup>172</sup>. The one at 1155 cm<sup>-1</sup> vibration and a sharp band at 1029 cm<sup>-1</sup> in pure SBE- $\beta$ -CD indicated C–O–C and sulfoxide stretch, respectively.

Superposition of oil and cyclodextrin infrared peaks found in physical mixture. The spectrum of the physical mixture was characterized by the intense band at 1638 cm<sup>-1</sup> (H–O–H). The band at 1228 cm<sup>-1</sup>, 1265 cm<sup>-1</sup> and 1030 cm<sup>-1</sup> also were associated to CEO and SBE-β-CD. In the case of inclusion complex between SBE-β-CD and CEO, all the sharp peaks belonging to the SBE-β-CD exist and only a few characteristics of CEO peaks are visible. IR spectra of CEO in inclusion complex were shifted, broadened, or disappeared because of the possible activation of some "host–guest" interaction. The band at 1228 cm<sup>-1</sup> and 1232 cm<sup>-1</sup> were not observed in inclusion complex.

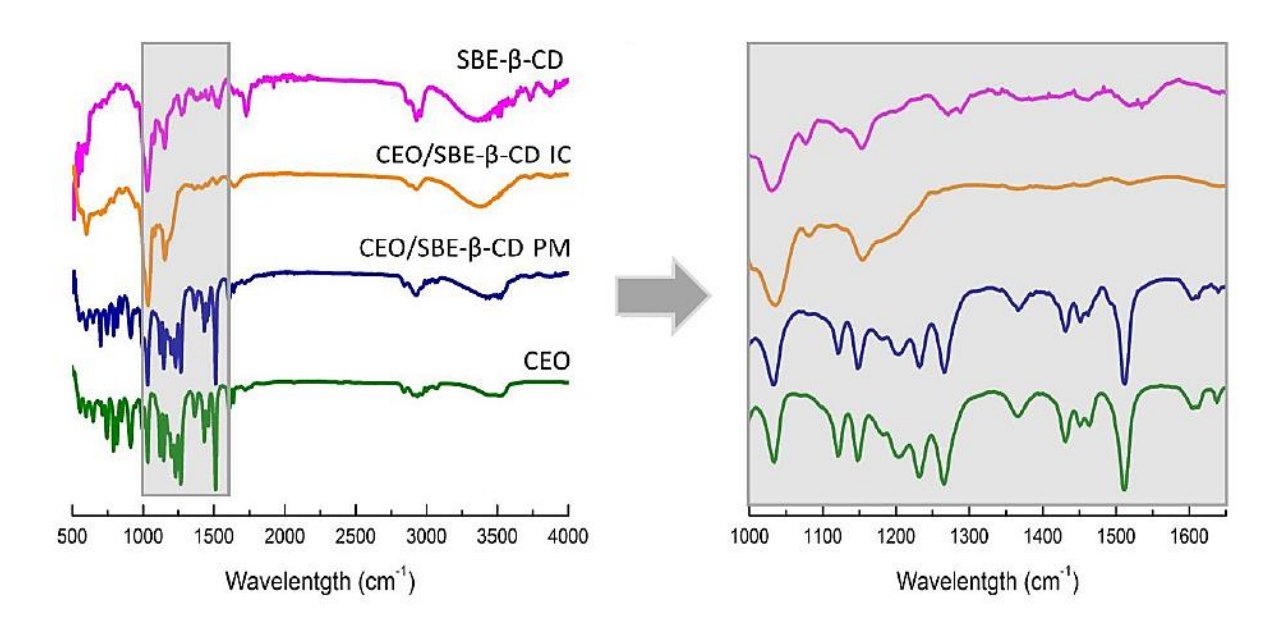


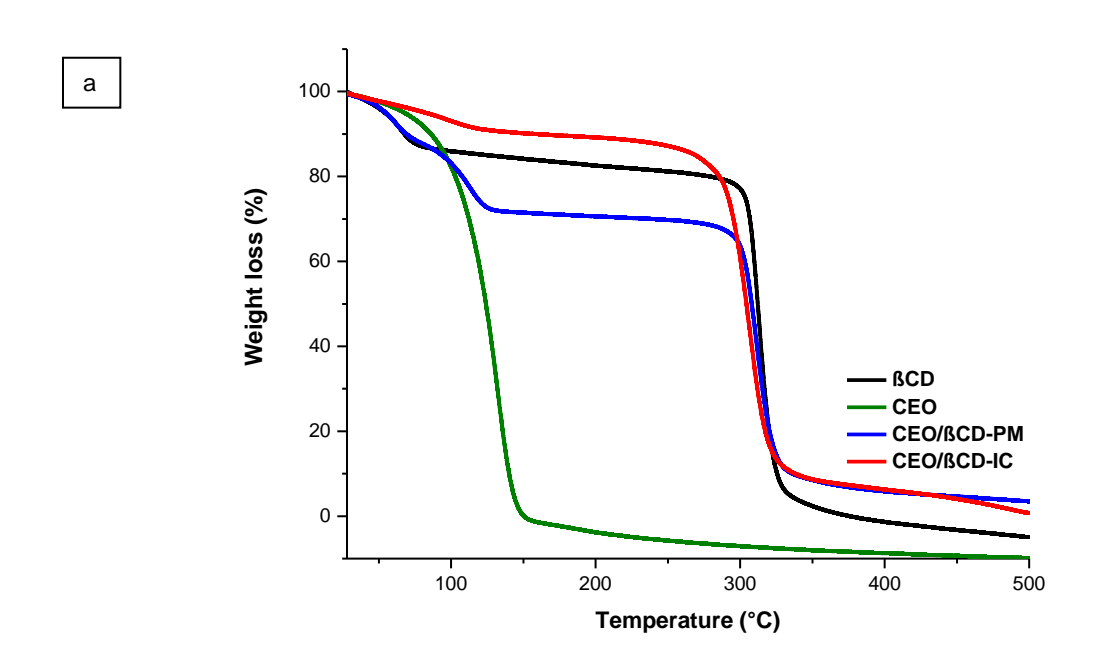
**Figure 18.** FTIR spectrum for SBE-β-CD, CEO, CEO/SBE-β-CD-PM and CEO/SBE-β-CD-IC

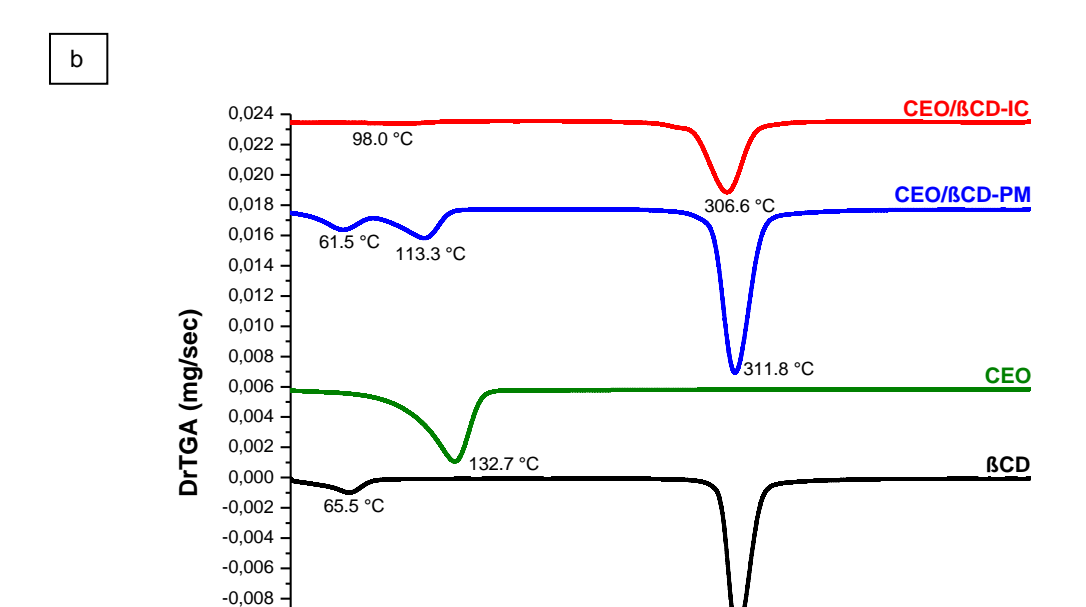
#### 3.6. Thermogravimetric Analysis

TGA is a frequently used technique for measuring a compound's thermal stability in which TGA will be done on samples to identify the changes in weight percent with respect to temperature change <sup>173</sup>. In this study, the thermal stability of inclusion complexes was evaluated using TGA and the results were compared with pure cyclodextrin, oil and physical mixture.

**Figure 19a** and **Figure 19b** show the TGA and the derivatives (DTG) for β-CD, CEO, CEO/β-CD-PM and CEO/β-CD-IC. The curves profile suggests that the process of thermal decomposition of CEO occurred apparently in one step. From 40 to 80 °C, CEO exhibited a sharp decrease with a mass loss of 97.33%. Within the temperature of 40–80 °C, the DTG profile of CEO exhibited one peak temperature ( $T_{\rm p,1}$  = 113 °C). It indicates that cinnamon oil has a volatile nature. It revealed that two stages of the thermal degradation of β-CD can be observed, with temperature increasing. The first stage occurred in the temperature range of 45 to 92 °C, and the mass loss of β-CD was about 10.8 %. The initial mass loss due to the endothermic behavior which corresponded to the loss of water molecules in β-CD cavity. At this stage, there was one peak temperature on the top of the DTG curve ( $T_{\rm p,1}$  = 65.4 °C). The second stage mass loss started at 287 °C and ended at 340 °C. This was the main mass loss stage as indicated and total mass loss was 75.5 %. The DTG profile of β-CD depicted one obvious peak temperature ( $T_{\rm p,2}$  = 313 °C). The physical mixture had undergone three major mass loss stages with a total mass loss of 85.8 %. The initial mass loss was attributed to the loss of water. The second weight loss between 80 °C and 145 °C was due to CEO. The third weight

loss between 275 °C and 350 °C was due to the degradation of  $\beta$ -CD. During this process, the DTG curve of physical mixture shows three evident peak temperatures ( $T_{p,1} = 61.5$  °C,  $T_{p,2} = 113.4$  °C and  $T_{p,3} = 311.8$  °C). As can be seen from the TG curve of CEO/ $\beta$ -CD IC, there were two stages of thermal decomposition, the first step of decomposition occurred from 67 to 135 °C, there was almost no loss of mass, meaning that  $\beta$ -CD-IC was almost not decomposed. The initial weight loss was attributed to the loss of water. The second mass loss step began at 275 and ended at 350 °C, the TG curves depict a very sharp decrease loss process with mass loss of 74.9 % of original mass. In this stage, the DTG curve of  $\beta$ -CD-IC had only one peak temperature ( $T_{p,1} = 306.6$  °C). Compared to physical mixture, inclusion complex showing that the thermal stability of CEO was significantly improved.





200

-0.010

-0.012

100

**Figure 19.** Thermogravimetric analysis (a) and DTG (b) of βCD, CEO, CEO/β-CD-PM and CEO/β-CD-IC.

Temperature (°C)

313.3 °C

400

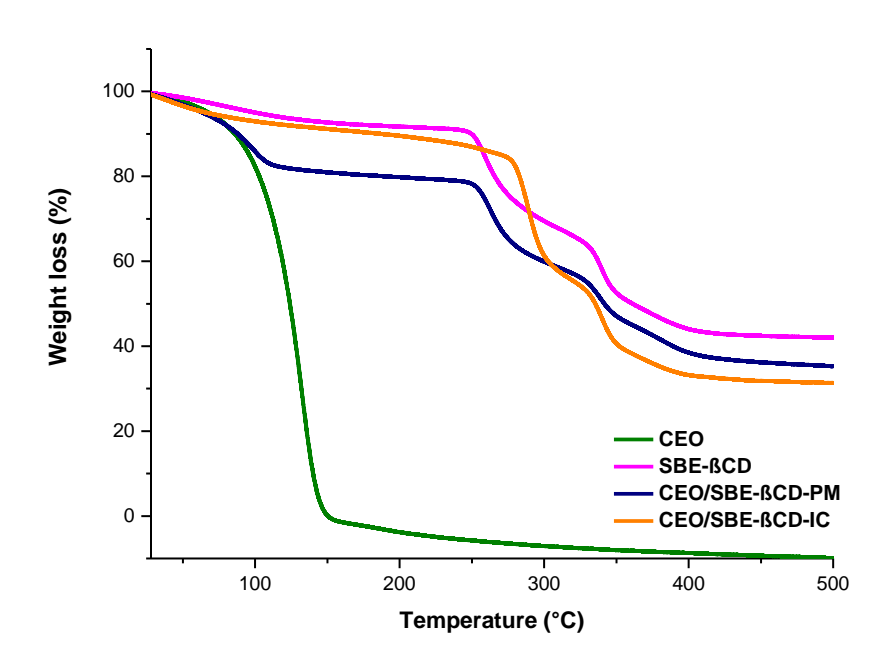
300

500

Figure 20a and Figure 20b show the TGA and the derivatives (DTG) for SBE-β-CD, CEO, CEO/SBE-β-CD-PM and CEO/SBE-β-CD-IC, respectively. This analysis showed evidence of three zones where the SBE-β-CD lost mass with temperature increasing. The first zone under 220 °C with an 8.3% mass loss due to the evaporation of superficial water associated with the cyclodextrin. The second process occurred in the temperature range of 220 to 310 °C with a 23.6% mass loss. Finally, a third process from 310 °C to 500 °C can be related to the degradation of the SBE-β-CD. At this point, 25.8% of the mass is reduced. DTG curve of SBE- $\beta$ CD exhibited three peak temperatures (Tp,1 = 72.2 °C, Tp,2 = 259.4 °C and Tp,3 = 339.6 °C). The process of thermal decomposition of CEO occurred apparently in one step. From 25 to 150 °C, CEO exhibited a sharp decrease with a mass loss of 102 %. Within the temperature of 25– 150 °C, the DTG curve of CEO exhibited one peak temperature (Tp,1 = 132.7 °C) which indicates to this volatilization. It can be observed that the thermogram associated with the physical mixture is very different from inclusion complexes. CEO/SBE-β-CD-PM had undergone three major mass loss stages with a total mass loss of 69,1% was presented. The initial weight loss between 25 °C and 220 °C was due to CEO. The second weight loss between 220 °C and 310 °C was due to the degradation of SBE-β-CD. The third weight loss step began at 310 and ended at 500 °C. During this process, the DTG curve of physical mixture shows three evident peak temperatures (Tp,1 = 98.6 °C, Tp,2 = 262.3 °C and Tp,3 = 338.5 °C). CEO/SBE- $\beta$ CD-IC show similar thermograms with SBE- $\beta$ CD. CEO/SBE- $\beta$ CD-IC had undergone three major mass loss stages with a total mass loss of 68% was presented. The first zone corresponds to the loss of water associated to the SBE- $\beta$ CD structure. The second and third mass loss step began around 220 °C and 310 °C, respectively. Although there was a slight shift in the degradation temperature of SBE- $\beta$ CD, the presence of CEO was not found in CEO/SBE- $\beta$ CD-IC. Compared to physical mixture, inclusion complex showing that the thermal stability of CEO was significantly improved. The DTG curve of inclusion complex shows three evident peak temperatures (Tp,1=39.3 °C, Tp,2=288.5 °C and Tp,3=339.8 °C).

The results indicated that the thermal stability of cinnamon oil was improved after encapsulation, because the decomposition reaction begin at 275 °C for CEO/ $\beta$ -CD IC and 220 °C for CEO/SBE- $\beta$ CD-IC, in contrast to cinnamon oil which thermal decomposition started at 25 °C. The higher thermal stability of CEO in the inclusion complexes suggested an existence of the interactions between CEO and the CDs cavity.

а



b

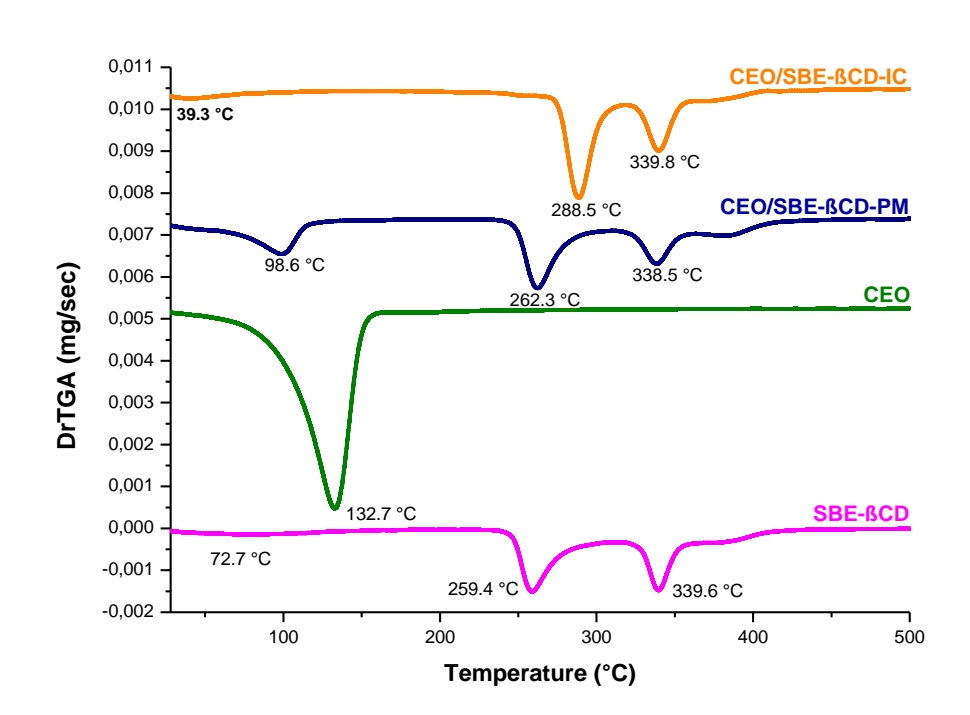


**Figure 20.** Thermogravimetric analysis (a) and DTG (b) of SBE- $\beta$ CD, CEO, CEO/ SBE- $\beta$ CD-IC.

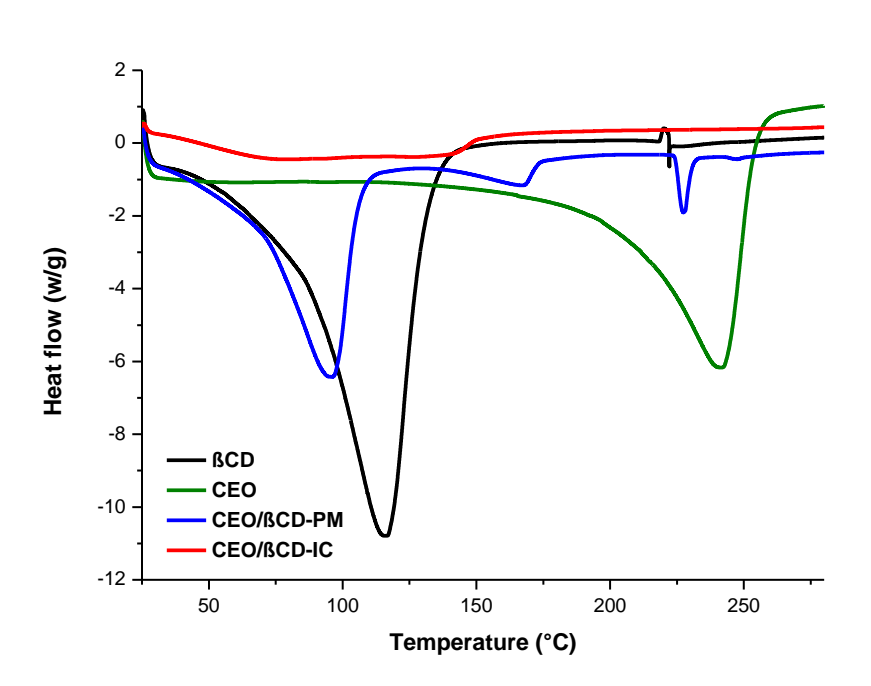
#### 3.7. Differential Scanning Calorimetry

DSC analysis was carried out to determine whether the solid product obtained was a physical mixture or true inclusion complexes. Thermograms curves of CEO, physical mixtures and inclusion complexes are shown in **Figure 21**. Results were characterized by a clear overlap of individual thermograms.

In the case of DSC thermogram of  $\beta$ -CD it was possible to evidence two endothermic peaks. The first one is attributed to the dehydration of the  $\beta$ -CD occurring around 116 °C, while the second peak centered at 300 °C corresponds to the decomposition of the  $\beta$ -CD (**Figure 21a**). On the other hand, cinnamon essential oil presents a single endothermic peak at 203 °C which is attributed to its boiling temperature. It is evidenced in the case of eugenol, with an endothermic peak at 254 °C (PubChem). About the physical mixtures, the DSC thermograms showed characteristic peaks of  $\beta$ -CD pure and essential oil components. On the contrary, as for the DSC thermograms of the inclusion complexes, it was only possible to evidence an endothermic peak at 300 °C related to the degradation of  $\beta$ -CD, there were no evidence of endothermic peaks related to the boiling point of cinnamon oil. This could be associated to the fact that the active compounds are protected within the  $\beta$ -CD cavity <sup>162</sup>.

DSC curve of SBE-βCD show a broad endothermic peak at around 85°C due to dehydration (loss of adsorbed or loosely held water molecules) and sharp endothermic peak at 263.6°C due to the beginning of decomposition events (Figure 21b). This observation was in accordance with the report by another studies on SBE- $\beta$ CD  $^{165,174}$ . On the other hand, CEO presents a single endothermic peak at 242.5°C which is attributed to its boiling temperature. It is evidenced in the case of eugenol, with an endothermic peak at 254 °C (PubChem). About the physical mixtures, the DSC thermograms showed four distinct thermal events at 80.23°C, 164.5°C, 263.6°C and 268.7°C. SBEβCD showed the similar thermal behavior in physical mixture. Peak at 80.23°C and 263.6°C were attributed to dehydration and decomposition of SBE-βCD, respectively. Melting of CEO appeared at 164.5°C in CEO/SBE-βCD-PM. Similar result was observed in βCD/CEO-PM showing peak at 167.7°C. It may have been possible to observe these peaks because of the endothermic process starting at 110°C for CEO. This result indicated partial complexation in physical mixture of both SBE-βCD and CEO. On the contrary, as for the DSC thermograms of the inclusion complexes, it was only possible to evidence an endothermic peak at 83.9 °C and 294.4 °C related to SBE-βCD. There was no evidence of endothermic peaks related to the boiling point of CEO. This could be associated to the fact that the active compounds are totally entrapped within the SBE-βCD cavity.

а



b

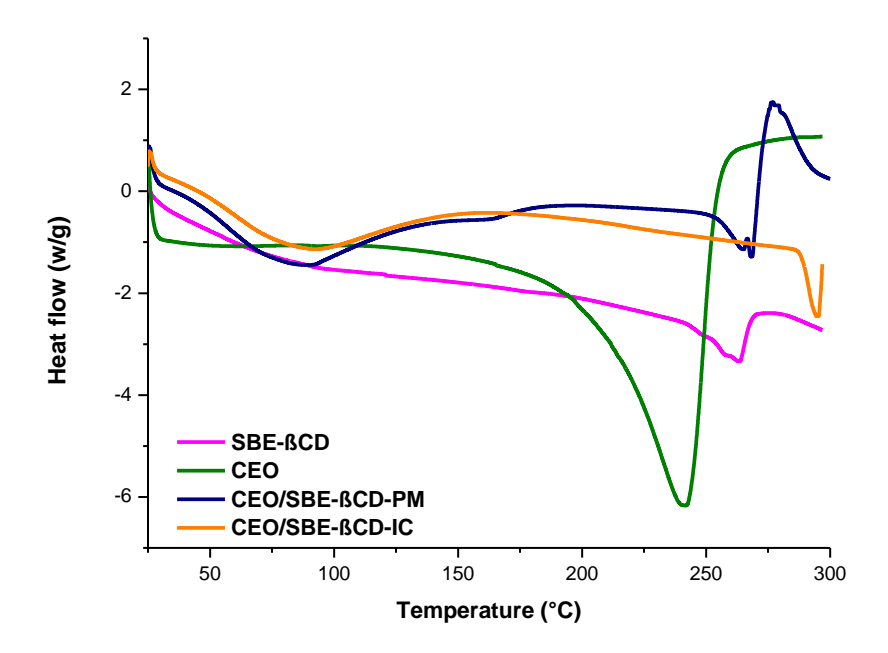


**Figure 21.** DSC thermograms of (a) βCD, CEO, CEO/βCD-PM and CEO/SBE-βCD-IC, and (b) SBE-βCD, CEO, CEO/SBE-βCD-PM and CEO/SBE-βCD-IC.

## 3.8. <sup>1</sup>H-NMR Spectroscopy

The ICs' formation can lead to changes of the significant chemical shifts of the free guest molecule forming a complex with CDs and these changes can provide information concerning the inclusion mode and binding affinity between CDs and guest molecule. The  $^{1}$ H-NMR spectra of spectroscopy of cinnamon leaf oil before and after the inclusion complex were shown in **Figure 22** and **Figure 23**. The decreased intensity of the essential oil in both of the complexes showed that there was an interaction between CDs and essential oil. The chemical shifts between CDs and the inclusion complex were checked in **Table 6 and Table 7** to understand the interaction better. After the formation of CEO/β-CD inclusion complex, chemical shifts were observed only in the H2 and H6 proton which are located on the surface of β-CD. These protons indicated that cinnamon leaf oil interacted with only the narrow hole of β-CD  $^{175}$ . Unlike β-CD, there were chemical shifts in the all-H protons of SBE-β-CD after the formation of the inclusion complex with cinnamon leaf oil. The observed shifting of H-3 and H-5 in the CEO/SBE-β-CD-IC may attribute to the hydrophobic interactions with the guest molecules (oil constituents), which are located inner surface of the SBE-β-CD cavity and confirmed the formation of CEO/SBE-β-CD inclusion complex  $^{176}$ .

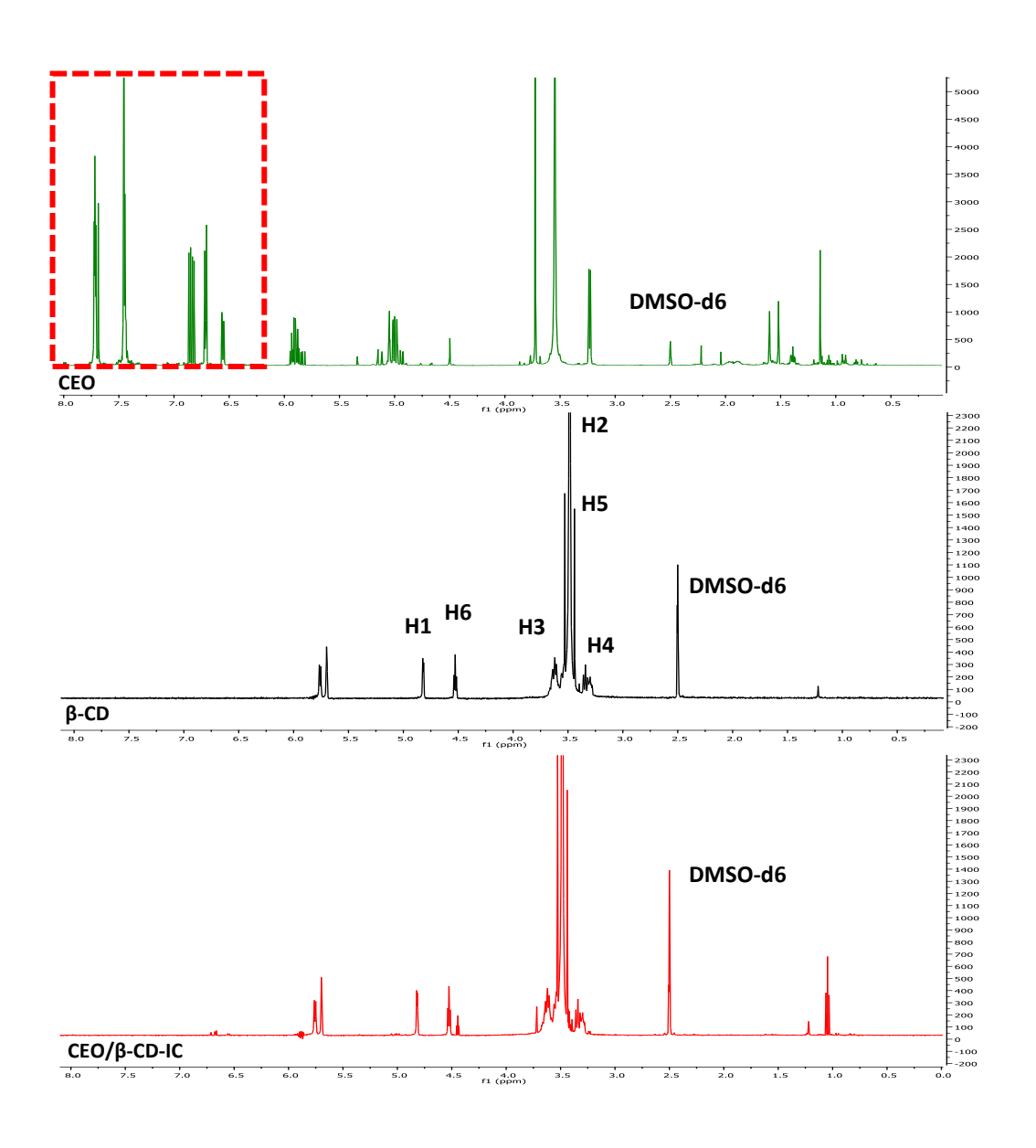


**Figure 22.** <sup>1</sup>H NMR spectrum of  $\beta$ -CD, CEO and CEO/ $\beta$ -CD-IC in DMSO-d6

**Table 6.** <sup>1</sup>H NMR chemical shifts ( $\delta$ ) of  $\beta$ -CD and CEO/ $\beta$ -CD-IC

H atom	δ (free)	δ (complex)	$\Delta \delta = \delta$ (complex)- $\delta$ (free)
H1	4.823	4.823	0
H2	3.620	3.624	+0.004
Н3	3.642	3.642	0
H4	3.562	3.562	0
H5	3.606	3.606	0
H6	4.527	4.525	-0.002

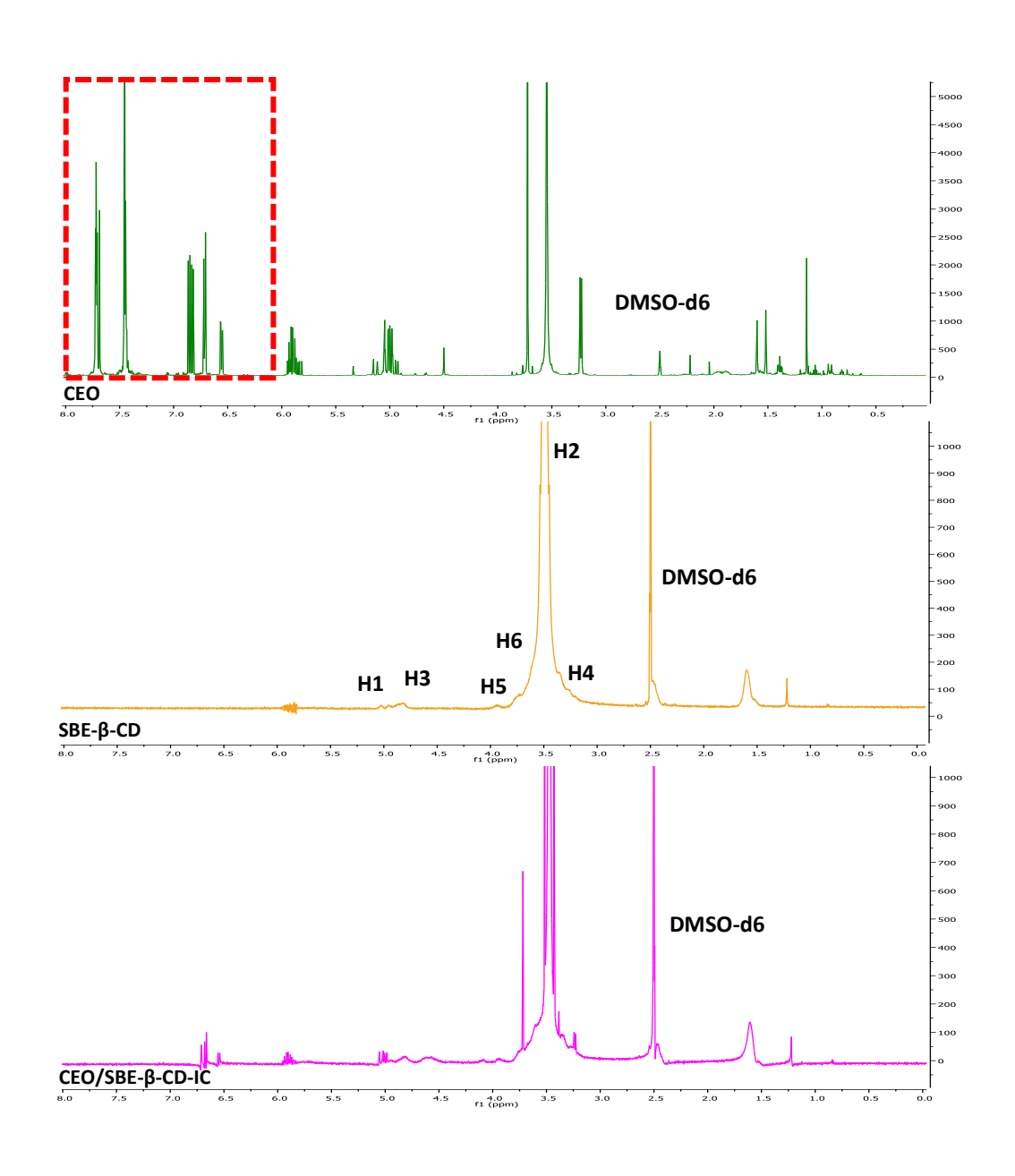


Figure 23.  $^1\text{H}$  NMR spectrum of SBE- $\beta$ -CD, CEO and CEO/SBE- $\beta$ -CD-IC in DMSO-d6

**Table 7.**  $^{1}$ H NMR chemical shifts ( $\delta$ ) of SBE- $\beta$ -CD and CEO/SBE- $\beta$ -CD-IC

H-atom	δ (free)	δ (complex)	$\Delta \delta = \delta$ (complex)- $\delta$ (free)
H1	5.031	5.030	-0.001
H2	3.360	3.366	+0.006
Н3	4.820	4.823	+0.003
H4	3.267	3.273	+0.006
H5	3.936	3.939	+0.003
Н6	3.734	3.737	+0.003

#### 3.9. Antibacterial activity of essential oil

#### 3.9.1. Agar disk diffusion test

The antibacterial effect of cinnamon leaf oil was determined by the disc diffusion method and the effect of this oil was compared with other oils as St. John's wort oil, coriander oil and clove oil (**Figure 24**). Among the tested essential oils, St. John's wort presented no antibacterial activity against *E. coli* and *S. aureus* while coriander oil presented similar antibacterial activity against *E. coli* and *S. aureus*. Since the major active component eugenol of cinnamon leaf oil and clove oil, similar results were obtained in both bacteria. *E. coli* was more sensitive to these oils than *S. aureus* because of damaging and disruption of cell membrane by eugenol <sup>177</sup>. The antibacterial activity of selected essential oils was ordered as cinnamon leaf oil =clove oil > coriander oil > St. John's wort oil against *E. coli* and coriander oil > cinnamon leaf oil > clove oil > St. John's wort oil against *S.aureus*. The zone of inhibition of cinnamon leaf oil was 20 mm for *E. coli* and 17 mm for *S. aureus*. It exhibited antibacterial activity as potent as ampicillin antibiotic (inhibition zone: 20 mm) against especially *E. coli*.

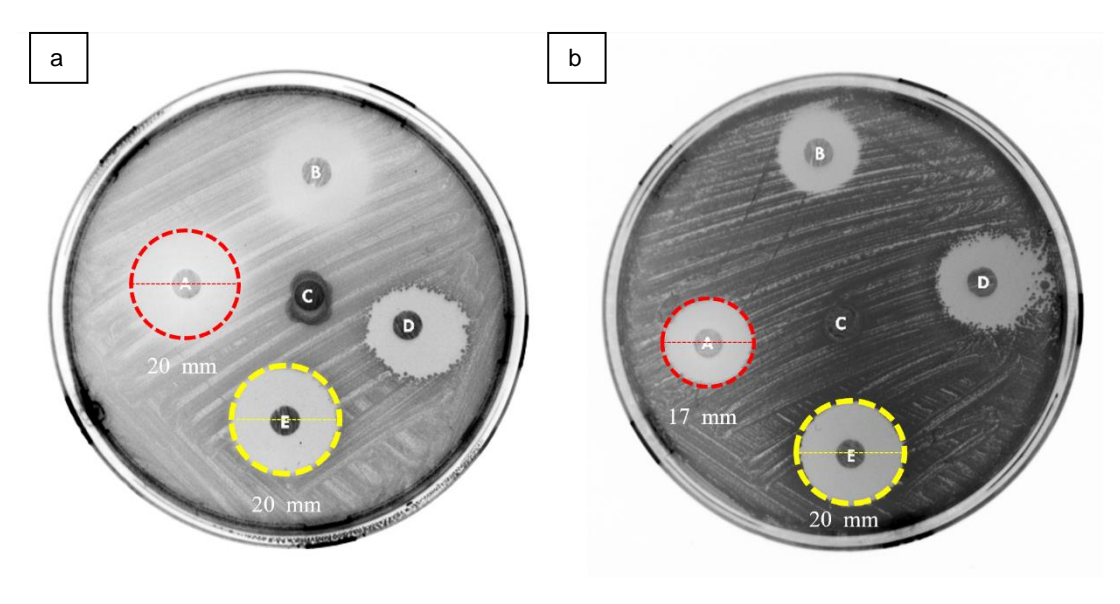


**Figure 24.** Inhibition zones of different essential oils against *E. coli* (a) and *S. aureus* (b). A: cinnamon leaf oil, B: clove oil, C: St. John's wort oil, D: coriander oil, E: ampicillin antibiotic

#### 3.9.2. MIC determination by serial dilution dose-response experiment

The MIC value of cinnamon leaf oil was investigated to observe at what concentration the essential oil started to show their effects. The **Figure 25** show the different concentrations of essential oils (1%-0.01%, v/v) on each bacterium. No growth was observed in the negative control tubes in the study. As a positive control, growth was observed in all test tubes studied

separately for each bacterium. Considering the results, the antibacterial activity of free CEO against both *E. coli* and *S. aureus* bacteria showed dose-dependent activity so that with increasing the concentrations of CEO, the growth of bacteria was reduced. Importantly, the corresponding MIC of cinnamon leaf oil for *E. coli* was 0.25 %, which was lower than that for S. aureus 0.5 %. These findings are mainly because Gram-positive bacteria with thicker and more compact walls are more stable than Gram-negative bacteria <sup>178</sup>. It was reasonable to reveal that *E. coli* was more sensitive to cinnamon leaf oil than *S. aureus*, which also aligned with other work. Cui et. al found the similar result that cinnamon leaf oil showed strong antibacterial activity against the *E. coli* with MIC (0.019%) than *S. aureus* MIC (0.039%) <sup>179</sup>.

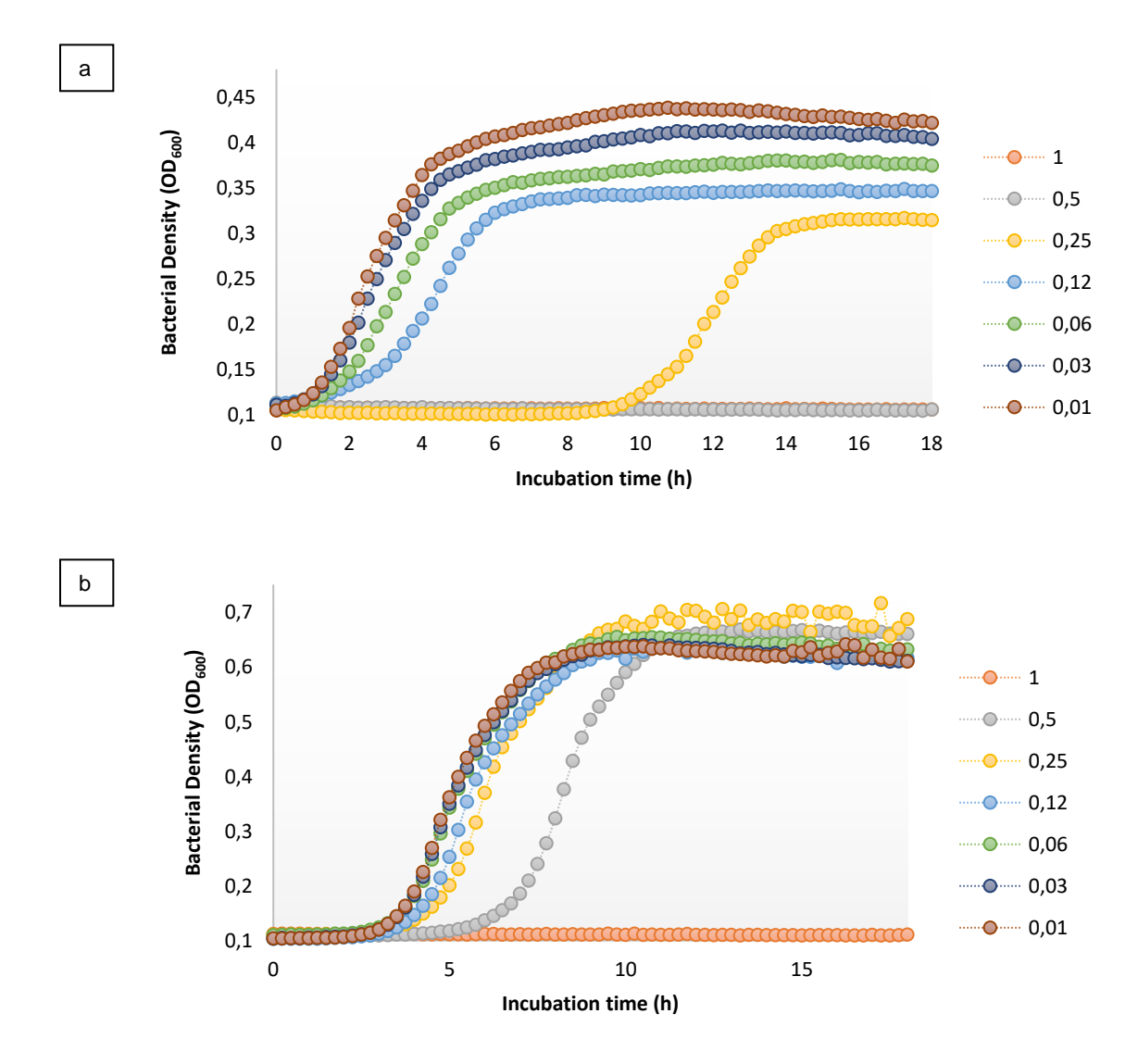


**Figure 25.** Bacterial growth curve of (a) *E. coli* and (b) *S. aureus* in LB medium in the presence of essential oil with different concentrations.

#### 3.10. Antibacterial activity of inclusion complexes

As evidenced by previous study, cinnamon leaf oil shows antibacterial activity against gram-positive and gram-negative bacteria. CEO/ $\beta$ -CD-IC and CEO/SBE  $\beta$ -CD-IC were checked to confirm the antibacterial activity of oil after inclusion with cyclodextrin.

The antibacterial effect of the inclusion complexes was determined against Escherichia coli and Staphylococcus aureus by the colony counting method. For this, the inclusion complexes were incubated in PBS containing bacteria for 24 hours. Sample images of bacterial colonies are given in **Figure 26**. Plates without inclusion complex were assumed as 100% for calculating growth inhibition rate. After being treatment with low concentration (15 mg/ml) of CEO/β-CD-IC and CEO/SBE-β-CD-IC for 24 hr, the surviving population of *E. coli* decreased compared to control group. Surviving population of E. coli were inhibited totally by using 30 mg/ml for both of inclusion complexes (Figure 26). They exhibited 100 % antibacterial activity against E. coli. Fully incubation occurred in the same amount of oil in CDs and cyclodextrins alone used as negative control didn't show antibacterial effect, as expected. However, different results were obtained in gram-positive bacteria experiments. When lower concentration (15 mg/ml) of CEO/β-CD-IC was applied, surviving population of S. aureus increased. It means that E. coli is more sensitive to CEO/β-CD-IC than S. aureus. After being treatment with high concentration (30 mg/ml) of CEO/β-CD-IC, the surviving population of S. aureus inhibited totally compared to control group (cell only). Likewise, CEO/SBE-β-CD-IC similar antibacterial effect against S. aureus. However, 30 mg/ml of the complex was not enough to completely inhibit the bacteria. CEO/SBE-β-CD-IC exhibited 22 % antibacterial activity against S.aureus while it was 100 % for CEO/β-CD-IC. Based on this information, results confirmed that CEO/β-CD-IC and CEO/SBE-β-CD-IC had a strong antibacterial activity against E. coli however CEO/β-CD-IC had better antibacterial activity against S. aureus than CEO/SBE-β-CD-IC. Similar finding was found by Halahlah that the antibacterial activity of rosemary oil  $\beta$ -CD-IC was higher than inclusion complexes with M- $\beta$ -CD and HP- $\beta$ -CD <sup>180</sup>. Likewise, euterpe oleracea mart oil/β-CD-IC showed better antibacterial activity when oil was encapsulated with HP-β-CD <sup>181</sup>. The differences of biological activity can be attributed to cyclodextrins that having different polarity <sup>180</sup>.

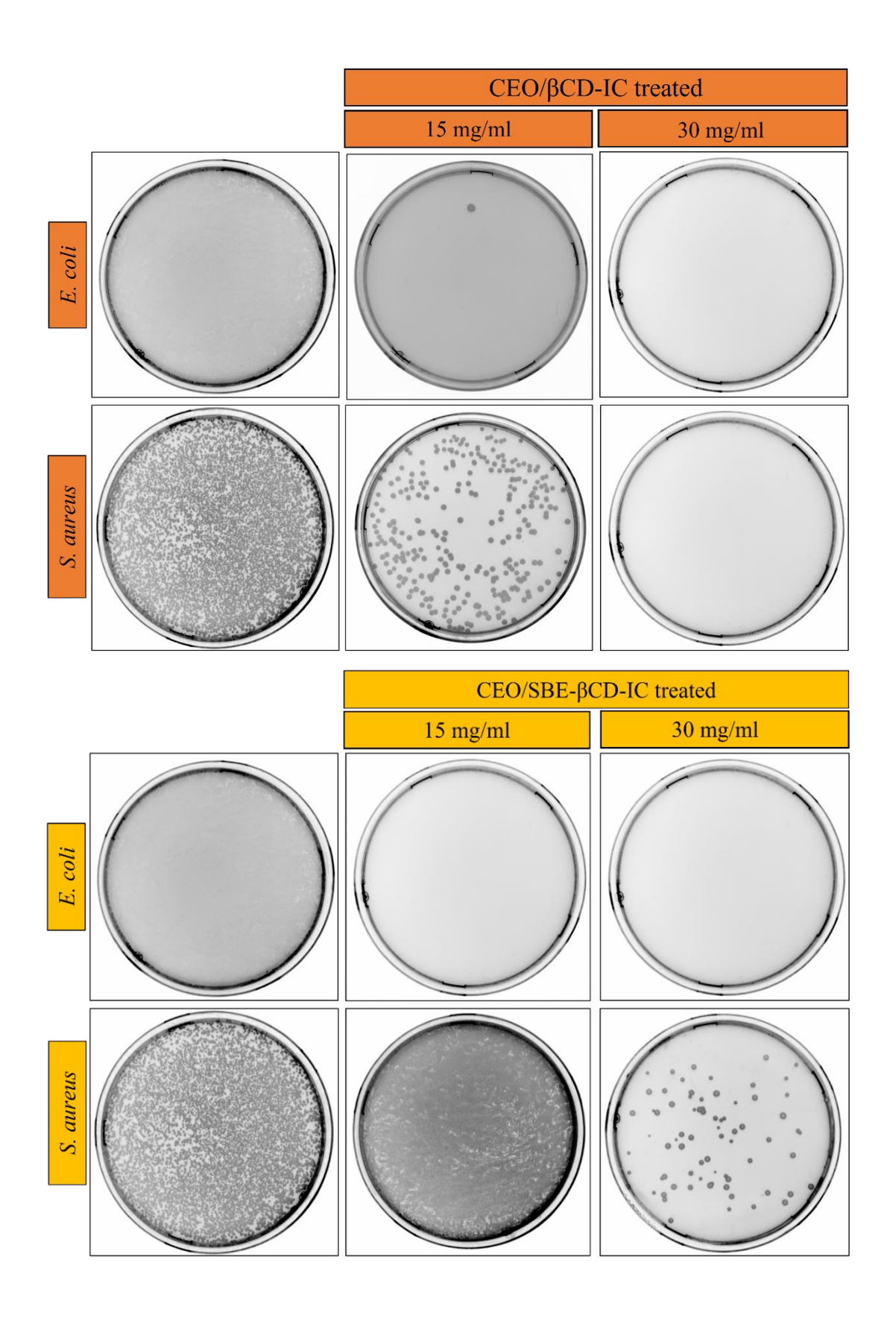


**Figure 26.** Images of plates showing bacterial growth of *E. coli* and *S. aureus* in term of colonies in the presence of inclusion complexes

#### 4. Conclusion

During this study, cinnamon leaf oil, as a type of hydrophobic antibacterial agent, was encapsulated within β-CD and SBE-β-CD via freeze drying method at a 1:1 molar ratio. CEO in CDs was determined spectrophotometrically using the UV-Vis spectrometer. Solubilizing and complexing ability of  $\beta$ -CD and SBE- $\beta$ -CD were confirmed via phase solubility assay, and it was indicated that CEO/β-CD-IC and CEO/SBE-β-CD-IC were classified as A<sub>L</sub> type which confirms presence of 1:1 stoichiometric ratio of inclusion complexes. Results of stability constant (K<sub>1:1</sub>) were showed that both of the complexes had capability to improve dissolution of poorly water-soluble drugs. However, SBE-β-CD showed superior solubilizing and complexing ability. K<sub>1:1</sub> value for CEO/SBE-β-CD-IC complex was found to be 337.08 M<sup>-1</sup> which is 1.9-fold higher than βCD. Encapsulation efficiency and loading efficiency after freezedrying were 18 % and 11 % for CEO/β-CD-IC and 23 % and 5 % for CEO/SBE-β-CD-IC. It has also showed high yield with CEO/SBE-β-CD-IC (77%) when compare with CEO/β-CD-IC (35 %). DLS analysis indicated that CEO/β-CD-IC and CEO/SBE-β-CD-IC are at nano size level with high monodispersity and quite stability in suspension. The formation of CEO/β-CD-IC and CEO/SBE-β-CD-IC was confirmed by several analysis includes SEM, FTIR, TGA, DSC and <sup>1</sup>H-NMR spectroscopy. Also, the results of TGA and DSC indicated that the thermal stability of cinnamon oil was improved after encapsulation. The antibacterial activity of free CEO against both E. coli and S. aureus bacteria showed dose-dependent activity so that with increasing the concentrations of cinnamon leaf oil, the growth of bacteria was reduced. They had better antibacterial activity against E. coli than S. aureus. Interestingly, the antibacterial activity of the oil was as potent as ampicillin antibiotic especially against E. coli. The antibacterial activity of CEO/β-CD-IC and CEO/SBE β-CD-IC were also checked, and they had strong antibacterial activities against E. coli, as expected. Interestingly, they showed different antibacterial activity against S. aureus so that CEO/β-CD-IC had higher antibacterial activity even at lower concentration. Accordingly, using CEO/β-CD-IC could be a good candidate for antibacterial applications such as skin infection caused by bacteria as E. coli and S. aureus.

# CHAPTER 2: Eudragit Electrospun Fibers Functionalized by Cinnamon Leaf oil Complexation with Cyclodextrins for Wound Dressing Application

#### 1. Introduction

#### 1.1. Wounds

Wound is defined as the deterioration of the integrity of the structures forming the skin and the temporary or complete loss of existing physiological properties due to disease, trauma, or surgery. Wounds are classified in 4 groups according to their thickness, closure style, clinical appearance/color, and healing time. This classification is detailed in **Table 8**.

Table 8. Classification of wound

Partial thickness wounds: The epidermis layer of the skin, that is, only the epidermis, is damaged. Healing of this type of wound takes place by regeneration (reepithelialization).

#### **Thickness**

Full thickness wounds: Subcutaneous layers, dermis and epidermis of the skin are damaged. These types of wounds may also involve muscle and bone tissue. The healing of these wounds is several stages and scarring is formed.

Primary intention wounds: These wounds do not cause any tissue loss (cuts, etc.) and can be closed with sutures.

#### Closure style

Secondary intention wounds: There is tissue loss in these wounds and heal with granulation.

Tertiary intention wounds: These wounds are deeper. They carry the risk of catching germs and infection.

Black-necrotic wounds: These wounds are covered with black/brown looking dead tissue. The presence of this tissue delays healing.

Green-infected wounds: Infection in such wounds prolongs the inflammatory phase of the healing process, delaying healing and requiring treatment.

## Clinical appearance/color

Red-granulation wounds: These wounds have a moist, tender, and bumpy texture. this tissue appears dull due to anemia or infection.

Pink-epithelialization wounds: This wound has a pink-white appearance due to epithelial cells migrating to the wound surface.

Mixed wounds: Multiple colors are observed in these wounds as they have two or more healing phases.

Acute wounds: These are wounds that heal in a short time without any complications. The cause of the wound is temporary. Generally, the factors that hinder recovery are few. In acute wounds, healing is continuous.

#### **Healing time**

Chronic wounds: These are wounds with a very long healing process depending on the severity of the wound or external factors such as infection. The factor that causes the wound is chronic. There are many systemic and local factors that prevent healing. Chronic wounds often recur.

#### 1.1.1 Wound healing

The whole of the biochemical and cellular responses that occur in the process of restoring the functional capacity and tissue integrity of the damaged tissue is called "wound healing". Wound healing, which begins with successive events with tissue damage, includes many well-organized cellular and molecular events as inflammation, vessel formation, fibroblast proliferation, wound closure, epithelialization, and matrix remodeling <sup>182</sup>. The healing process of the wound is directly affected by the area of the wound, the health status of the person and the severity of the damage. The healing process generally consists of four phases. These are the stages of hemostasis, inflammation, proliferation, and remodeling (**Figure 27**) <sup>182,183</sup>.

Hemostasis and inflammation stages begins immediately after the injury, and at this stage, redness, pain, swelling, warmth, and loss of function occur <sup>184</sup>. The inflammatory phase prepares the wound for healing and removes damaged tissue. The predominant cells 72 hours after injury are macrophages. Meanwhile, new vessel formations begin with the release of angiogenic growth factor. As new blood vessels form, oxygenated blood reaches the wound area and nourishes the area. Fibroblasts form collagen around the new vessels, allowing the proteoglycans they produce to bind to each other and make them more flexible. It consists of 2 stages, Early period (hemostasis) and late stage (phagocytosis). In early period, bleeding can be stopped, and clot formation can be achieved, and bacterial formation can be prevented. In late stage, leukocytes destroy damaged tissues and bacteria. **The proliferation stage** leads to the restructuring of the epidermis. Epithelialization occurs at this stage, where epithelial cells migrate to the wound area and reduce the risk of infection <sup>185</sup>. During re-epithelialization, a reduction in wound size occurs. At this stage, the wound is rich in blood vessels. Fibroblasts

synthesize abundant collagen. With the synthesis of collagen, resistance against tearing is provided in the wound. New blood vessels are formed, and this vascularization continues until the end of wound healing. During the healing process of the wound, the wound edges begin to recede. Epithelial cells seal the wound bed. **The remodeling stage** is the final stage of wound healing. Collagen synthesized in the proliferation phase is shaped by cross-links. Soft and gelatinous type III collagen turns into firmer type I collagen after a while. The tension of the formed granulation tissue increases even more <sup>186</sup>. The cells and vascularity of the newly formed tissue decrease over time. This phase can take up to 2 years.

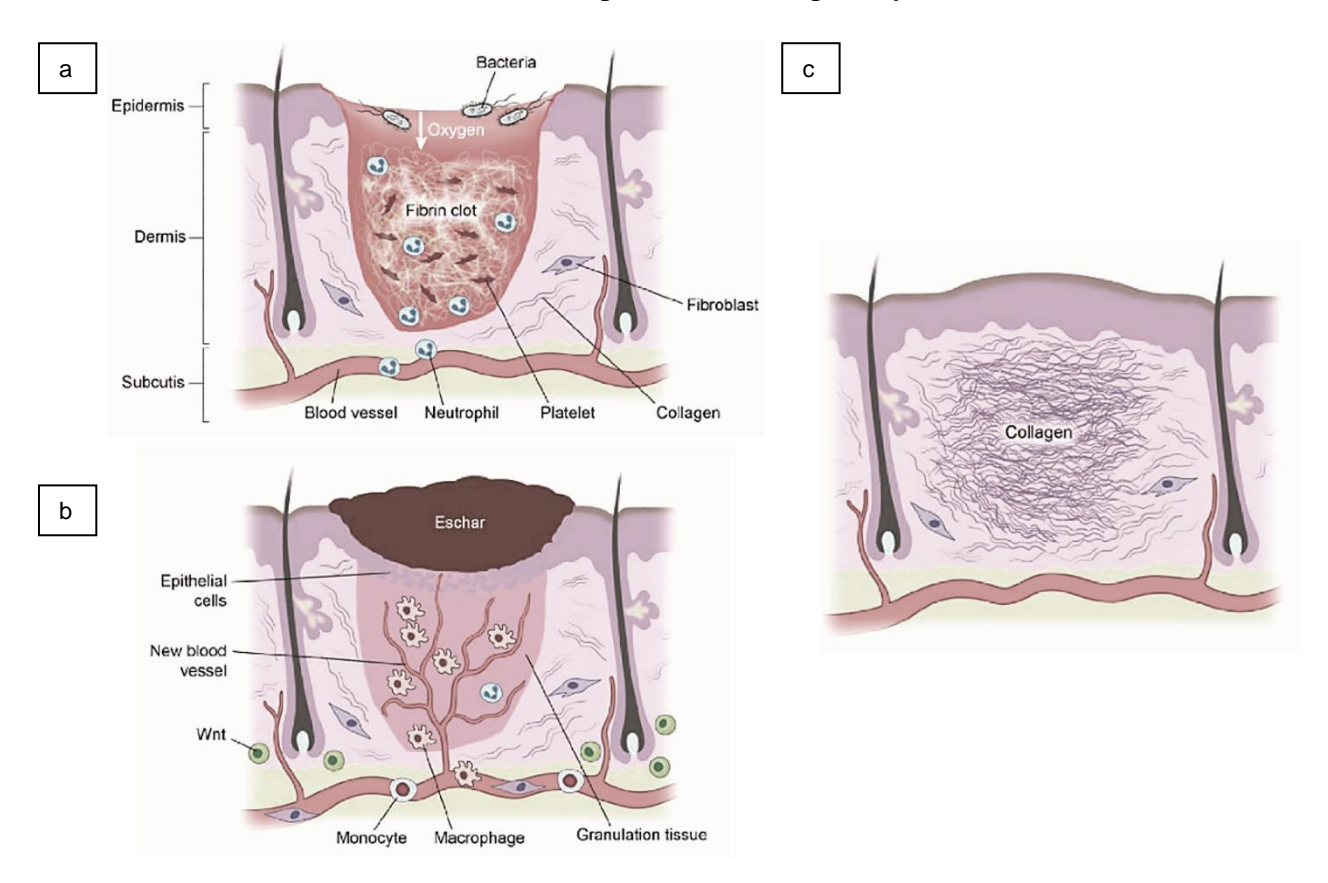


**Figure 27.** Stages of wound healing (a) hemostasis and inflammation stage (b) proliferation stage and (c) remodeling stage <sup>187</sup>.

#### 1.1.2. The Importance of pH in Wound Healing

Although the importance of pH value during the healing of wounds was known many years ago, not many studies have been done on it until recently. However, after the 2000s, interest in this subject has increased and the relationship between wound healing and pH has been closely examined. The pH value of the wound can give important information about the condition of the wound. pH change during the wound healing process for acute and chronic wounds is given in **Figure 28**. It has been observed that the pH value of the wound exudate changes as the wound

heals or becomes infected. The pH value of healthy skin (pH 4.8-6.0) is slightly acidic. Increasingly alkaline pH in wounds is an indication that they will not heal or become chronic <sup>188</sup>. During a wound healing process, the pH of the wound is initially basic, then neutral and eventually reaches the pH of healthy skin. The first stage of the inflammatory phase is one hour after injury and within hours the blood clots to form a temporary plug. In this case, the approximate pH value of the wound is 7.4, which is very close to the blood. After about two weeks, the wound heals and returns to normal pH. Wounds heal more slowly in alkaline media. Because the contact of the tissue with oxygen is not enough. When the wound becomes infected; produces ammonia, ammonia raises the pH and blocks oxygen access, resulting in longer wound healing time.

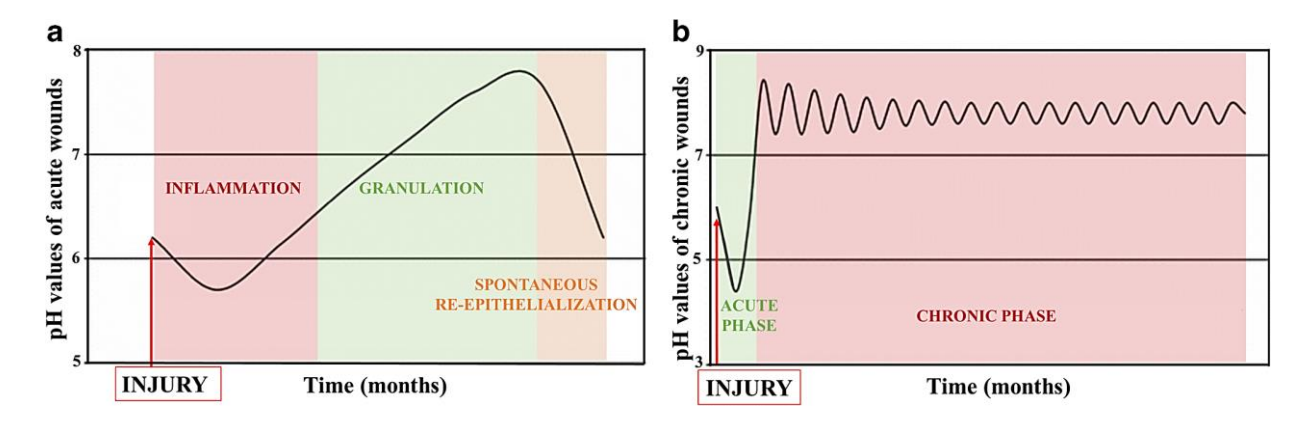
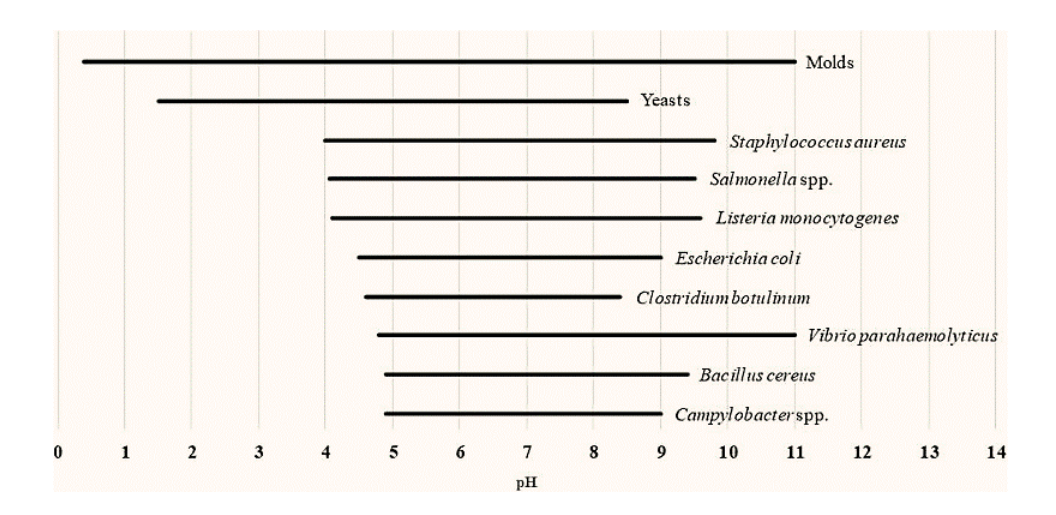


Figure 28. Changes of pH on acute wounds (a) and chronic wounds (b) on healing <sup>189</sup>.

The pH of the wound environment can vary significantly depending on the stage of the healing process, the type of wound or other factors such as infection. Wound healing described above, which operates in an interlocking and sequential manner, does not occur in patients with diabetes. A wound that will heal in a short time does not heal immediately in diabetic patients. Diabetes is among the major diseases that impair the defense system. An important stage of wound healing depends on the defense system and the cells of the defense system involved in this stage. Their malfunctioning not only impairs wound healing, but also reduces resistance to microbes and causes diabetic wounds to become easily infected. Diabetic foot ulcers are infected by gram-positive aerobes as *S. aureus*, *S. epidermidis*, *S. haemolyticus* and gram negative aerobes as *E. faecalis*, *C. striatum*, *A. calcoaceticus*, *E. cloacae*, *E. coli*, *K. oxytoca* and *K. pneumoniae* <sup>190,191</sup>. The growth abilities of microbials at different pH are shown in **Figure 29**.



**Figure 29.** Microbial growth in different pH range <sup>187</sup>.

All of the wound healing processes described above are active works, that is, they require energy. Energy in the body is only possible in the presence of sufficient nutrients and oxygen. However, disease of the large and small vessels of diabetics disrupts the nutrition and oxygenation of the tissues. Failure of the vessels to fulfill their function and not carrying enough blood to the tissues is called ischemia. The energy requirement cannot be met in ischemic tissues, and therefore, wound healing cannot occur normally like other activities. Diabetic wound healing, if defined in the order described above (inflammation), can be considered to be stuck in the <u>inflammation stage</u>. Wounds caused by ulcers is a serious global health problem affecting millions of people. Treating ulcers before they reach a <u>chronic stage</u> can help reduce patients' pain. In the treatment of diabetic foot ulcer, infected tissue must be cleaned in order to initiate secondary intension of healing. Since the pH of stage I pressure ulcers is around 5.5-5.6, the treatment of these wounds can be treated with wound dressings that release therapeutic agents at acidic pH <sup>192</sup>.

#### 1.2. Wound Dressings

Largest organ in our body, skin, is the first line of defense against infection. Damages due to trauma to the skin may heal spontaneously or may require direct medical intervention depending on the severity of the damage. Wound dressings are materials used to cover wounds, thereby replacing the natural epithelium lost because of injury and helping wounds heal faster than open wounds.

Basic function of wound dressing is absorbing blood and wound fluid and allowing oxygen to pass through. An ideal dressing should be easy to apply and easily removable; prevent leakage from the winding; apply pressure to stop bleeding; adapt to the shape of the wound; allow the

passage of oxygen and provide thermal insulation <sup>193</sup>. It should also provide a moist environment on its inner surface. Because it is known that moisture has an inhibitory effect on tissue drying and crust formation. As a result of the drying of the wound, a scab or scar is formed. Unclosed, air-drying wounds develop thicker scabs and re-epithelialize more slowly. Another feature of an ideal bandage is providing a protective feature against infection and microorganisms. It should be able to absorb the wound discharge and remove it from the environment without increasing bacterial growth and causing excessive drying and should prevent the passage of bacteria. All these properties are important especially in the early stage of acute inflammation for rapid healing.

The structure of the wound dressing is also an important issue. Wound dressings can be classified as passive dressings such as gauze, bandage and plasters, and modern dressings such as hydrocolloid, alginate, polyurethane foam, polyurethane film, and hydrogel. Modern dressings developed in recent years prevent dehydration and preserve the viability of tissues and the ability of cells to proliferate. These dressings also accelerate angiogenesis (new vessel formation) and increase the effectiveness of some endogenous molecules that have an active role in wound healing. While isotonic wet dressing and hydrocolloid dressings are an option, recent advances in nanotechnology have offered new approaches for drug delivery applications, particularly in chronic wound healing. Treatment of chronic wounds are classified into new therapeutic way as nanoparticles (inorganic, polymeric, lipids); self-forming nanocarriers (micelles, liposomes, nanogels) and nanofibers, and these have been found to have positive effects especially in diabetic wound models <sup>194</sup>.

#### 1.2.1. Nanofibers based wound dressing

Fibers, whose diameter can vary in the order of nanometers, are defined as "nanofiber". Nanofibers provide convenience in many application areas with their high porosity, controllable pore size, soft and stable structure, high specific surface area and low specific gravity <sup>195,196</sup>. The most researched subject about nanofibers is the biomedical application areas of nanofibers (**Figure 30**). It is predicted that nanofibers will contribute to developing medical applications such as organogenesis, genetic medicine, smart wound dressings. Especially promising research topics are nanofiber-based three-dimensional scaffolds used in tissue engineering, design of nanofiber devices for controlled drug delivery, and nanofiber wound dressing materials. Drug delivery with nanofiber is a promising field of biomedical application <sup>197</sup>. Drugs or other functional substances are added into nanofibers and nanofibers act both as drug carriers and

drug delivery systems. Through nanofibers, controlled and slow release of compounds can be achieved, special compounds can be better protected and more stable in nanofibers <sup>198–200</sup>.

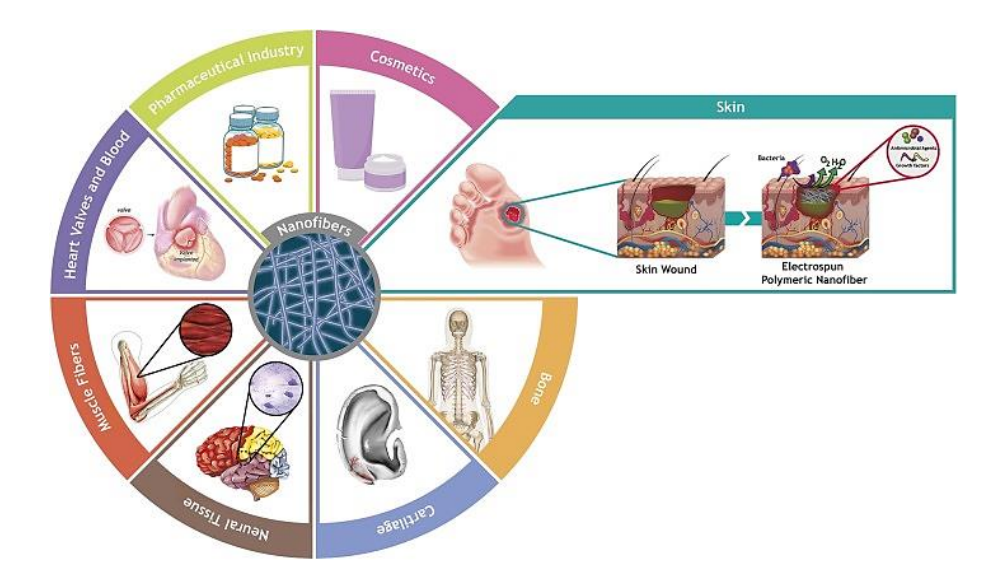


**Figure 30.** The use of nanofibers in different fields of biomedicine <sup>201</sup>.

The most important feature of nanofibrous structures in the wound healing process is that they can form structures similar to the extracellular matrix (ECM). The ECM is a complex structure found among cells within mammalian tissues. Liu et al. stated that nanofibrous structures can mimic ECM due to their large surface area, porosity and 3-dimensional network structure <sup>202</sup>. They stated that the ECM-like physical form can be provided by network structures consisting of nanofibers and can be used effectively in wound treatments. Nanofiber wound dressings produced have a hemostatic (stopping bleeding) effect. Due to their high surface area, they have a good fluid absorption capacity, and this feature has been stated to be an important feature in terms of absorbing wound exudates. Nanofiber structures provide good oxygen permeability thanks to their small pores and allow the wound to breathe. In addition, these small pores protect the wound against microorganisms coming from the outside. It can be easily applied to many places with its thin and flexible structures. Nanofiber dressings can accelerate wound healing by creating minimal scar tissue <sup>203</sup>.

Nanofiber-based wound dressings can be produced from synthetic and natural polymers with technologies such as drawing, template synthesis, phase separation, self-assembly, meltblown, bicomponent and electrospinning. However, electrospinning, which is a simple and economical method, is the most interesting production technique among them. In the literature, there are many studies in which nanofibers obtained by electro-spinning method are evaluated as wound dressing. These fibers are obtained various polymers as chitosan <sup>204</sup>, carboxyethyl chitosan <sup>205</sup>,

polyurethane <sup>206</sup>, polycaprolactone <sup>207</sup>, polyethylene oxide <sup>208</sup>, polyvinyl alcohol <sup>209</sup>, polyvinyl alcohol pyrrolidone <sup>210</sup>, alginate <sup>211</sup>, cellulose acetate <sup>212</sup>, hyaluronic acid <sup>213</sup> and collagen <sup>214</sup>.

## 1.3. Electrospinning

Electrospinning is a simple and effective manufacturing technique used to create ultrafine fibers from a wide variety of materials such as polymers, composites, and ceramics. This technique is based on positioning an electrically charged liquid polymer in the form of a continuous fiber on a grounded surface <sup>193</sup>. Electrospinning is the most effective method to produce polymer-based nanofibers. Nanofibers with diameters ranging from 3 nm to 1 micron and above are successfully obtained from many polymers with this method <sup>215</sup>.

Experimental set-up of electrospinning is shown in **Figure 31**. The polymer solution prepared with a suitable solvent, the electrode in contact with this solution, a high voltage direct current power supply and a g rounded collector plate are the basic components of the electrospinning process <sup>193</sup>. In this method, the polymer solution is taken into a suitable syringe and the solution is allowed to flow from the syringe with the help of a pump. Meanwhile, a high voltage potential is applied between the collector plate and the tip of the syringe. The polymer solution at the tip of the metal syringe is in the form of a spherical droplet up to a certain voltage value. When the critical voltage value is reached, the surface tension of the polymer solution and the electrostatic forces are equalized, and the polymer drop takes the form of a cone (Taylor cone). After this point, with the slightest increase in voltage, continuous fibers form from the metal tip of the syringe to the collector plate. Meanwhile, the solvent in the polymer solution evaporates rapidly <sup>216,217</sup>

In an ideal electrospinning process should provide suitable and controllable fiber diameters, defect-free structure or controllable defect on the fiber surface and continuous nanofiber formation in the form of monofilaments. In order to provide these properties, a controlled electrospinning process must be performed. Although the electrospinning method provides advantages as a cheap and simple nanofiber production technique, it is a very difficult process to control. Because there are many technical parameters that affect the process. These parameters are generally examined in three main groups as solution parameters, process parameters and ambient parameters.

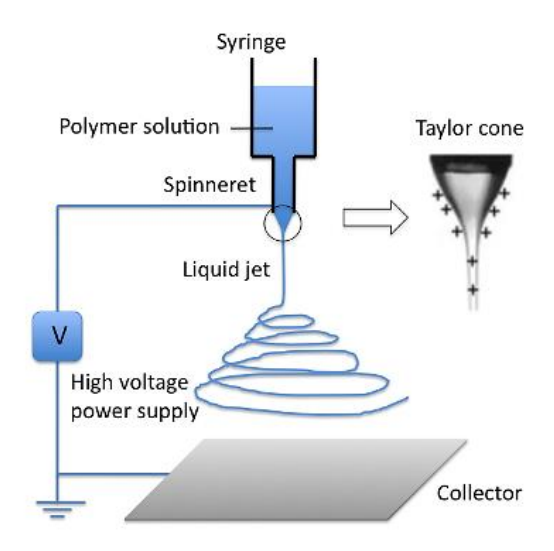


**Figure 31.** Experimental set-up of electrospinning <sup>218</sup>.

The properties of the polymer solution are the most important parameters affecting the electrospinning process and the morphology of the fiber formed. When the **concentration** of the polymer is too low, (electro spraying) occurs instead of electro-spinning, thus microparticles are obtained. When the concentration is slightly high, beaded fiber formation occurs. When the concentration is sufficient, smooth, and homogeneous fibers can be obtained. When the concentration is too high, helical microstrips are obtained <sup>219</sup>. **Viscosity** is another important parameter. Continuous and smooth fibers cannot be obtained at very low viscosity. For a low viscosity solution, **surface tension** is the dominant factor. In such a case, only beads or fibers containing beads are formed. By the way, due to the high chain complexity, more resistance to electrostatic charges occurs at very high viscosity and a suitable fiber spinning process does not occur. If the solution has sufficient viscosity, continuous fibers can be obtained <sup>219</sup>.

Another important parameter affecting the electrospinning process is process parameters. These factors are applied voltage, feed rate, solution temperature, collector type, nozzle diameter and distance between nozzle and collector. A critical voltage threshold must be exceeded for a Taylor cone to form. When the **voltage** is increased, the amount of polymer withdrawn from the nozzle increases and a thicker fiber is formed. When it is increased too much, multijets are formed and fine fibers are obtained <sup>219,220</sup>. In order to obtain a smooth and uniform nanofibrous structure, the critical distance must be maintained. In the studies, when the distance between the nozzle and the collector is kept short, large diameter nanofibers were obtained. It has been observed that the fiber diameter decreases when the **distance** between the nozzle and the collector is kept long. It is also recommended to use **small nozzles** to obtain small diameter

fibers. Also, electrospinning with a **low feed rate** is generally preferred as it. takes time for the solvent to evaporate <sup>221</sup>.

The effects of the ambient conditions in which electrospinning is carried out on the polymer jet is a subject that has been little researched. However, the humidity of the environment in which the jet is located, the type and pressure of the atmosphere are the factors affecting the electrospinning jet and the structure of the fibers obtained. **Relative humidity** also determines the evaporation rate of the solvent. At very low relative humidity, the solvent can evaporate very quickly. In fact, evaporation can take place while the solution is still at the tip of the nozzle, and solidification occurs at the nozzle tip. This leads to blockages and hinders electro attraction <sup>195</sup>. The **composition of the air** in the environment where electro-gravitation takes place is also important. Because some gases behave differently under high electric field. When electrospinning is performed at a pressure lower than atmospheric pressure, the solution in the syringe tends to flow out more and this causes unstable jet initiation <sup>195</sup>. When the relationship between the relative humidity of the environment and the fiber diameters formed was examined, it was observed that the fiber diameters obtained increased as the humidity increased. This is explained by the increase in the electrical charge of the polymer as the humidity increases.

#### 1.4. Studies on electrospun fibers with cyclodextrin inclusion complexes

Inclusion complexes and electrospinning methods have been used for encapsulation of essential oils and active substances with superior properties. In recent years, these methods have been combined to take advantage of the encapsulation benefits of each method and it is suggested that future research on the biomedical application of encapsulation of plant extracts should focus on this combination. Inclusion complexes can be mixed with electrospinnable polymers or used as key components of electrospun nanofibers. Cyclodextrin functional electrospun fibers are categorized in three ways; cyclodextrin/drug blended polymeric fiber, polycyclodextrin/drug fiber and polymer free-cyclodextrin/drug fiber. Schematic representation of obtaining electrospun fibers with cyclodextrin inclusion complexes are shown in **Figure 32**.

For obtaining cyclodextrin/drug blended polymeric fiber, cyclodextrin is dissolved in water and the active compound is added slowly and mixed for a certain time. After obtaining the inclusion complex, the complex can be added to the polymer solution in two forms; (i) in aqueous form or (ii) solid form that dried by techniques such as freeze dryer and vacuum <sup>222</sup>. In both cases,

inclusion complex loaded fibers are obtained that have longer dissolution time and sustained release <sup>101</sup>. Unlike the first method, while preparing poly-cyclodextrin/drug fiber, the active substance is added last. For this, the polymeric solution is first prepared. Cyclodextrin was then added to the solution and mixed. Then active compound is added and dispersed under constant stirring <sup>222</sup>. At the end of this, poly-cyclodextrin/drug fibers are obtained to be used in especially controlled drug releases <sup>101</sup>. No polymer is required to obtain polymer free-cyclodextrin/drug fiber. Cyclodextrin is dissolved in water and the active compound is added slowly and mixed for a certain time <sup>222</sup>. After obtaining the inclusion complex, they are electrospun directly without the need for polymer. Unlike other fibers, these fibers rapidly dissolve on contact with water and no controlled release <sup>101</sup>. Because of this feature, they are especially using in fast dissolving drug delivery systems <sup>223–225</sup>.

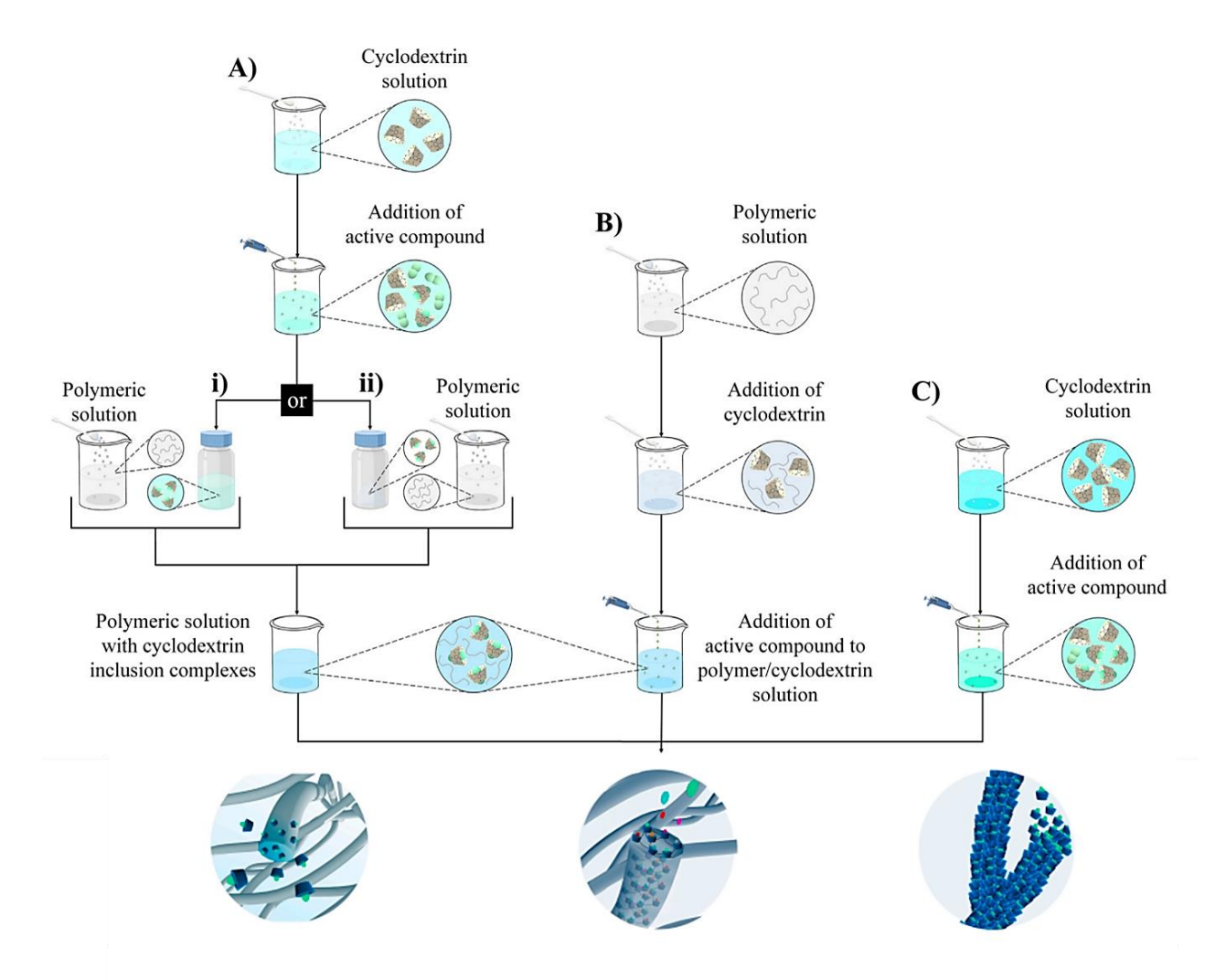


**Figure 32.** Schematic representation of obtaining electrospun fibers with cyclodextrin inclusion complexes in different ways (a) cyclodextrin/drug blended polymeric fiber, (b) polycyclodextrin/drug fiber and (c) polymer free-cyclodextrin/drug fiber <sup>101,222</sup>.

Most of the research in this area has focused on blending cyclodextrin-drug inclusion complexes with various polymers. Literature review on this research is listed in **Table 9**. As shown in Table 9, cyclodextrin/drug blended polymeric fiber have often been used to increase the thermal stability, water solubility and control release of plant extract compounds encapsulated in electrospun fibers. Due to antibacterial properties of these fibers, they are also used in antibacterial dressing and antimicrobial packaging. As the antibiotic, essential oil and active substance can be incorporated into the fibers, studies with essential oil have been examined in detail in relation to the thesis. When a comprehensive literature review was conducted, two studies were found on essential oil-inclusion complexes published in 2016 and 2017.

Antunes et al. incorporated eucalyptus essential oil/β-CD inclusion complexes into the zein via electrospinning method to obtain antibacterial cyclodextrin/drug blended polymeric fiber <sup>120</sup>. For this, first, eucalyptus essential oil was molecularly encapsulated with β-CD by coprecipitation method and then dried form of the complex added to the zein polymer solution. The parameters used in electrospinning are as follows; 1 mL/h flow rate, +18 kV voltage, 15 cm distance,  $23 \pm 2$  °C temperature,  $45 \pm 2\%$  relative humidity, 1 mL syringe with 0.7 mm diameter. FT-IR, SEM and TGA analysis indicated the presence of the complex in the fiber and homogeneous, cylindrical bead-free fibers obtained. Before examining the antibacterial effect of the fiber, the effect of eucalyptus essential oil alone first tested with the disk method, MIC and MBC and found that the eucalyptus essential oil showed higher sensitivity against Gram (S.positive and B. cereus) than Gram aureus. L. monocytogenes negative bacteria (S. typhimurium, E. coli, P. aeruginosa and S. dysenteriae). The antibacterial activity result of electrospun eucalyptus essential oil/β-CD-IC-zein membrane confirmed the presence of essential oil inside of fiber by micro-atmosphere technique with cell counting method. While fibers without the addition of inclusion complexes did not inhibit bacteria, it was found that bacterial inhibition increased as the amount of complex increased. In same method, Wen et al. was produced cinnamon bark essential oil/ β-CD inclusion complex loaded fiber by using polylactic acid <sup>138</sup>. After characterizing the inclusion complex with SEM, FTIR and TGA analyzes, wetting ability and thermal property of cinnamon essential oil/β-CD-IC-polylactic acid nanofilm was analyzed. A decrease in the water contact angle value was observed on the film surface due to the presence of the inclusion complex. Also, the antibacterial property of the complex loaded fibers (containing 80% trans-cinnamaldehyde) was evaluated against S. aureus and E. coli by both agar diffusion assay and broth dilution method. It was found that it had a higher antibacterial effect than the uncomplexed oil loaded fibers. Also, Wen et al. checked the antibacterial effect of these fibers on pork for use in packaging by viable microbial counts and found that electrospun cinnamon essential oil/ $\beta$ -CD-IC-polylactic acid nanofilm increased the shelf life of pork <sup>138</sup>.

In addition to the use of antibacterial electrospun fibers with cyclodextrin inclusion complexes in food packaging, these fibers are also used to accelerate wound healing. Li et al. produced enrofloxacin and flunixin meglumine/ $\beta$ -CD inclusion complex loaded thermoplastic polyurethane fiber via electrospinning and the fiber examined whether it is suitable for use as a dressing  $^{226}$ . The results indicated that these fibers showed high water uptake capacity, hydrophobic outer surface, sustained drug release and antibacterial activity, that is, they have the perfect characteristics of an ideal dressing. Wound healing effect of these fiber was also confirmed on mouse model by in-vivo experiment. However, antibiotics were used in this study and there are no studies on wound healing application of essential oil/cyclodextrins loaded fibers. Instead of antibiotic, using natural oils with wound healing properties such as cinnamon leaf essential oil has promising potential.

It is known to be advantageous to use pH sensitive polymers since the wound pH changes during the healing process, especially for diabetic wounds. The pH of the wound increases in the presence of bacteria proliferation on the ulcer which is chronic complications of diabetes <sup>227,228</sup>. These microbial infections cause high inflammatory responses and cause incomplete and longterm healing of the wound <sup>229</sup>. Considering the slow recovery time of these patients, controlled drug release systems are of interest. Thanks to this system, drugs are delivered at controlled rate according to the pathophysiological need of the disease, thus allowing prolonged release, reduced dose frequency and improved patient therapeutic efficacy and compliance <sup>230,231</sup>. Eudragit S100 and Eudragit L100 are a "smart" and "stimulus-responsive" polymeric materials because of responding to changes in the environment as pH <sup>232</sup> and effective carriers for controlled drug release and drug encapsulation <sup>233</sup>. However, there are no studies done with these pH sensitive Eudragit polymers and essential oil/cyclodextrin inclusion complexes. For targeted and controlled delivery, Coban et al. was incorporated niclosamide/HPβ-CD-IC into pH sensitive Eudragit L100 polymer by electrospinning <sup>234</sup>. For this, niclosamide was encapsulated with HPβ-CD by freeze-drying method at 1:1 molar ratio and then dried form of the complex added to the Eudragit L100 polymer solution that dissolved in DMAc: methanol. The parameters used in electrospinning are as follows; 1 mL/h flow rate, +15 kV voltage, 20 cm distance,  $23 \pm 2$  °C temperature, 20 % relative humidity, 3 mL syringe with 0.6 mm diameter. Niclosamide/HP $\beta$ -CD-IC-Eudragit L100 fiber was characterized by XRD, FT-IR, SEM, DSC and TGA. Niclosamide/HP $\beta$ -CD-IC-Eudragit L100 fiber also dissolved at pH 1.2 (simulating stomach) and pH 7.4 (simulating colon) conditions to obtain a pH-sensitive release profile and to prevent the immediate release of the antibiotic. It was found that that niclosamide releases less in the stomach when it encapsulated with HP $\beta$ -CD and Eudragit L100.

Table 9. A literature research on electrospun fibers with cyclodextrin inclusion complexes

Cyclodextrin	Active molecule	Polymer	Results/Applications	References
β-CD	Dexamethasone	Poly(lactic-co-	Dental pulp therapy	235
		glycolic acid)		
HP- β-CD	Curcumin	-	Antioxidant	236
β-CD	Amino	Poly-ε-caprolactone	Biomedical	237
HP-βCD, M-	Linalool	-	Antibacterial,	238
βCD, and			Prolonged release	
HP-γCD				
β-CD	Quercetin	Polyacrylic acid	Slow release, High	239
			solubility	
HP-βCD, M-	Thymol	-	High thermal	117
βCD, and			stability	
HP-γCD				
НР-βСД	Metronidazole	-	Fast-dissolving oral	223
			drug delivery	
НР-βСD	Thiabendazole	-	Antifungal	240
HP-βCD, M-	Limonene	-	Antibacterial,	241
βCD, and			Prolonged release	
HP-γCD				
НР-βСD,	Cinnemaldehyde	-	Antibacterial, High	242
HP-γCD	-		thermal stability	
НР-ВСД	Vitamin E	-	Enhanced water	243
•			solubility,	
			Prolonged release	

НР-βСD,	Alpha-lipoic acid		Antioxidant	244
HP-γCD				
β-CD	Xylanase	Polyvinyl alcohol	Improved enzyme	245
			activity	
HP-βCD	Ciprofloxacin	Gelatin	Enhanced wettability	246
SBE-βCD	Sulfisoxazole	-	Enhanced wettability	247
HP-βCD, M-	Eugenol	-	High thermal	143
$\beta$ CD, and			stability	
HP-γCD				
НР-βСД	Curcumin	Polylactic acid	Enhanced water	248
			solubility, slow	
			release	
НР-βСД	Gallic acid	Polylactic acid	Prolonged release	249
НР-βСД	Sulfisoxazole	Hydroxypropyl	Prolonged release	250
		cellulose		
НР-βСД	Ibuprofen	-	Fast-dissolving oral	224
			drug delivery	
НР-βСД	Rutin	Poly(vinyl alcohol)	Ultraviolet resistant	251
HP-βCD, M-	Vanillin	-	Enhanced water	126
βCD, and			solubility, High	
HP-γCD			thermal stability	
γ-CD	Thymol	Zein	Antibacterial,	252
			Prolonged release	
β-CD	Eucalyptus	Zein	Antibacterial	120
	essential oil			
HP-βCD	Hydrocortisone	-	Fast-dissolving oral	225
			drug delivery	
M-βCD	Isoflavone formo	Polyvinyl-alcohol	Enhanced water	253
	nonetin		solubility, Fast-	
			dissolving oral drug	

Niclosamide	Eudragit® L100	Colon targeted	234
		delivery	
Menthol	Poly(methyl	High thermal	254
	methacrylate)	stability	
Cinnamon	Polylactic acid	Antimicrobial	138
essential oil		packaging	
Eugenol	Polyvinyl alcohol	High thermal	255
		stability, Prolonged	
		release	
Quercetin	Star-shaped	Antibacterial	229
	polylactides	dressing	
Enrofloxacin and	Polyurethane	Wound healing	226
flunixin			
meglumine			
	Menthol  Cinnamon essential oil  Eugenol  Quercetin  Enrofloxacin and flunixin	Menthol Poly(methyl methacrylate)  Cinnamon Polylactic acid essential oil  Eugenol Polyvinyl alcohol  Quercetin Star-shaped polylactides  Enrofloxacin and Polyurethane flunixin	Menthol Poly(methyl High thermal methacrylate) stability  Cinnamon Polylactic acid Antimicrobial essential oil packaging  Eugenol Polyvinyl alcohol High thermal stability, Prolonged release  Quercetin Star-shaped Antibacterial polylactides dressing  Enrofloxacin and Polyurethane Wound healing flunixin

## 1.5. Aim of the study

The aim of this study was to produce cinnamon leaf oil/β-CD-inclusion complex loaded Eudragit S100 fiber and cinnamon leaf oil/SBE-β-CD-inclusion complex loaded Eudragit S100 fiber by electrospinning method for antibiotic-free wound healing applications and characterize the physico-chemical properties, wetting ability, and water uptake capacity of the electrospun fibers. Cinnamon leaf oil/β-CD-inclusion complex and cinnamon leaf oil/SBE-β-CD-inclusion complex were aimed to impart antibacterial activity to Eudragit S100 fibers. It was also aimed to achieve controlled and sustainable release of essential oils from fibers, which are obtained by using 'smart' and "stimulus-sensitive" polymeric material and inclusion complex, depend on pH of environment. Also, cytotoxic effect of these fibers was tested on L929 fibroblast cell line. According to best knowledge, this is the first study in which complex of cyclodextrin and essential oil are used in the structure of Eudragit S100 electrospun fibers for wound healing application.

#### 2. Materials and Methods

#### 2.1. Materials

Eudragit® S100 polymer (anionic copolymer, methyl methacrylate and methacrylic acid) was gifted from Evonik Industry in Gebze. The materials required to form the inclusion complexes and antibacterial assay were listed in Chapter 1. For cell viability fetal bovine serum, Dulbecco's modified Eagle's medium-high glucose (DMEM-HG), penicillin/streptomycin, and trypsin/EDTA were obtained from Biological Industries (BI). L929 cell line (mouse fibroblast cell) was purchased from Sigma. WST-1 assay kit was purchased from Abcam.

#### 2.2. Methods

#### 2.2.1. Preparation of Eudragit polymeric solution with and without inclusion complexes

Eudragit S100 polymer was used as electrospinning solution for the production of electrospun fibers. Before producing inclusion complex loaded Eudragit S100 fibers, optimization studies were carried out on pristine fibers. For this, Eudragit S100 powder (1.2 g and 0.6 g) was dissolved in 4 ml ethanol to obtain 25% (w/v) and 12% (w/v) Eudragit solution, respectively. These solutions were stirred for approximately for 24 hours yield a homogenous solution. Then, CEO-β-CD-IC loaded Eudragit S100 fiber and CEO-SBE-β-CD-IC loaded Eudragit S100 fiber were fabricated with selected concentration. To produce these fibers, 12% (w/v) Eudragit S100 powder was dissolved in ethanol for approximately for 24 hours to be homogeneous. Then 100 mg of the inclusion complex was added the Eudragit S100 solution and mixed for 2 hours until complete dissolution of inclusion complexes.

## 2.2.2. Production of pristine and Cinnamon leaf oil/Cyclodextrin-Inclusion Complex loaded Eudragit S100 fiber by electrospinning

Each electrospinning solution was separately taken into a 5 ml plastic syringe, and it was placed in the syringe pump. The electrospun fibers were collected on collector covered with aluminum foil. The distance between the collector plate and the tip of the injector was 12 cm, the solution feed rate was 5 mL/h, and the voltage value was 18 kV. All electrospinning processes were carried out at room temperature and the produced nanofibers were stored at +4 °C. Experimental setup for electrospinning synthesis of fibers is illustrated in **Figure 33**.

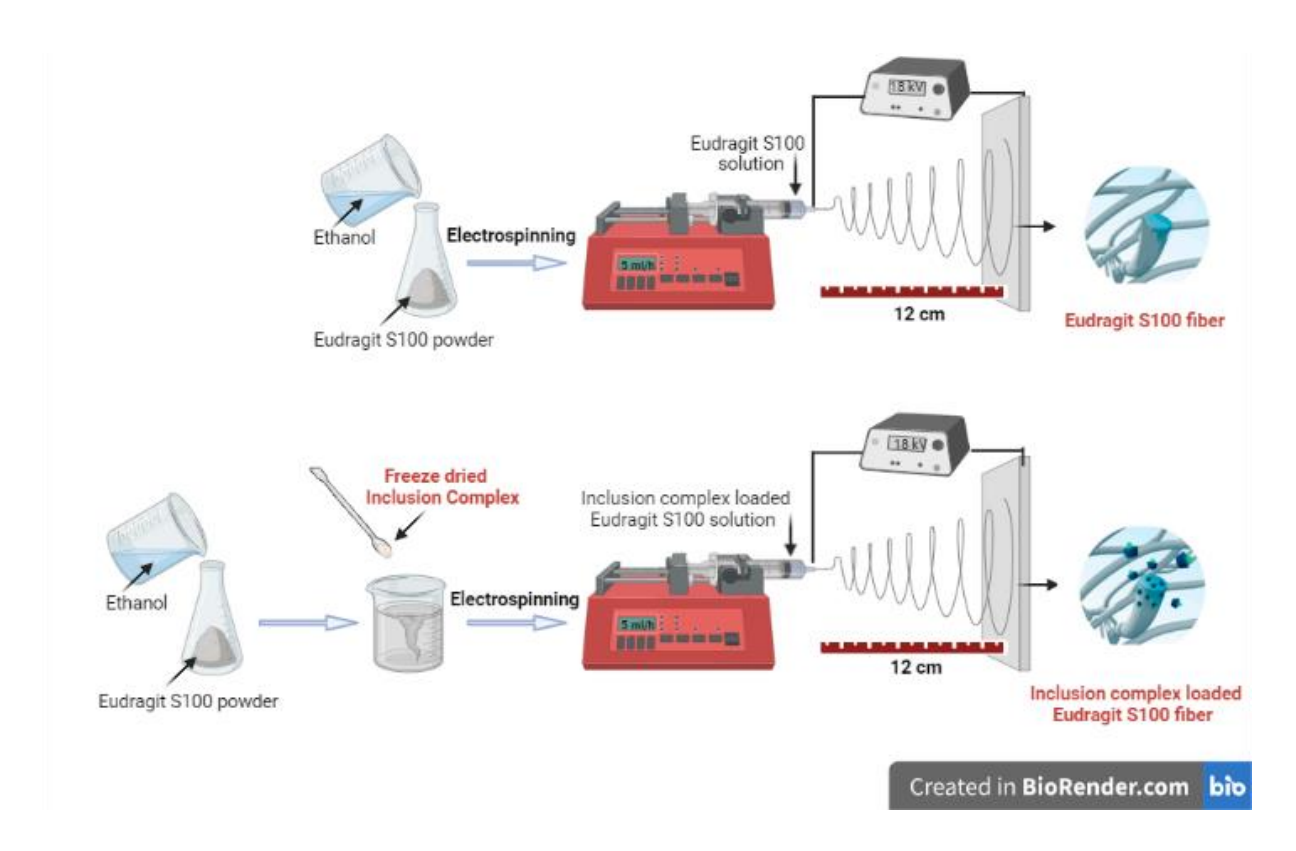


**Figure 33.** Experimental setup for solution preparation and electrospinning process fibers with and without inclusion complexes

# 2.2.3. Encapsulation efficiency of Cinnamon leaf oil/Cyclodextrin-Inclusion Complex loaded Eudragit S100 electrospun fiber

The amount of CEO in the CEO/β-CD-IC and CEO/SBE-β-CD-IC loaded Eudragit S100 fibers was determined by solvent extraction method using UV-Vis Spectroscopy <sup>148,149</sup>. Briefly, fibers (14 mg) was weighted into falcon tube and resuspended with 1 ml of ethanol <sup>256</sup>. This solution was vortexed for 5 minutes with high speed to totally dissolve them in solvent. After adding 9 ml of hexane, they were again vortexed at the highest speed for 1 minute. CEO was extracted from CD cavities and fibers with hexane by heating the samples in a glass tube at 45°C in a water bath in heater shaker with intermittent mixing during 2 hr. After the heating period, the solution was kept cooling to room temperature and centrifuged at 4,000 rpm for 20 minutes in order to have supernatant containing the oil. After centrifuging, supernatant was collected by pasteur pipette.

The percentage of EE was determined using the following equation <sup>256</sup>:

EE (%) = 
$$\frac{\text{weight of oil in the nanofiber}}{\text{theoretical weight of oil in the fiber}} \times 100$$

### 2.2.4. Morphology and diameter distribution of electrospun fibers

In order to characterize the fiber diameters and surface morphologies (such as smoothness, uniformity, bead defect formation) of the produced nanofibrous surfaces, gold-palladium coating was applied and analyzed in Scanning Electron Microscope (SEM). The nanofibers morphology was examined in the photographs taken at different magnifications using a 3- kV acceleration voltage. The diameter of 100 fibers was measured on the photographs using ImageJ software.

#### 2.2.5. Functional and thermal properties of electrospun fiber

Functional and thermal properties of prepared electrospun fibers with and without inclusion complexes were obtained with Fourier transform infrared – attenuated total reflection (FTIR – ATR) spectrometer and thermogravimetric analyzer (TGA), respectively. Same parameters and procedures were used as mentioned in **Chapter 1**.

### 2.2.6. Wettability of electrospun fibers

The contact angle measurement was carried out by analyzing the drop shape using the "sessile drop technique". 5 ul of pure water was dropped on the surface of electrospun fibers with the help of a micropipette and the image of the drop on the surface was obtained with the image capture software on the computer integrated into the device.

#### 2.2.7. Water uptake of electrospun fibers

The water uptake study was carried out by immersing 3 mg of electrospun fibers with and without inclusion complexes in water at 37 °C. After overnight incubation, the fibers were removed from the water. The surface water was taken onto the Whatman 1 filter paper, gently wiped and weighed.

The percentage of water uptake was determined using the following equation <sup>257</sup>:

Water uptake (%) = 
$$\frac{\text{weight of the wet fiber} - \text{starting dry weight of the fiber}}{\text{starting dry weight of the fiber}} \times 100$$

### 2.2.8. Antibacterial activity of electrospun fibers

Antibacterial activity of prepared electrospun fibers with and without inclusion complexes determined on *E. coli* (Gram-negative) and *S. aureus* (Gram-positive) bacteria according to

method proposed by Unalan et al. with some modifications  $^{258}$ . For this, the bacterial strains were grown in LB broth medium for 18 h on a 200-rpm shaker at 37 °C. 10 ul of adjusted cultures ( $OD_{600}=0.1$ ) of bacterium were added separately in tubes containing 3 mL of PBS. UV irradiation was applied on electrospun fibers for 10 minutes for both sides. 150 mg of UV-sterilized inclusion complex loaded fibers added to the culture and incubated at 37 °C for 24 h. 0.1 ml of the above culture containing PBS, bacteria and fiber was spread on a LB agar plate. It was incubated again at 37 °C for 24 hr. Same amount of essential oil that was in electrospun fibers was used as a positive control and electrospun fibers alone were used as a negative control. The images of plates were taken with Bio-Rad Gel Imaging System. The colonies are counted and the percentage of antibacterial activity of fibers were measured determined using the equation  $^{152}$ :

% Antibacterial activity = (population number of control bacteria - population number of experimental bacteria) / population number of control bacteria x 100

## 2.2.9. Drug release assay

The release profile of cinnamon leaf oil from pH sensitive nanofibers was investigated by UV-Vis spectrometry. For this, fibers loaded with inclusion complex weighing 10 mg were immersed in a flask with 20 ml of PBS at normal pH and acidic pH. Solution was continuously stirred at 37 °C for 160 h. 3 ml of medium was taken at the specified time intervals and read in UV-Vis spectrometry. The amount released was determined by the detection of eugenol in the medium. For this, a wavelength of 280 nm was used. After completion of reading, same sample dropped back to the flask and continued to be stirred.

#### 2.2.10. Cell viability assay

In vitro cytotoxicity of CEO/β-CD-IC and CEO/SBE-β-CD-IC loaded Eudragit S100 fiber, CEO and pristine Eudragit S100 fiber on L929 fibroblast cell line was investigated by WST-1 assay according to method proposed by Napavichayanun et al and Unalan et. al <sup>259,260</sup>. L929 cells were cultured in DMEM-HG included %5 FBS, %1 L-glutamine and %1 antibiotic (penicillin and streptomycin) at 37 °C under 5 % CO<sub>2</sub>. The cells (10<sup>4</sup> cells/well) were seeded in 96 well plates and incubated until they reached 80% density. At the same time, samples were prepared for cytotoxicity test. For this, each sterilized samples were and soaked in 5 ml DMEM and incubated at 37 °C. The extracted solutions were replaced with the growth medium in 96 well plates and incubated for 24 and 48 hr at 37 °C under 5 % CO<sub>2</sub>. At the end of the period, the viability of the cells was analyzed with the WST-1 agent. For this, 10 μl of WST solution

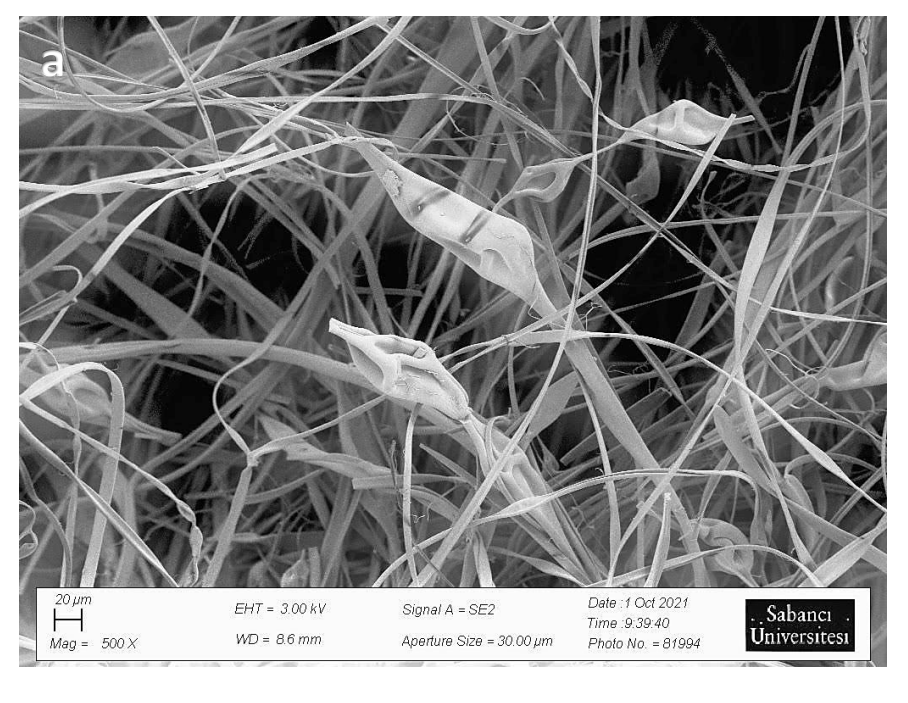
was added into each well of 96 well and the plates were incubated at 37°C for 2 hours. After incubation, optical density (OD) was evaluated using a micro-plate reader at 460 nm wavelength. Each experiment was repeated three times. Cell media (DMEM) was used as a negative control.

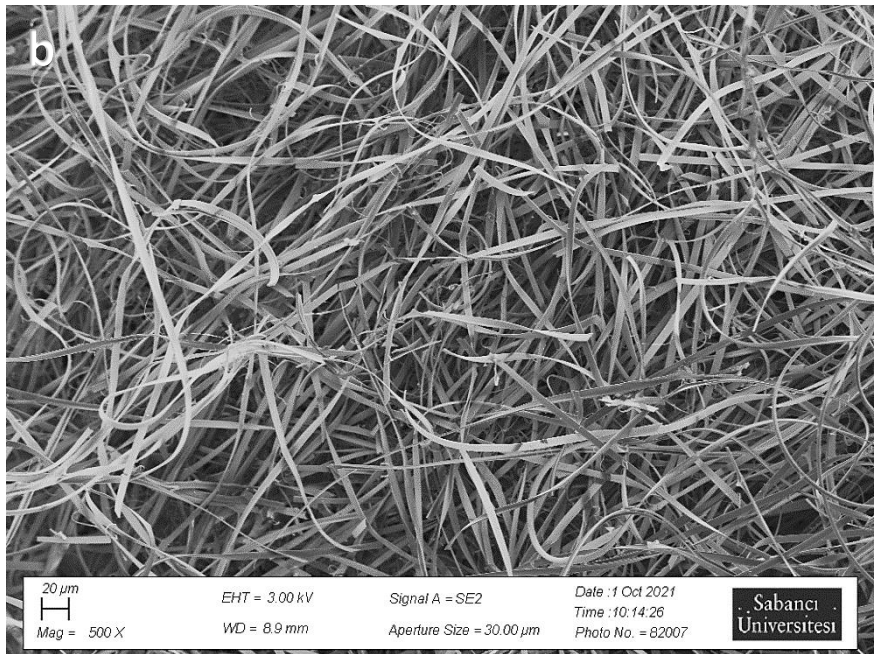
#### 3. Results and Discussion

### 3.1. Morphology and diameter distribution of electrospun fibers

One of the most important factors for the successful preparation of electrospun polymer nanofibers is the selection of the appropriate solvent <sup>261</sup>. The solvent should be able to spin the polymer solution and at the same time should be able to easily dissolve the drug placed in it <sup>262</sup>. Polymers can be dissolved by using toxic solvent as DMF, THF and DMAC. Although these toxic solvents evaporate during electrospinning, the fibers should be kept under UV for overnight or in a vacuum desiccator to eliminate the toxicity completely. This may damage the capsules that will be loaded into the fiber. Polymers such as Eudragit is able to be electrospun when they are dissolved in ethanol which is not particularly toxic solvent <sup>256,263</sup>. In this study, Eudragit S100 polymer was dissolved in ethanol overnight until it has homogenous appearance.

It is known that Eudragit fibers alone show good spinnability <sup>264</sup>. Before producing inclusion complex loaded Eudragit S100 fibers, optimization studies were carried out on pristine fibers. For this, firstly parameters as the distance between the collector plate and the tip of the injector, the solution flow rate and the voltage value were optimized. Low voltage and flow rate in the experiments caused <u>no continuous jets</u>. 5 ml/hr flow rate, 12 cm distance and 18 kV voltage were applied for electrospinning process, and it was resulting with creating no drops on the fibers web. These parameters were selected to compare the morphological difference of the electrospinning fiber with different Eudragit S100 polymer concentrations ((25% (w/v) and 12% (w/v)). Although the fibers prepared with Eudragit S100 polymer at a concentration of 25% had the ability to form fibers, they formed a large amount of half-hollowed beads (**Figure 34a**). As the concentration decreased, bead-free fibers were formed and its general distribution improved (**Figure 34b**). For this reason, it was continued with 12% (w/v) Eudragit S100 in further studies.

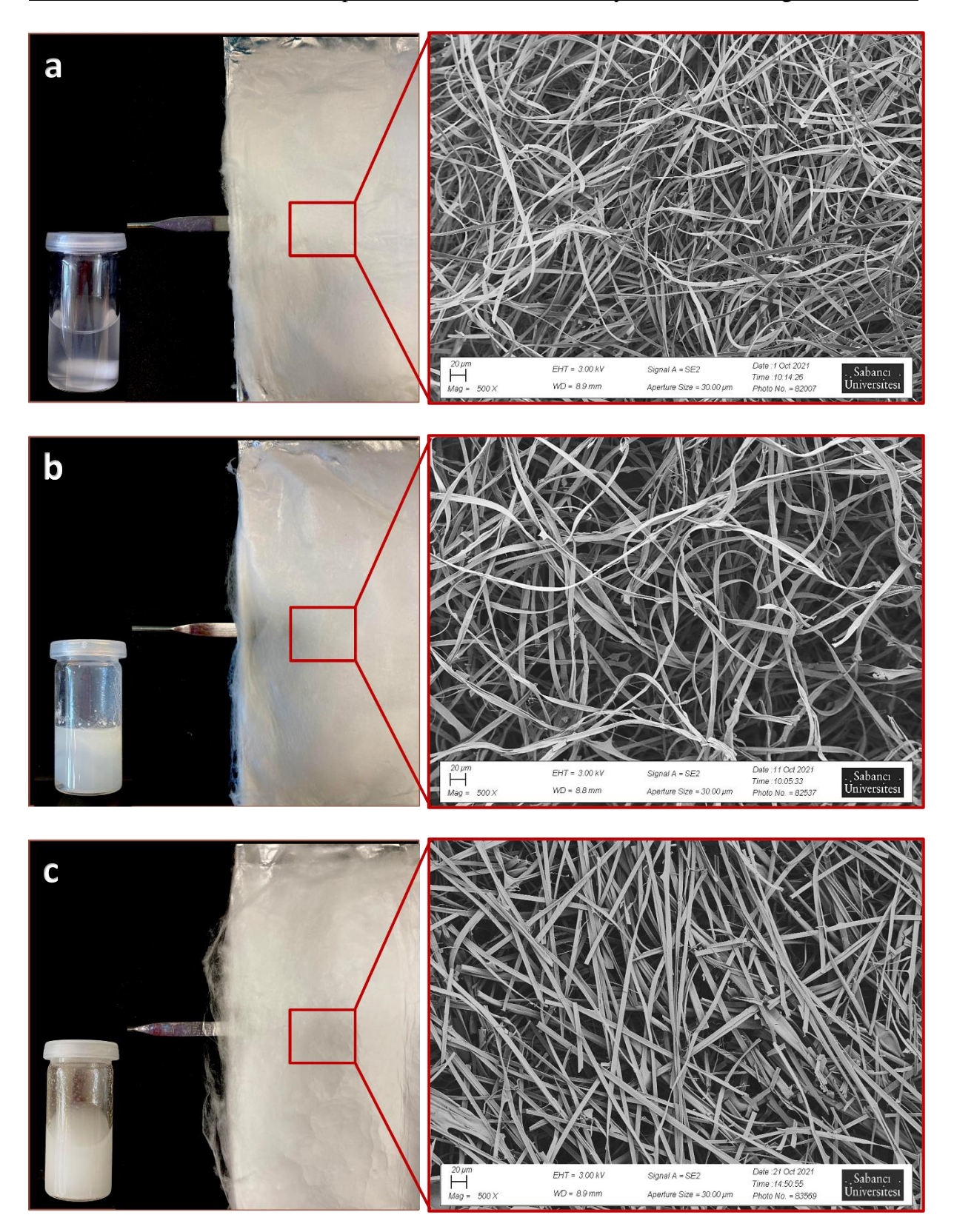




**Figure 34.** SEM micrographs of pristine Eudragit S100 fiber at different concentrations 25 % (a) and 12 % (b) at magnification 500 X.

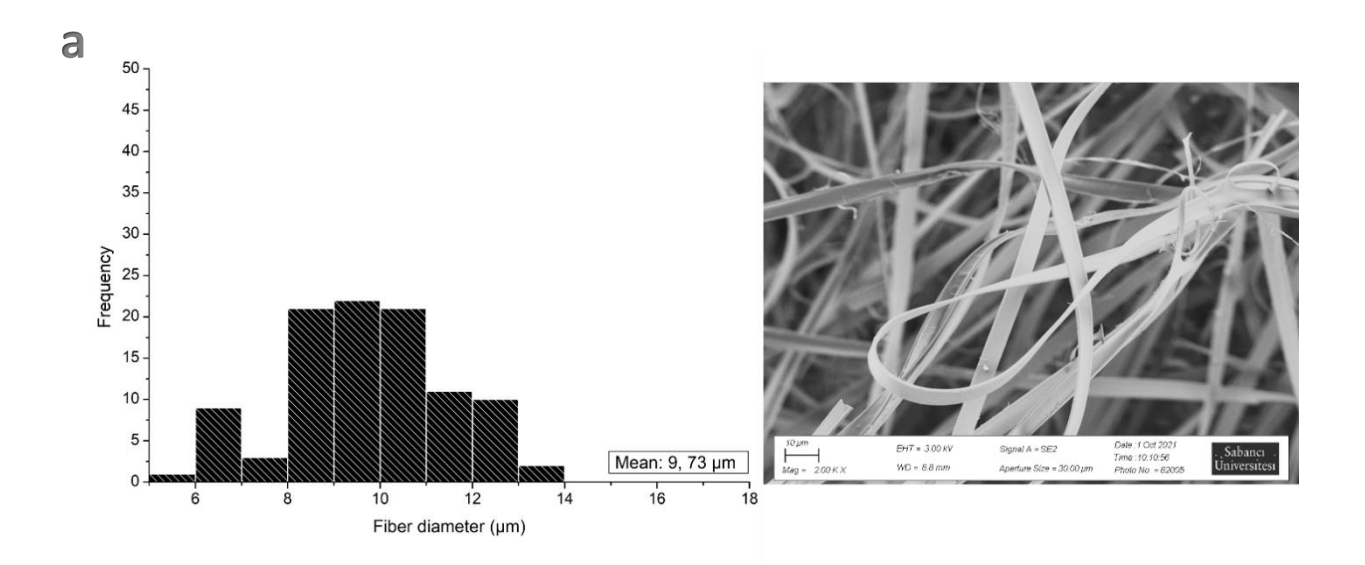
**Figure 35** show SEM micrographs of pristine Eudragit S100 fiber, CEO/βCD-IC loaded Eudragit S100 fiber and CEO/SBE-βCD-IC loaded Eudragit S100 fiber with objective values ranging 500 X. It can be seen in these images that pristine electrospun fiber and inclusion complex loaded fibers have a highly homogeneous structure. Although they have some broken fibers, it was shown that fiber with Eudragit polymer tend to be a flat and shorter shape with ribbon-like  $^{255,264}$ . They have a smooth surface and bead-free form with no drug crystals visible.

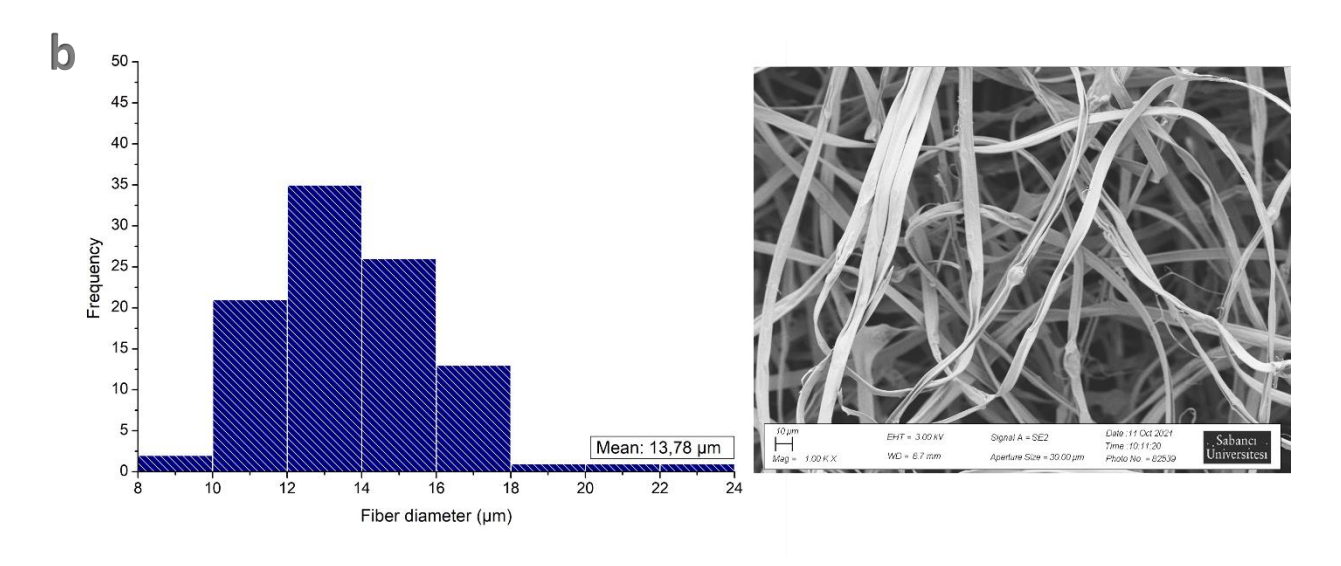
There is also no aggregation due to inclusion complexes in inclusion complex-loaded fibers. This indicates that inclusion complexes have been successfully loaded in Eudragit S100 fiber.



**Figure 35.** SEM micrographs of (a) pristine Eudragit S100 fiber, (b) CEO/βCD-IC loaded Eudragit S100 fiber and (c) CEO/SBE-βCD-IC loaded Eudragit S100 fiber at 500X.

After comparing the morphological differences by SEM, fiber diameters were measured using Image J2x program. The viscosity of the electrospun polymer solution is one of the most important factors affecting the size of the fiber <sup>265</sup>. It was explained that higher viscosity caused larger fiber diameter <sup>266</sup>. In this study, the viscosity of the Eudragit S100 polymer solution alone was lower before adding the complex. However, the viscosity of the solution increased when the inclusion complex was added, as there was interaction between Eudragit S100 polymer chains and the cinnamon leaf oil and cyclodextrin molecule. Fiber diameter distribution of the (a) pristine Eudragit S100 fiber, (b) CEO/βCD-IC loaded Eudragit S100 fiber and (c) CEO/SBE-βCD-IC loaded Eudragit S100 fiber are depicted in Figure 36. The mean fiber diameter of pristine Eudragit S100 fiber was measured to be 9, 73 µm. On the other hand, inclusion complex loaded Eudragit S100 fibers led to an increase in fiber diameters. The average diameter of fiber was 13,78 μm for CEO/βCD-IC loaded Eudragit S100 fiber and 13,02 μm for CEO/SBE-βCD-IC loaded Eudragit S100 fiber. These results support the reports which showed thicker nanofiber when PVA nanofibers encapsulating eugenol/β-CD-IC <sup>255</sup> and Eudragit L100 fibers encapsulating niclosamide/β-CD-IC <sup>234</sup>. Ao et al. also found similar results that the diameter of quercetin loaded Eudragit L100 fiber was 7-9 µm <sup>264</sup>.





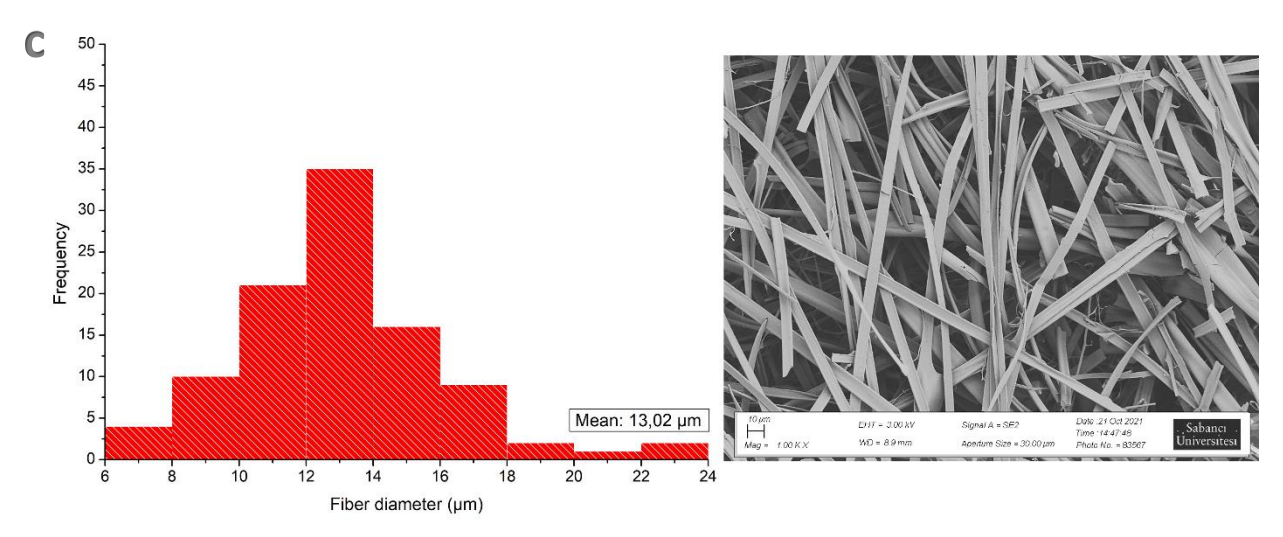


**Figure 36**. Fiber diameter distribution of the (a) pristine Eudragit S100 fiber, (b) CEO/ $\beta$ CD-IC loaded Eudragit S100 fiber and (c) CEO/SBE- $\beta$ CD-IC loaded Eudragit S100 fiber.

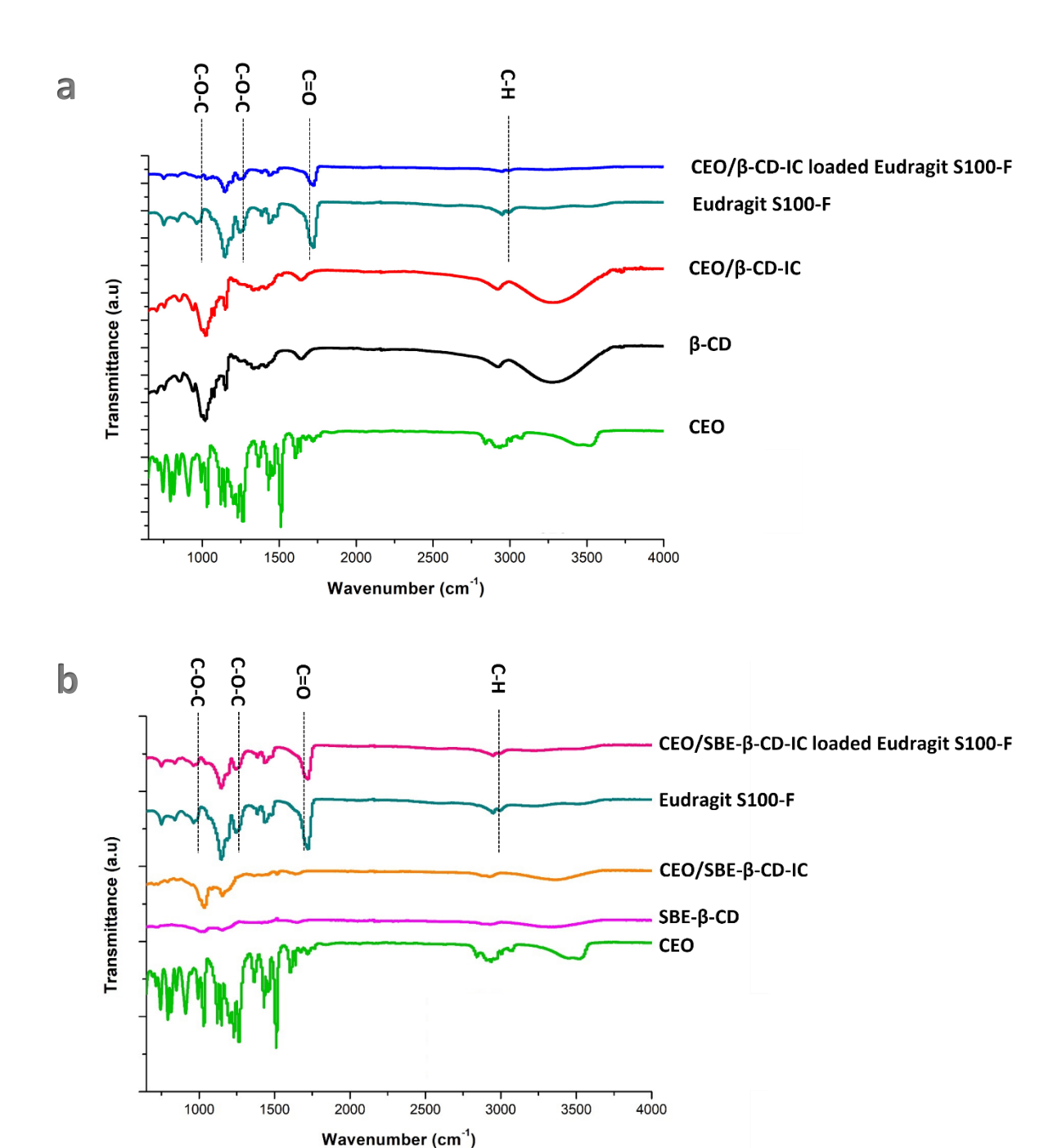
## 3.2. Encapsulation efficiency of Cinnamon leaf oil/Cyclodextrin-Inclusion Complex loaded Eudragit S100 electrospun fiber

Encapsulation efficiency of inclusion complex loaded Eudragit S100 fiber was determined by using by UV-Vis spectroscopy. The standard curve (y=0.0243x+00789,  $R^2=0.997$ ) was used to determine the oil content in fiber. The percentage of encapsulation efficiency was 51% for CEO/ $\beta$ CD-IC loaded Eudragit S100 fiber and 45% for CEO/SBE- $\beta$ CD-IC loaded Eudragit S100 fiber. Studies with essential oil or its active component in fiber showed that the encapsulation efficiency of polyacrylonitrile nanofibers containing lavender essential oil was 32.4%  $^{267}$  and pullupan nanofibers containing eugenol was 22.5%  $^{268}$ . The low encapsulation efficiency of these fibers is due to the fact that these volatile compounds evaporate from the polymeric matrix easily during preparation of solution and electrospinning process. However,

the encapsulation efficiency of eugenol/gamma cyclodextrin ( $\gamma$ CD) loaded pullupan nanofibers was 92% <sup>268</sup>. High encapsulation efficiency was also found for menthol/HP- $\beta$ CD-IC nanofibers (75%) and menthol/HP- $\gamma$ CD-IC nanofibers (70%) <sup>269</sup>. It means that by forming an inclusion complex of active component with cyclodextrin, a high amount of component was preserved and high efficiency was achieved in electrospinning <sup>268</sup>.

### 3.3. Functional and thermal properties of electrospun fibers

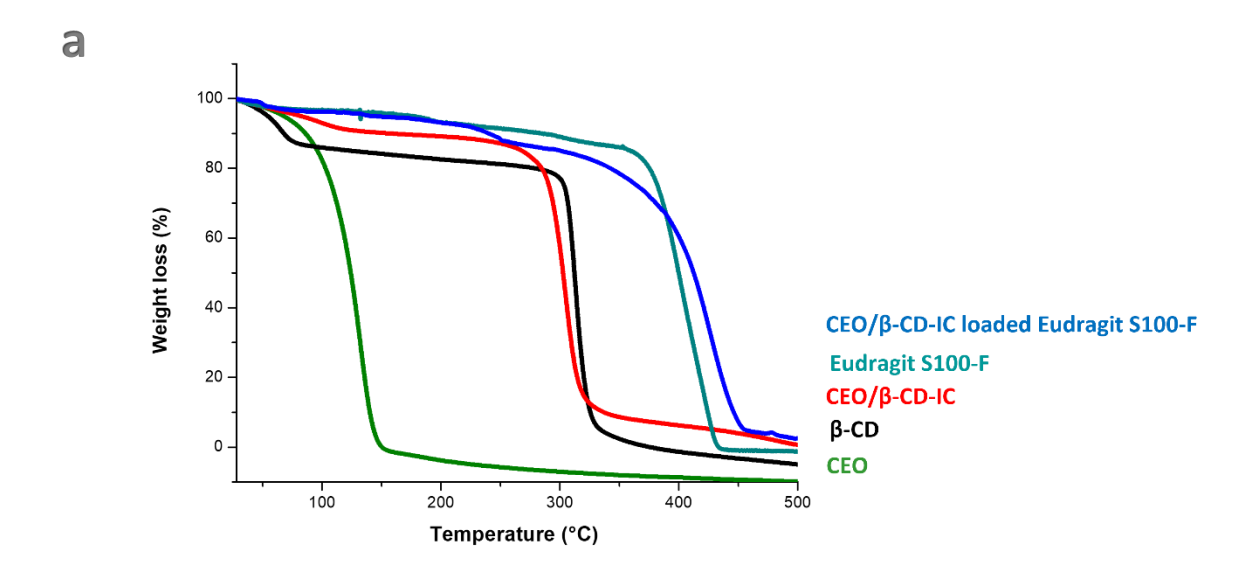
ATR-FTIR spectra of pristine Eudragit S100 fiber and the electrospun fibers with the inclusion complexes were shown in Figure 37. For comparison, ATR-FTIR spectra of pure cinnamon leaf oil, cyclodextrin and inclusion complexes were displayed in same figure. The ATR-FTIR spectra of Eudragit S100 show characteristic peaks at 2950.46 cm<sup>-1</sup> caused by C-H stretching of vibration. It has C=O stretching vibrations at 1722.70 cm<sup>-1</sup> and peaks at 1245.22 cm<sup>-1</sup> and 1148.55 cm<sup>-1</sup> assigned to the C-O-C stretching vibration <sup>270</sup>. Upon the incorporation of inclusion of the CEO/ βCD-IC, the C=O band from the pristine fibers shifted from 1722.70 cm<sup>-1</sup> to 1723.12 cm<sup>-1</sup> and the C-H band shifted from 2950.46 cm<sup>-1</sup> to 2949.65 cm<sup>-1</sup>. C-O-C stretching vibration was shifted to  $1244.21~\text{cm}^{-1}$  and  $1148.72~\text{cm}^{-1}$  in CEO/ $\beta$ CD-IC loaded Eudragit S100 fiber. Interactions among Eudragit S100 and inclusion complexes were proved by the band shifts observed in the FTIR-ATR spectra of pristine fiber and inclusion complex loaded Eudragit S100 electrospun fibers. Also, characteristic peak of cinnamon leaf oil at 1637 cm<sup>-1</sup> and 1674 cm<sup>-1</sup> and inclusion complex at 1604 cm<sup>-1</sup> C=C stretching vibration indicating inclusion complex formation were absent in case of incorporating inclusion complex into Eudragit S100 electrospun fibers. Similar results were found for CEO/SBE-βCD-IC loaded Eudragit S100 fiber. Upon the incorporation of inclusion of the CEO/SBE-βCD-IC, the C=O band from the pristine fibers shifted from 1722.70 cm<sup>-1</sup> to 1721.95 cm<sup>-1</sup> and the C-H band shifted from 2950.46 cm<sup>-1</sup> to 2950.15 cm<sup>-1</sup>. C-O-C stretching vibration was shifted to 1244.21 cm<sup>-1</sup> and 1147.56 cm<sup>-1</sup> in CEO/SBE-βCD-IC loaded Eudragit S100 fiber. These data suggest that CEO/βCD-IC and CEO/SBE-β-CD inclusion complexes were efficiently incorporated in the Eudragit S100 fiber. These findings are is in agreement with similar studies <sup>117,271</sup>.



**Figure 37.** FTIR spectra of pristine fiber, CEO/βCD-IC loaded Eudragit S100 fiber (a) and CEO/SBE-βCD-IC loaded Eudragit S100 fiber (b)

The thermal stability of pristine Eudragit fiber, CEO/βCD-IC loaded Eudragit S100 fiber and CEO/SBE-βCD-IC loaded Eudragit S100 fiber were evaluated using TGA analysis and the results were shown in **Figure 38**. For comparison, weight loss of cinnamon leaf oil, cyclodextrin and inclusion complexes were displayed in same figure. As shown in **Figure 38a** and **Figure 38b**, TGA profile of Eudragit S100 fiber has the main degradation between 360 °C and 440 °C with 85.6% mass loss. When the thermogram of the inclusion complex loaded Eudragit S100 fiber was

examined, there were three weight loss: (i) dehydration of water, (ii) volatilization of complexed cinnamon leaf oil, and (iii) main degradation of Eudragit S100. The main degradation occurs in between 270°C-350 °C for CEO/βCD-IC and 220°C-310°C for CEO/SBE- βCD-IC. The degradation peak of inclusion complexes was shifted to higher temperature (360 °C-440 °C) in case of incorporating in Eudragit S100 fiber as can be seen from the results, cinnamon leaf oil could be effectively preserved to higher temperatures by making an inclusion complex, and this value was maximized by loading the complexes into the Eudragit S100 fiber. In other words, the thermal stability and durability of cinnamon leaf oil were increased by an inclusion complex incorporated in pH sensitive Eudragit S100 fiber.



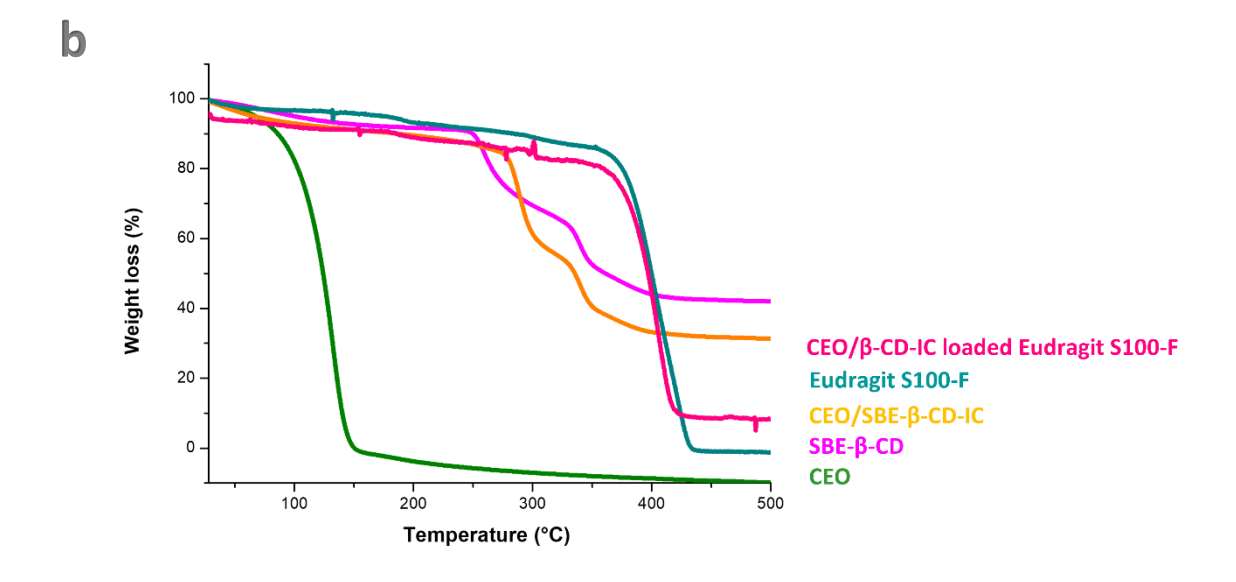


**Figure 38.** TGA of pristine fiber, CEO/ $\beta$ CD-IC loaded Eudragit S100 fiber (a) and CEO/SBE- $\beta$ CD-IC loaded Eudragit S100 fiber (b)

### 3.4. Wettability of electrospun fibers

The fibers to be used as a wound dressing should have certain degree of hydrophilic properties because this feature allows the dressing to adhere to the biological surface and increases the attachment and proliferation of cells <sup>272</sup>. Although Eudragit S100 is hydrophobic, addition of inclusion complex should make them certain degree of hydrophilic. To assess the effect of CEO/βCD-IC loaded Eudragit S100 fiber and CEO/SBE-βCD-IC loaded Eudragit S100 fiber, Eudragit S100 fiber with and without inclusion complexes were characterized by using water contact angle. The surface of the membrane is defined as wet with a contact angle of less than 90 degrees and non-wetting with a contact angle of higher than 90 degrees <sup>273</sup>. The appearance of water on the surface of Eudragit S100 fiber was depicted in Figure 39. Pristine Eudragit S100 fiber was highly hydrophobic as represented by a contact angle of 126.31°, whereas the addition of inclusion complexes changed the surface wettability of electrospun fiber (Figure 39). It was measured 102.1° for CEO/βCD-IC loaded Eudragit S100 fiber and 123.3° for CEO/SBE-BCD-IC loaded Eudragit S100 fiber. Based on this finding, although all fibers produced within the scope of this study exhibited hydrophobic behavior due to the chemical structure of Eudragit S100 polymer, incorporation of inclusion complex to Eudragit S100 fiber make them more hydrophilic with decreasing average water contact angle. It is undesirable for a material that will be used in wound dressing to be excessively hydrophobic (contact angle value higher than 150°) and excessively hydrophilic (contact angle value lower than 10°) <sup>273,274</sup>, because being super-hydrophobic causes irritation on the wound, and being super hydrophilic causes cell adhesion and proliferation on the membrane <sup>275</sup>. Considering this information, it has been found that CEO/BCD-IC loaded Eudragit S100 fiber had a balanced hydrophilic property and more suitable for wound dressing application.

These finding is in agreement with study that contact angle value of electrospun polylactic acid membrane decreased with addition of cinnamon bark essential oil/ $\beta$ -cyclodextrin inclusion complexes <sup>138</sup>. This result might be increasing –OH substituent on the surface of fiber and surface hydrophobicity-modifying effect of cyclodextrin which is an amphiphilic compound <sup>138</sup>

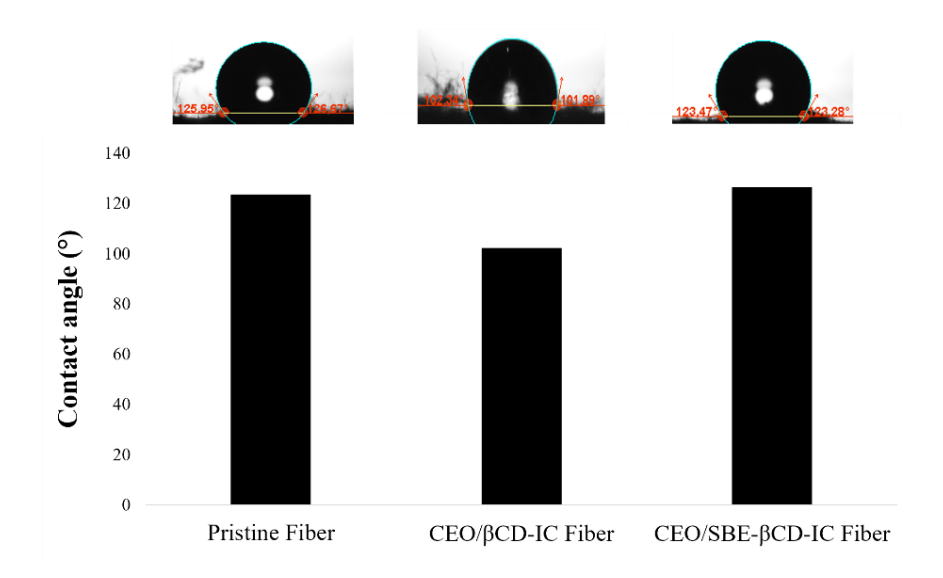
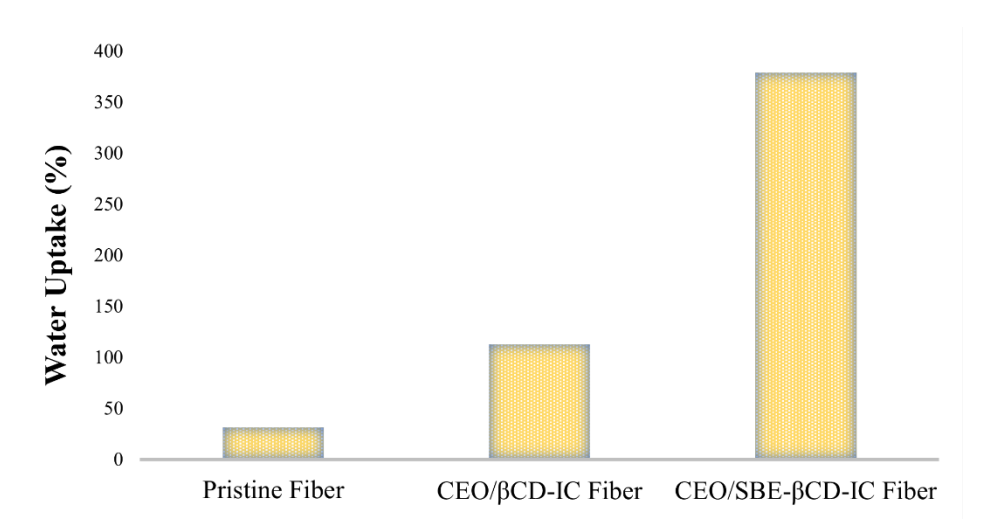


Figure 39. Contact angle of obtained electrospun fibers

#### 3.5. Water uptake of electrospun fibers

The water uptake of Eudragit S100 fiber, CEO/βCD-IC loaded Eudragit S100 fiber and CEO/SBE-βCD-IC loaded Eudragit S100 fiber was examined after 24 hr incubation at 37 °C (**Figure 40**). Although it has hydrophobic character, Eudragit S100 fiber was found to have 31 % water absorption capacity. Similar finding was found for hydrophobic molecule, polycaprolactone when it was electrospinned. These capabilities of fibers to be due to the porosity in the matrix <sup>276</sup>. The water uptake of the electrospun fibers with inclusion complexes were increased compared to pristine fiber. Water uptake capacity was 113 % for CEO/βCD-IC loaded Eudragit S100 fiber and 379 % for CEO/SBE-βCD-IC loaded Eudragit S100 fiber. It is known that increasing the concentration of essential oil was result in lower water uptake <sup>277</sup>. The higher capacity in CEO/SBE-βCD-IC loaded Eudragit S100 fiber can be attributed the solubility effect of SBE-βCD and lower amount of oil inside.



**Figure 40**. Water uptake percentage for Eudragit S100 fiber, CEO/βCD-IC loaded Eudragit S100 fiber and CEO/SBE-βCD-IC loaded Eudragit S100 fiber

### 3.6. Antibacterial activity of electrospun fibers

The antibacterial activity of Eudragit S100 fiber, CEO/βCD-IC loaded Eudragit S100 fiber and CEO/SBE-βCD-IC loaded Eudragit S100 fiber was tested against *E. coli* and *S. aureus*. For this, same amount of all fibers was UV sterilized as shown in **Figure 41**. These fibers were incubated in PBS media includes bacteria for 24 hr and then, spreaded on LB agar. After incubation, CEO/βCD-IC loaded Eudragit S100 fiber showed higher antibacterial activity to both *E. coli* and *S. aureus*. Surviving population of *E. coli* were inhibited totally by using 50 mg/ml CEO/βCD-IC loaded Eudragit S100 fiber (**Figure 42**). Whereas the same amount of CEO/SBE-βCD-IC loaded Eudragit S100 fiber didn't show any antibacterial activity. The higher antibacterial activity of CEO/βCD-IC loaded Eudragit S100 fiber was attributed to having higher encapsulation efficiency. These fibers also exhibited similar antibacterial effect of the CEO/βCD-IC. CEO/βCD-IC loaded Eudragit S100 fiber was more sensitive in its action to *E. coli* than *S. aureus*. The fiber had 100% antibacterial activity to *E. coli* and 83% antibacterial activity to *S. aureus*.

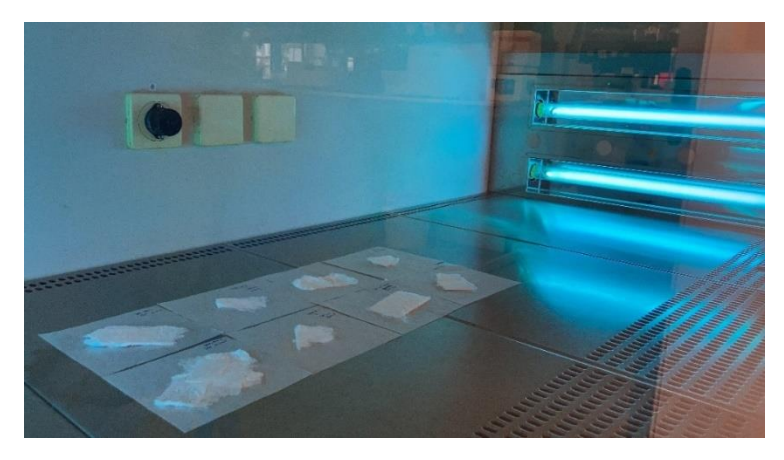
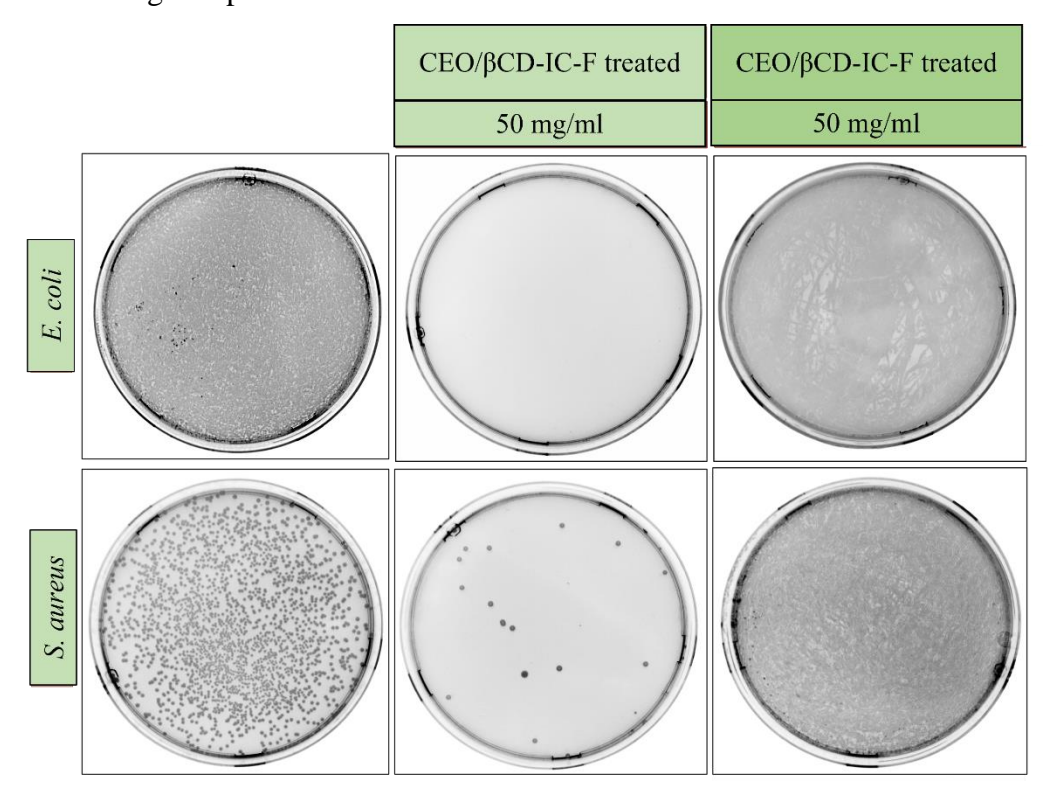


Figure 41. UV light exposure on obtained fibers



**Figure 42.** Images of plates showing bacterial growth of *E. coli* and *S. aureus* in term of colonies in the presence of inclusion complexes loaded fibers

## 3.7. Drug release assay

In vitro release of essential oil from CEO/ $\beta$ CD-IC loaded Eudragit S100 fiber and CEO/SBE- $\beta$ CD-IC loaded Eudragit S100 fiber was investigated in PBS medium with different pH. The amount of cinnamon leaf oil present in the release medium was quantified by measuring absorbance with spectrophotometer at 280 nm using PBS as reference. The content of CEO was calculated by means of a calibration curve for CEO in PBS at various concentrations (**Figure 43**).

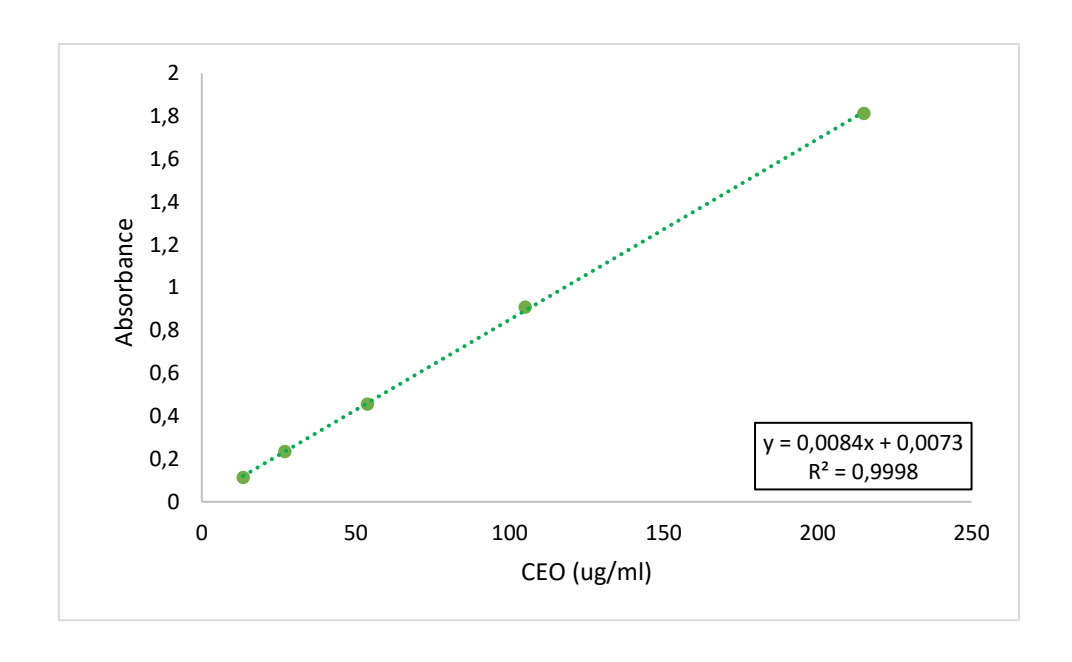
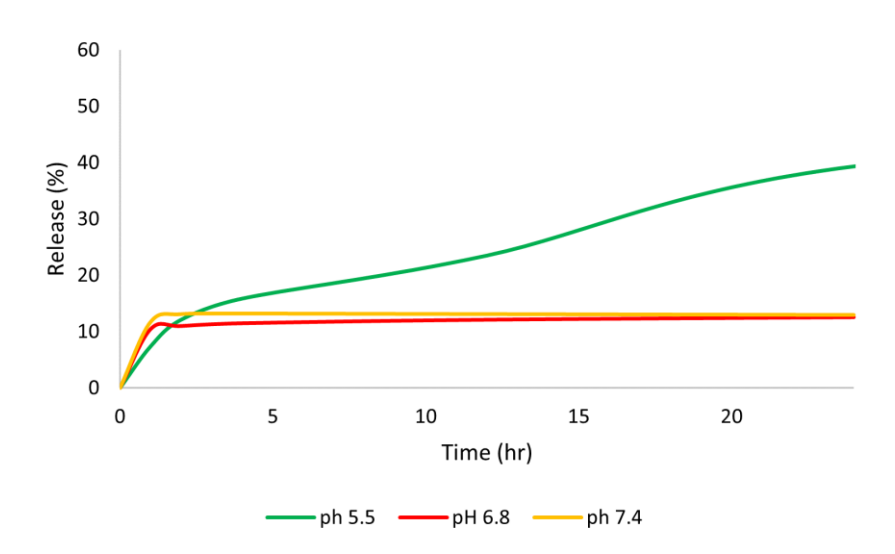


Figure 43. Calibration curve of pure cinnamon leaf essential oil in PBS at 280 nm.

CEO/βCD-IC loaded Eudragit S100 fiber was dispersed in PBS (pH 5.5, 6.8 and 7.4) at 37°C and 140 rpm. At different interval times, 3 mL of solution extracted and readed by UV-Visible spectroscopy at 280 nm. As a control, blank Eudragit S100 fiber was added to PBS solution and the solution readed from 200 nm to 800 nm after 1 hr. However, the peak was found at 207 nm. The release graph of fibers loaded with inclusion complexes during 24 h is shown in **Figure 44**. CEO/βCD-IC loaded Eudragit S100 fiber in PBS pH 6.8 and 7.4 showed burst release with about 10% and 12% of loaded oil, respectively, within 1 h. Then, both samples released a small amount cinnamon leaf oil in 24 h. The initial fast release of fiber in these solutions is due to the fiber's tendency to dissolve quickly in normal and weak acidic pH. Burst release also occurs due to the active substance in the outermost layer of the nanofibers passing into the release medium rapidly <sup>278</sup>. Since fibers releasing shows a similar response at pH 6.8 and pH 7.4, the release study continued only with pH 7.4 Monitoring the release pattern of the oil was continued until 168 h. The release of oil from CEO/βCD-IC loaded Eudragit S100 fiber in PBS pH 7.4 was reached from 12% to 17% at the end of 168 h. In contrast to pH 7.4, CEO/βCD-IC loaded Eudragit S100 fiber showed controlled sustained release behavior in PBS pH 5.5. Cinnamon oil from CEO/βCD-IC loaded Eudragit S100 fiber was gradually released in PBS pH 5.5 during 24 hour. It was seen that CEO/βCD-IC loaded Eudragit S100 fiber in PBS pH 5.5 reached the maximum release (57%) in 168 h, and then the release was stopped (**Figure 45**).



**Figure 44.** Effect of pH on the release of cinnamon leaf oil from CEO/ $\beta$ CD-IC loaded Eudragit S100 fiber.

As seen in **Figure 45**, the rate of cinnamon leaf oil from CEO/SBE-βCD-IC loaded Eudragit S100 fiber was higher than CEO/βCD-IC loaded Eudragit S100 fiber at initial stage in PBS pH 5.5. Initially, 7% cinnamon leaf oil release from fiber was detected, then this rate gradually reached 72% at the end of the 12th h. In the next 168-h period, cinnamon leaf oil was released in a controlled manner and the release rate reached 88%. Although the rate of cinnamon leaf oil from CEO/SBE-βCD-IC loaded Eudragit S100 fiber was higher than CEO/βCD-IC loaded Eudragit S100 fiber in PBS pH 7.4, it showed similar release behavior. The fiber showed burst release with about 15% oil released within 1 h. Then, release was reached 28% at the end of 168 h. Results showed that pH values significantly affect the release of cinnamon leaf oil from the CEO/βCD-IC loaded Eudragit S100 fiber and CEO/SBE-βCD-IC loaded Eudragit S100 fiber. They showed negligible essential oil release at pH:7.4 (normal pH) and controlled sustained release at pH 5.5 (acidic pH). The greater cinnamon leaf oil release from both fibers at pH 5.5 allows them to be used as a dressing for treatment of diabetic ulcer because pathological environment is pH 5.5–5.6 for infected chronic wounds.

It is known that the solubility and dispersibility of active substances in the polymeric system and the release medium could affect the release pattern  $^{281}$ . However, we have the similar percentage of encapsulation efficiency for both CEO/ $\beta$ CD-IC loaded Eudragit S100 fiber and CEO/SBE- $\beta$ CD-IC loaded Eudragit S100 fiber, they showed different release pattern which maybe due to their different solubilizing ability. Indeed, SBE- $\beta$ CD could increase the solubility of oil in the system and so it showed more amount of oil released during 168 h. Also, the results of released test could confirm our results from phase solubility test.

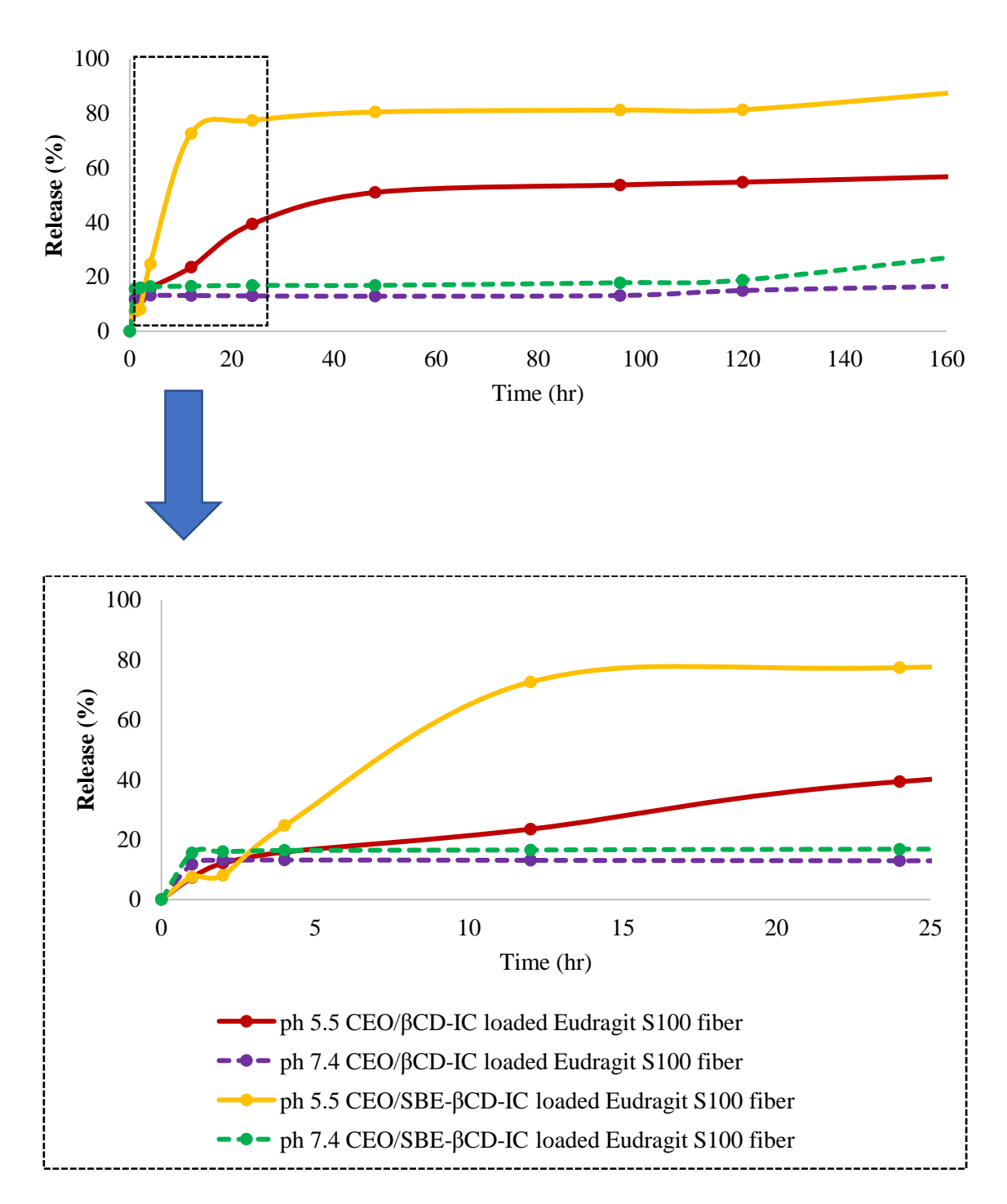


**Figure 45.** Time dependent release profiles of CEO/ $\beta$ CD-IC loaded Eudragit S100 fiber and CEO/SBE- $\beta$ CD-IC loaded Eudragit S100 fiber at pH 5.5 and pH 7.4.

## 3.8. Cell viability assay

The cytotoxicity of Eudragit fiber with and without inclusion complexes (20 mg/ml) were tested on L929 cell line (**Figure 46**). According to the WST-1 cytotoxicity assay results on the 24 hours, L929 cell treated with CEO/ $\beta$ CD-IC loaded Eudragit S100 fiber and free CEO (equivalent amount of CEO in the fiber) do not have cytotoxic characteristics. Moreover, pristine Eudragit fiber and CEO/ $\beta$ CD-IC loaded Eudragit S100 fiber were showed proliferative

effect on L929 when compared to medium only (control). After 48 hr, cell viability of free CEO was decreased to 77% which means it was toxic. The effect of CEO/SBE-βCD-IC loaded Eudragit S100 fiber and free CEO (equivalent amount of CEO in the fiber) were also tested on L929 cell. Likewise, CEO in CEO/βCD-IC loaded Eudragit S100 fiber, CEO was toxic after 48 hr and CEO/βCD-IC loaded Eudragit S100 fiber didn't increase the cytocompatibility of the CEO. This fiber had a toxic effect at both 24 and 48 hr.

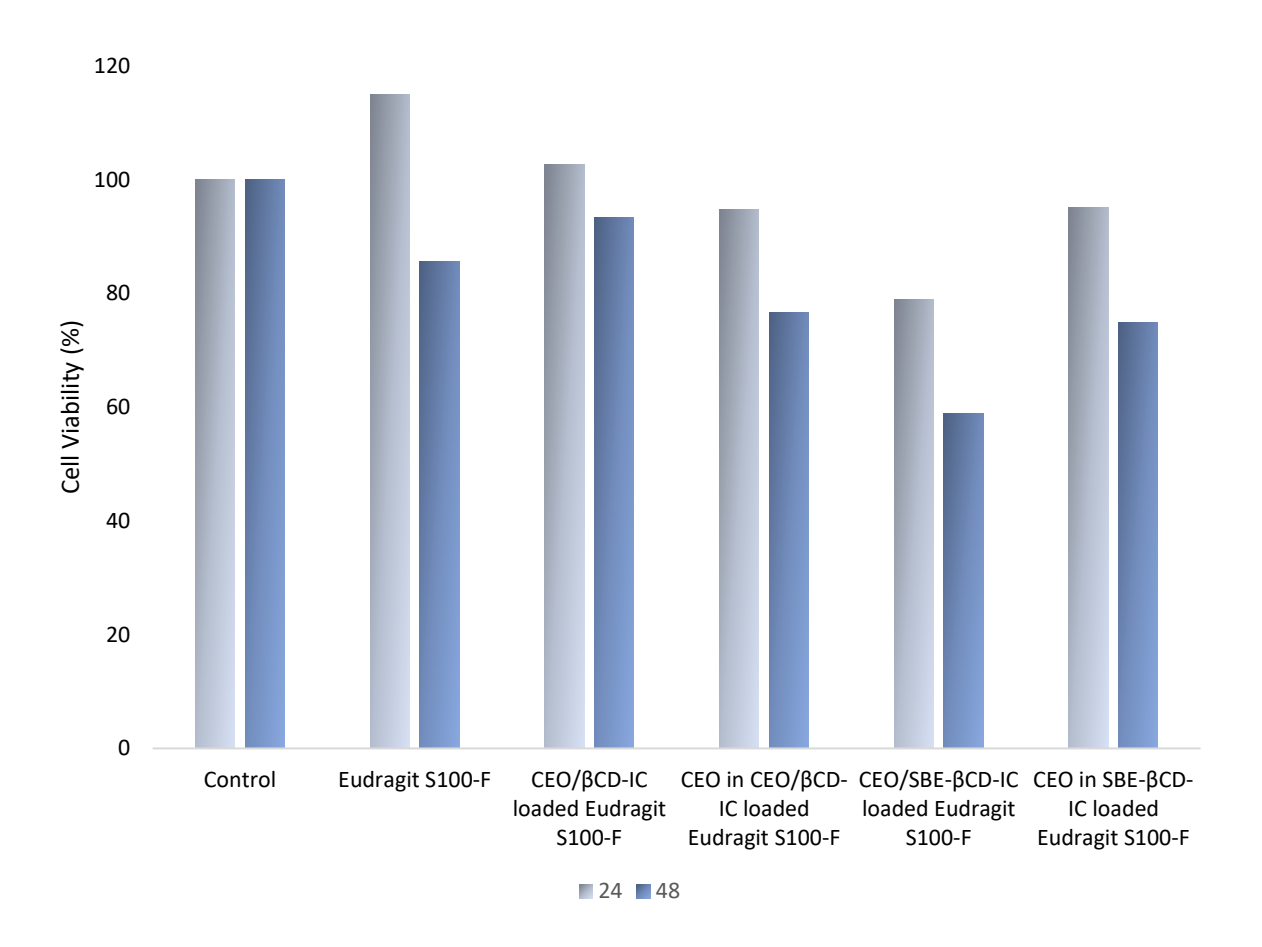


**Figure 46**. *In vitro* cytotoxicity test of Eudragit fiber with and without inclusion complexes, and equivalent amount of CEO in the fibers against L929 cell line

Considering the results, 20 mg/ml of CEO/ $\beta$ CD-IC loaded Eudragit S100 fiber showed non-toxic effects against L929. The concentration of these fiber was also increased to understand the effect on cell. Cells were treated with 40 mg/ml of pristine Eudragit fiber, 40 mg/ml of CEO/ $\beta$ CD-IC loaded Eudragit S100 fiber and free CEO (equivalent amount of CEO in the fiber, 9.28 mg/ml) at both 24 and 48 hr (**Figure 47**). It was shown that pristine Eudragit fiber (40 mg/ml) and CEO in 40 mg of CEO/ $\beta$ CD-IC loaded Eudragit S100 fiber were highly toxic compared to control. However, CEO/ $\beta$ CD-IC loaded Eudragit S100 fiber didn't show any toxic effect even 40 mg/ml.

These cytotoxicity tests showed that it was not appropriate to use CEO/SBE-βCD-IC loaded Eudragit S100 fiber because it was highly toxic even 20 mg/ml. However, CEO/βCD-IC loaded Eudragit S100 fiber was safe even at concentrations below 40 mg/ml. Therefore, it was suitable for use as a wound dressing.

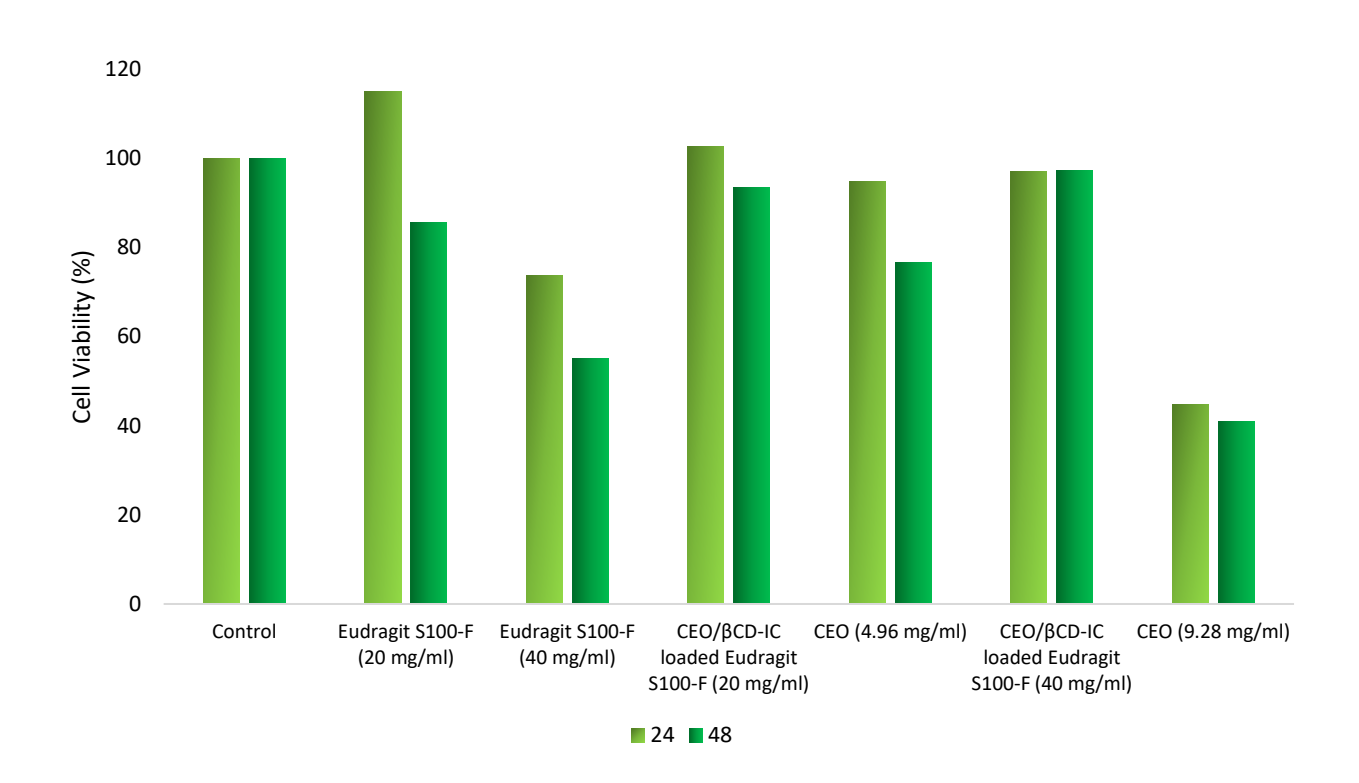


**Figure 47**. *In vitro* cytotoxicity test of pristine Eudragit fiber, CEO/βCD-IC loaded Eudragit S100 fiber and equivalent amount of CEO in the fibers against L929 cell line

#### 4. Conclusion

During this study cinnamon leaf oil/β-CD-inclusion complex loaded Eudragit S100 fiber and cinnamon leaf oil/SBE-β-CD-inclusion complex loaded Eudragit S100 fiber were produced by electrospinning method. High encapsulation efficiency was achieved during electrospinning. Fiber formations were confirmed by SEM, FTIR, and TGA. SEM analysis indicated that these fibers had a smooth surface and bead-free form with an average diameter ranging from 13-14 µm. Interactions between Eudragit S100 and inclusion complexes were proved by the band shifts observed in the FTIR-ATR spectra of pristine fiber. TGA analysis showed that the thermal stability and durability of cinnamon leaf oil were increased by an inclusion complex incorporated in Eudragit S100 fiber. The electrospun fibers were also examined whether they were suitable for use as a dressing. Although all fibers produced within the scope of this study exhibited hydrophobic behavior due to the chemical structure of Eudragit S100 polymer, while the incorporation of inclusion complex to Eudragit S100 fiber makes them more hydrophilic with decreasing average water contact angle. It has been found that CEO/βCD-IC loaded Eudragit S100 fiber had a balanced hydrophilic property and was more suitable for wound dressing application. The water uptake of the inclusion complex loaded fibers was increased compared to pristine Eudragit S100. The antibacterial activity of these electrospun fibers was also checked, and it was found that CEO/βCD-IC loaded Eudragit S100 fiber had better antibacterial activities against E. coli and S. aureus compared to CEO/SBE-βCD-IC loaded Eudragit S100 fiber. Drug release assays indicated that both fibers showed negligible essential oil release at pH:7.4 (normal pH) and controlled sustained release at pH 5.5 (acidic pH). Cell viability assay showed that CEO/SBE-βCD-IC loaded Eudragit S100 fiber was highly toxic; however, CEO/βCD-IC loaded Eudragit S100 fiber was compatible with cells. Accordingly, using CEO/BCD-IC loaded Eudragit S100 fiber could be a good candidate for wound healing applications because of having high water uptake, balanced hydrophilic outer surface, non-toxic property, high antibacterial activity, and controlled drug release.

#### 5. References

- 1. Cseke LJ, Kaufman PB, Kirakosyan A. The biology of essential oils in the pollination of flowers. *Nat Prod Commun*. 2007. doi:10.1177/1934578x0700201225
- 2. Masotti V, Juteau F, Bessière JM, Viano J. Seasonal and Phenological Variations of the Essential Oil from the Narrow Endemic Species Artemisia molinieri and Its Biological Activities. *J Agric Food Chem.* 2003. doi:10.1021/jf034621y
- 3. Angioni A, Barra A, Coroneo V, Dessi S, Cabras P. Chemical composition, seasonal variability, and antifungal activity of Lavandula stoechas L. ssp. stoechas essential oils from stem/leaves and Flowers. *J Agric Food Chem.* 2006. doi:10.1021/jf0603329
- 4. Bakkali F, Averbeck S, Averbeck D, Idaomar M. Biological effects of essential oils A review. *Food Chem Toxicol*. 2008. doi:10.1016/j.fct.2007.09.106
- 5. Butnariu M, Sarac I. Essential Oils from Plants. *J Biotechnol Biomed Sci.* 2018. doi:10.14302/issn.2576-6694.jbbs-18-2489
- 6. Koul O, Walia S, Dhaliwal G. Essential oils as green pesticides: Potential and Constraints. *Biopestic Int.* 2008.

- 7. Price S, Price L. Aromatherapy for Health Professionals: Third Edition.; 2007.
- 8. Bayram E, Kırıcı S, Tansı S, Yılmaz G. Tıbbi ve aromatik bitkilerin üretiminin arttırılması olanakları. *Türkiye Ziraat Mühendisliği VII Tek Kongresi Bildir Kitabı-I*. 2010.
- 9. Chao SC, Young DG, Oberg CJ. Screening for inhibitory activity of essential oils on selected bacteria, fungi and viruses. *J Essent Oil Res.* 2000. doi:10.1080/10412905.2000.9712177
- 10. Xiang F, Zhao Q, Zhao K, Pei H, Tao F. The efficacy of composite essential oils against Aflatoxigenic fungus Aspergillus flavus in Maize. *Toxins* (*Basel*). 2020. doi:10.3390/toxins12090562
- 11. Kim YG, Lee JH, Kim S II, Baek KH, Lee J. Cinnamon bark oil and its components inhibit biofilm formation and toxin production. *Int J Food Microbiol*. 2015. doi:10.1016/j.ijfoodmicro.2014.11.028
- 12. Kunyanga CN, Imungi JK, Okoth MW, Biesalski HK, Vadivel V. Total phenolic content, antioxidant and antidiabetic properties of methanolic extract of raw and traditionally processed Kenyan indigenous food ingredients. *LWT Food Sci Technol*. 2012. doi:10.1016/j.lwt.2011.08.006
- 13. Hepokur C. Investigation of cytotoxic effects of Eugenia caryophyllus (Clove). *Cumhur Dent J.* 2018. doi:10.7126/cumudj.444426
- 14. Bazı Tıbbi ve Aromatik Bitkilerde Esansiyel Yağların Antimikrobiyal Aktivitelerinin Belirlenmesi. *Ziraat Fakültesi Derg.* 2015.
- 15. KILIÇ Bartın Orman Fakültesi A. Uçucu Yağ Elde EtmeYöntemleri Methods of Essential Oil Production. *Bartın Orman Fakültesi Derg.* 2008.
- 16. Lawrence R, Lawrence K. Antioxidant activity of garlic essential oil (Allium Sativum) grown in north Indian plains. *Asian Pac J Trop Biomed*. 2011. doi:10.1016/S2221-1691(11)60122-6
- 17. Grassmann J, Elstner EF. ESSENTIAL OILS | Properties and Uses. In: *Encyclopedia of Food Sciences and Nutrition*.; 2003. doi:10.1016/b0-12-227055-x/00425-9
- 18. Wallace RJ. Antimicrobial properties of plant secondary metabolites. *Proc Nutr Soc.*

- 2004. doi:10.1079/pns2004393
- 19. Moumni S, Elaissi A, Trabelsi A, et al. Correlation between chemical composition and antibacterial activity of some lamiaceae species essential oils from Tunisia. *BMC Complement Med Ther*. 2020. doi:10.1186/s12906-020-02888-6
- Mugao LG, Gichimu BM, Muturi PW, Mukono ST. Characterization of the Volatile Components of Essential Oils of Selected Plants in Kenya. *Biochem Res Int.* 2020. doi:10.1155/2020/8861798
- 21. Elsharif SA, Banerjee A, Buettner A. Structure-odor relationships of linalool, linalyl acetate and their corresponding oxygenated derivatives. *Front Chem.* 2015. doi:10.3389/fchem.2015.00057
- 22. Elsharif SA, Buettner A. Structure-Odor Relationship Study on Geraniol, Nerol, and Their Synthesized Oxygenated Derivatives. *J Agric Food Chem.* 2018. doi:10.1021/acs.jafc.6b04534
- 23. Dorman HJD, Deans SG. Antimicrobial agents from plants: Antibacterial activity of plant volatile oils. *J Appl Microbiol*. 2000. doi:10.1046/j.1365-2672.2000.00969.x
- 24. Burt S. Essential oils: Their antibacterial properties and potential applications in foods A review. *Int J Food Microbiol*. 2004. doi:10.1016/j.ijfoodmicro.2004.03.022
- 25. Cristani M, D'Arrigo M, Mandalari G, et al. Interaction of four monoterpenes contained in essential oils with model membranes: Implications for their antibacterial activity. *J Agric Food Chem.* 2007. doi:10.1021/jf070094x
- 26. Saad NY, Muller CD, Lobstein A. Major bioactivities and mechanism of action of essential oils and their components. *Flavour Fragr J.* 2013. doi:10.1002/ffj.3165
- 27. Rai M, Paralikar P, Jogee P, et al. Synergistic antimicrobial potential of essential oils in combination with nanoparticles: Emerging trends and future perspectives Synergistic antimicrobial potential of essential oils in combination with nanoparticles: Emerging trends and future perspect. *Int J Pharm.* 2017;519(1-2):67-78. doi:10.1016/j.ijpharm.2017.01.013
- 28. Lakehal S, A M. Essential Oil Composition and Antimicrobial Activity of Artemisia herba— alba Asso Grown in Algeria. *Med Chem (Los Angeles)*. 2016. doi:10.4172/2161-0444.1000382

- 29. Cui H, Zhang X, Zhou H, Zhao C, Lin L. Antimicrobial activity and mechanisms of Salvia sclarea essential oil. *Bot Stud.* 2015. doi:10.1186/s40529-015-0096-4
- 30. Yap PSX, Yusoff K, Lim SHE, Chong CM, Lai KS. Membrane disruption properties of essential oils-a double-edged sword? *Processes*. 2021. doi:10.3390/pr9040595
- 31. Cox SD, Mann CM, Markham JL, et al. The mode of antimicrobial action of the essential oil of Melaleuca alternifolia (Tea tree oil). *J Appl Microbiol*. 2000. doi:10.1046/j.1365-2672.2000.00943.x
- 32. Alves Carneiro V, Soares Melo R, Mateus Gomes Pereira A, et al. Essential Oils as an Innovative Approach against Biofilm of Multidrug-Resistant Staphylococcus aureus . In: *Bacterial Biofilms*.; 2020. doi:10.5772/intechopen.91833
- 33. Swetha CS,. Evaluation of Selected Essential Oils as Biocontrol Agents Against Listeria monocytogenes. *J Anim Res.* 2020. doi:10.30954/2277-940x.05.2020.19
- 34. Jeong EJ, Lee NK, Oh J, et al. Inhibitory effect of cinnamon essential oils on selected cheese-contaminating fungi (Penicillium spp.) during the cheese-ripening process. *Food Sci Biotechnol*. 2014. doi:10.1007/s10068-014-0163-8
- 35. Farahpour MR, Habibi M. Evaluation of the wound healing activity of an ethanolic extract of Ceylon cinnamon in mice. *Vet Med (Praha)*. 2012. doi:10.17221/4972-VETMED
- 36. Dugoua JJ, Seely D, Perri D, et al. From type 2 diabetes to antioxidant activity: A systematic review of the safety and efficacy of common and cassia cinnamon bark. *Can J Physiol Pharmacol*. 2007. doi:10.1139/Y07-080
- 37. Muhammad DRA, Dewettinck K. Cinnamon and its derivatives as potential ingredient in functional food—A review. *Int J Food Prop.* 2017. doi:10.1080/10942912.2017.1369102
- 38. Cheng SS, Chung MJ, Chen YJ, Chang ST. Antipathogenic activities and chemical composition of cinnamomum osmophloeum and cinnamomum zeylanicum leaf essential oils. *J Wood Chem Technol*. 2011. doi:10.1080/02773813.2010.486462
- 39. Rezq A, Elmallh M. Anti-ulcer Effect of Cinnamon and Chamomile Aqueous Extracts in Rat Models. *J Am Sci.* 2010.

- 40. Jakhetia V, Patel R, Khatri P, et al. CINNAMON: A PHARMACOLOGICAL REVIEW. *J Adv Sci Res.* 2010.
- 41. Zainol NA, Ming TS, Darwis Y. Development and characterization of cinnamon leaf oil nanocream for topical application. *Indian J Pharm Sci.* 2015. doi:10.4103/0250-474X.164785
- 42. Lee JS, Jeon SM, Park EM, et al. Cinnamate Supplementation Enhances Hepatic Lipid Metabolism and Antioxidant Defense Systems in High Cholesterol-Fed Rats. *J Med Food*, 2003. doi:10.1089/10966200360716599
- 43. Kim SS, Oh OJ, Min HY, et al. Eugenol suppresses cyclooxygenase-2 expression in lipopolysaccharide-stimulated mouse macrophage RAW264.7 cells. *Life Sci.* 2003. doi:10.1016/S0024-3205(03)00288-1
- 44. Huss U, Ringbom T, Perera P, Bohlin L, Vasänge M. Screening of ubiquitous plant constituents for COX-2 inhibition with a scintillation proximity based assay. *J Nat Prod*. 2002. doi:10.1021/np020023m
- 45. Kumar S, Vasudeva N, Sharma S. Pharmacological and pharmacognostical aspects of Cinnamomum tamala Nees & Eberm. *J Pharm Res.* 2012.
- 46. Soliman KM, Badeaa RI. Effect of oil extracted from some medicinal plants on different mycotoxigenic fungi. *Food Chem Toxicol*. 2002. doi:10.1016/S0278-6915(02)00120-5
- 47. Carmo ES, Lima EDO, De Souza EL, De Sousa FB. Effect of Cinnamomum zeylanicum Blume essential oil on the growth and morphogenesis of some potentially pathogenic Aspergillus species. *Brazilian J Microbiol*. 2008. doi:10.1590/S1517-83822008000100021
- 48. Campaniello D, Corbo MR, Sinigaglia M. Antifungal Activity of Eugenol against Penicillium, Aspergillus, and Fusarium Species. *J Food Prot.* 2010. doi:10.4315/0362-028X-73.6.1124
- 49. Leite AM, Lima EDO, De Souza EL, Diniz MDFFM, Trajano VN, De Medeiros IA. Inhibitory effect of β-pinene, α-pinene and eugenol on the growth of potential infectious endocarditis causing Gram-positive bacteria. Rev Bras Ciencias Farm J Pharm Sci. 2007. doi:10.1590/S1516-93322007000100015
- 50. Ali SM, Khan AA, Ahmed I, et al. Antimicrobial activities of Eugenol and

- Cinnamaldehyde against the human gastric pathogen Helicobacter pylori. *Ann Clin Microbiol Antimicrob*. 2005. doi:10.1186/1476-0711-4-20
- 51. de Oliveira ÉR, Campini PAL, de Souza AG, da Silva CG, Yudice EDC, dos Santos Rosa D. Antibacterial cellulose papers loaded with different isolated active compounds for food packaging applications. *Iran Polym J (English Ed.* 2021. doi:10.1007/s13726-021-00958-1
- 52. Ouattara B, Simard RE, Holley RA, Piette GJP, Bégin A. Antibacterial activity of selected fatty acids and essential oils against six meat spoilage organisms. *Int J Food Microbiol*. 1997. doi:10.1016/S0168-1605(97)00070-6
- 53. Chouhan S, Sharma K, Guleria S. Antimicrobial Activity of Some Essential Oils—
  Present Status and Future Perspectives. *Medicines*. 2017;4(3):58.
  doi:10.3390/medicines4030058
- 54. HADRI Z, ALLEM R, Marin GP. Effect of essential oil of Cinnamomum zeylanicum on some pathogenic bacteria. *African J Microbiol Res.* 2014. doi:10.5897/ajmr2013.6519
- 55. Zhang Y, Liu X, Wang Y, Jiang P, Quek SY. Antibacterial activity and mechanism of cinnamon essential oil against Escherichia coli and Staphylococcus aureus. *Food Control*. 2015. doi:10.1016/j.foodcont.2015.05.032
- 56. Singh G, Maurya S, deLampasona MP, Catalan CAN. A comparison of chemical, antioxidant and antimicrobial studies of cinnamon leaf and bark volatile oils, oleoresins and their constituents. *Food Chem Toxicol*. 2007. doi:10.1016/j.fct.2007.02.031
- 57. Shahidi F, Han XQ. Encapsulation of Food Ingredients. *Crit Rev Food Sci Nutr*. 1993. doi:10.1080/10408399309527645
- 58. Desai KGH, Park HJ. Recent developments in microencapsulation of food ingredients. *Dry Technol.* 2005. doi:10.1081/DRT-200063478
- 59. Anal AK, Singh H. Recent advances in microencapsulation of probiotics for industrial applications and targeted delivery. *Trends Food Sci Technol*. 2007. doi:10.1016/j.tifs.2007.01.004
- 60. Greay SJ, Hammer KA. Recent developments in the bioactivity of mono- and diterpenes: anticancer and antimicrobial activity. *Phytochem Rev.* 2015. doi:10.1007/s11101-011-9212-6

- 61. Başyiğit B ve ark. Kekik esansiyel yağı ve mikroenkapsülasyon uygulamaları. *Batman Üniversitesi Yaşam Bilim Derg.* 2017.
- 62. Baldwin EA, Hagenmaier RD, Bai J. Edible Coatings and Films to Improve Food Ouality, Second Edition.; 2011.
- 63. Jafari SM, Assadpoor E, He Y, Bhandari B. Encapsulation efficiency of food flavours and oils during spray drying. *Dry Technol*. 2008. doi:10.1080/07373930802135972
- 64. de la Cruz Pech-Canul A, Ortega D, García-Triana A, González-Silva N, Solis-Oviedo RL. A brief review of edible coating materials for the microencapsulation of probiotics. Coatings. 2020. doi:10.3390/coatings10030197
- 65. Marques HMC. A review on cyclodextrin encapsulation of essential oils and volatiles. Flavour Fragr J. 2010. doi:10.1002/ffj.2019
- 66. Gökmen S, Palamutoğlu R, Sariçoban C, et al. Gıda Endüstrisinde Enkapsülasyon Uygulamaları. *Electron J Food Technol Gıda Teknol Elektron Derg Electron J Food Technol*. 2012.
- 67. de Miranda JC, Martins TEA, Veiga F, Ferraz HG. Cyclodextrins and ternary complexes: Technology to improve solubility of poorly soluble drugs. *Brazilian J Pharm Sci.* 2011. doi:10.1590/S1984-82502011000400003
- 68. Cyclodextrin A Versatile Ingredient.; 2018. doi:10.5772/intechopen.69187
- Luda MP, Zanetti M. Cyclodextrins and cyclodextrin derivatives as green char promoters in flame retardants formulations for polymeric materials. A review. *Polymers (Basel)*. 2019. doi:10.3390/polym11040664
- 70. Sun X, Sui S, Ference C, et al. Antimicrobial and mechanical properties of β-cyclodextrin inclusion with essential oils in chitosan films. *J Agric Food Chem.* 2014. doi:10.1021/jf5027873
- 71. Pinho E, Grootveld M, Soares G, Henriques M. Cyclodextrins as encapsulation agents for plant bioactive compounds. *Carbohydr Polym*. 2014. doi:10.1016/j.carbpol.2013.08.078
- 72. Szente L, Szejtli J. Cyclodextrins as food ingredients. *Trends Food Sci Technol*. 2004. doi:10.1016/j.tifs.2003.09.019

- 73. Szejtli J. Past, present, and future of cyclodextrin research. In: *Pure and Applied Chemistry*.; 2004. doi:10.1351/pac200476101825
- 74. Campos EVR, de Oliveira JL, Fraceto LF, Singh B. Polysaccharides as safer release systems for agrochemicals. *Agron Sustain Dev.* 2014. doi:10.1007/s13593-014-0263-0
- 75. Leemhuis H, Kragh KM, Dijkstra BW, Dijkhuizen L. Engineering cyclodextrin glycosyltransferase into a starch hydrolase with a high exo-specificity. *J Biotechnol*. 2003. doi:10.1016/S0168-1656(03)00126-3
- Banchero M, Ronchetti S, Manna L. Characterization of ketoprofen/methyl-βcyclodextrin complexes prepared using supercritical carbon dioxide. *J Chem.* 2013. doi:10.1155/2013/583952
- 77. Banjare MK, Behera K, Satnami ML, Pandey S, Ghosh KK. Host-guest complexation of ionic liquid with α- And β-cyclodextrins: A comparative study by 1H-NMR, 13C-NMR and COSY. *New J Chem.* 2018. doi:10.1039/c8nj01840e
- 78. Aksamija A, Polidori A, Plasson R, Dangles O, Tomao V. The inclusion complex of rosmarinic acid into beta-cyclodextrin: A thermodynamic and structural analysis by NMR and capillary electrophoresis. *Food Chem.* 2016. doi:10.1016/j.foodchem.2016.04.008
- 79. Rabus JM, Pellegrinelli RP, Khodr AHA, Bythell BJ, Rizzo TR, Carrascosa E. Unravelling the structures of sodiated β-cyclodextrin and its fragments. *Phys Chem Chem Phys.* 2021. doi:10.1039/d1cp01058a
- 80. Rajbanshi B, Saha S, Das K, et al. Study to Probe Subsistence of Host-Guest Inclusion Complexes of α and β-Cyclodextrins with Biologically Potent Drugs for Safety Regulatory Dischargement. *Sci Rep.* 2018. doi:10.1038/s41598-018-31373-x
- 81. Cal K, Centkowska K. Use of cyclodextrins in topical formulations: Practical aspects. *Eur J Pharm Biopharm*. 2008. doi:10.1016/j.ejpb.2007.08.002
- 82. Pinho E, Grootveld M, Soares G, Henriques M. Cyclodextrin-based hydrogels toward improved wound dressings. *Crit Rev Biotechnol*. 2014. doi:10.3109/07388551.2013.794413
- 83. Valle DEMM. Cyclodextrins and their uses: A review. *Process Biochem.* 2004. doi:10.1016/S0032-9592(03)00258-9

- 84. Carrier RL, Miller LA, Ahmed I. The utility of cyclodextrins for enhancing oral bioavailability. *J Control Release*. 2007. doi:10.1016/j.jconrel.2007.07.018
- 85. Lee JU, Lee SS, Lee S, Oh H Bin. Noncovalent complexes of cyclodextrin with small organic molecules: Applications and insights into host–guest interactions in the gas phase and condensed phase. *Molecules*. 2020. doi:10.3390/molecules25184048
- 86. Betlejewska-Kielak K, Bednarek E, Budzianowski A, Michalska K, Maurin JK. Comprehensive characterisation of the ketoprofen-β-cyclodextrin inclusion complex using x-ray techniques and nmr spectroscopy. *Molecules*. 2021. doi:10.3390/molecules26134089
- 87. Mundhara N, Majumder A, Panda D. Methyl-β-cyclodextrin, an actin depolymerizer augments the antiproliferative potential of microtubule-targeting agents. *Sci Rep.* 2019. doi:10.1038/s41598-019-43947-4
- 88. Stella VJ, he Q. Cyclodextrins. *Toxicol Pathol*. 2008. doi:10.1177/0192623307310945
- 89. Jodál I, Nánási P, Szejtli J. Investigation of the Hemolytic Effect of the Cyclodextrin Derivatives. In: *Proceedings of the Fourth International Symposium on Cyclodextrins*.; 1988. doi:10.1007/978-94-009-2637-0 61
- 90. Loftsson T, Duchêne D. Cyclodextrins and their pharmaceutical applications. *Int J Pharm.* 2007. doi:10.1016/j.ijpharm.2006.10.044
- 91. Müller BW, Brauns U. Hydroxypropyl-β cyclodextrin derivatives: Influence of average degree of substitution on complexing ability and surface activity. *J Pharm Sci.* 1986. doi:10.1002/jps.2600750609
- 92. Haroon Khalid S, Bashir M, Asghar S, Hussain Mallhi T, Ullah Khan I. Effect of Cyclodextrin Derivatization on Solubility and Efficacy of Drugs. In: *Colloid Science in Pharmaceutical Nanotechnology*.; 2020. doi:10.5772/intechopen.90364
- 93. Zia V, Rajewski RA, Bornancini ER, Luna EA, Stella VJ. Effect of alkyl chain length and degree of substitution on the complexation of sulfoalkyl ether β-cyclodextrins with steroids. *J Pharm Sci.* 1997. doi:10.1021/js960236u
- 94. Stella VJ, Rajewski RA. Sulfobutylether-β-cyclodextrin. *Int J Pharm*. 2020. doi:10.1016/j.ijpharm.2020.119396

- 95. Fauvelle F, Debouzy JC, Crouzy S, Göschl M, Chapron Y. Mechanism of α-cyclodextrin-induced hemolysis. 1. The two-step extraction of phosphatidylinositol from the membrane. *J Pharm Sci.* 1997. doi:10.1021/js9602453
- 96. Dodziuk H. Cyclodextrins and Their Complexes: Chemistry, Analytical Methods, Applications.; 2006. doi:10.1002/3527608982
- 97. Pereva S, Nikolova V, Angelova S, Spassov T, Dudev T. Water inside β-cyclodextrin cavity: amount, stability and mechanism of binding. *Beilstein J Org Chem.* 2019. doi:10.3762/bjoc.15.163
- 98. Liu L, Guo QX. The driving forces in the inclusion complexation of cyclodextrins. *J Incl Phenom.* 2002. doi:10.1023/A:1014520830813
- 99. Szejtli J. CYCLODEXTRIN TECHNOLOGY.; 2013.
- 100. Boonyarattanakalin K, Viernstein H, Wolschann P, Lawtrakul L. Influence of ethanol as a Co-Solvent in cyclodextrin inclusion complexation: A Molecular Dynamics Study. *Sci Pharm.* 2015. doi:10.3797/scipharm.1412-08
- 101. Topuz F, Uyar T. Electrospinning of cyclodextrin functional nanofibers for drug delivery applications. *Pharmaceutics*. 2019. doi:10.3390/pharmaceutics11010006
- 102. Higuchi T, Connors KA. Phase Solubility Techniques. In: *Advances in Analytical Chemistry and Instrumentation*.; 1965.
- 103. Williams HD, Trevaskis NL, Charman SA, et al. Strategies to address low drug solubility in discovery and development. *Pharmacol Rev.* 2013. doi:10.1124/pr.112.005660
- 104. Saokham P, Muankaew C, Jansook P, Loftsson T. Solubility of cyclodextrins and drug/cyclodextrin complexes. *Molecules*. 2018. doi:10.3390/molecules23051161
- 105. Vyas A. Preparation and characterization of the inclusion complex of ursolic acid with polymerized hydrophilic cyclodextrin. *Planta Med.* 2015. doi:10.1055/s-0035-1545237
- 106. Küçüktürkmen B, Bozkir A. A new approach for drug targeting to the central nervous system. In: *Nanoarchitectonics in Biomedicine*.; 2019. doi:10.1016/B978-0-12-816200-2.00014-1
- 107. Trotta F, Zanetti M, Camino G. Thermal degradation of cyclodextrins. *Polym Degrad Stab*. 2000. doi:10.1016/S0141-3910(00)00084-7

- 108. Cheirsilp B, Rakmai J. Inclusion complex formation of cyclodextrin with its guest and their applications. *Biol Eng Med*. 2017. doi:10.15761/bem.1000108
- 109. Del Valle EMM. Cyclodextrins and their uses: A review. *Process Biochem*. 2004. doi:10.1016/S0032-9592(03)00258-9
- Lin L, Dai Y, Cui H. Antibacterial poly(ethylene oxide) electrospun nanofibers containing cinnamon essential oil/beta-cyclodextrin proteoliposomes. *Carbohydr Polym*. 2017. doi:10.1016/j.carbpol.2017.09.043
- 111. Ayala-Zavala JF, Soto-Valdez H, González-León A, Álvarez-Parrilla E, Martín-Belloso O, González-Aguilar GA. Microencapsulation of cinnamon leaf (Cinnamomum zeylanicum) and garlic (Allium sativum) oils in β-cyclodextrin. *J Incl Phenom Macrocycl Chem.* 2008. doi:10.1007/s10847-007-9385-1
- 112. Cui H, Siva S, Lin L. Ultrasound processed cuminaldehyde/2-hydroxypropyl-β-cyclodextrin inclusion complex: Preparation, characterization and antibacterial activity. *Ultrason Sonochem*. 2019. doi:10.1016/j.ultsonch.2019.04.001
- 113. Abada M Ben, Hamdi SH, Gharib R, et al. Post-harvest management control of Ectomyelois ceratoniae (Zeller) (Lepidoptera: Pyralidae): new insights through essential oil encapsulation in cyclodextrin. *Pest Manag Sci.* 2019. doi:10.1002/ps.5315
- 114. Das S, Gazdag Z, Szente L, et al. Antioxidant and antimicrobial properties of randomly methylated β cyclodextrin captured essential oils. Food Chem. 2019. doi:10.1016/j.foodchem.2018.11.047
- 115. Galvão JG, Cerpe P, Santos DA, et al. Lippia gracilis essential oil in β-cyclodextrin inclusion complexes: an environmentally safe formulation to control Aedes aegypti larvae. *Pest Manag Sci.* 2019. doi:10.1002/ps.5138
- 116. Gaur S, Lopez EC, Ojha A, Andrade JE. Functionalization of Lipid-Based Nutrient Supplement with β-Cyclodextrin Inclusions of Oregano Essential Oil. *J Food Sci.* 2018. doi:10.1111/1750-3841.14178
- 117. Celebioglu A, Yildiz ZI, Uyar T. Thymol/cyclodextrin inclusion complex nanofibrous webs: Enhanced water solubility, high thermal stability and antioxidant property of thymol. *Food Res Int.* 2018. doi:10.1016/j.foodres.2017.12.062
- 118. Cui H, Bai M, Lin L. Plasma-treated poly(ethylene oxide) nanofibers containing tea tree

- oil/beta-cyclodextrin inclusion complex for antibacterial packaging. *Carbohydr Polym*. 2018. doi:10.1016/j.carbpol.2017.10.011
- 119. Wang J, Qiu C, Narsimhan G, Jin Z. Preparation and characterization of ternary antimicrobial films of β-cyclodextrin/allyl isothiocyanate/polylactic acid for the enhancement of long-term controlled release. *Materials* (*Basel*). 2017. doi:10.3390/ma10101210
- 120. Dias Antunes M, da Silva Dannenberg G, Fiorentini ÂM, et al. Antimicrobial electrospun ultrafine fibers from zein containing eucalyptus essential oil/cyclodextrin inclusion complex. *Int J Biol Macromol*. 2017. doi:10.1016/j.ijbiomac.2017.06.095
- 121. Azzi J, Danjou PE, Landy D, et al. The effect of cyclodextrin complexation on the solubility and photostability of nerolidol as pure compound and as main constituent of cabreuva essential oil. *Beilstein J Org Chem.* 2017. doi:10.3762/bjoc.13.84
- 122. Siqueira-Lima PS, Brito RG, Araújo-Filho HG, et al. Anti-hyperalgesic effect of Lippia grata leaf essential oil complexed with β-cyclodextrin in a chronic musculoskeletal pain animal model: Complemented with a molecular docking and antioxidant screening. *Biomed Pharmacother*. 2017. doi:10.1016/j.biopha.2017.05.009
- 123. Andrade TA, Freitas TS, Araújo FO, et al. Physico-chemical characterization and antibacterial activity of inclusion complexes of Hyptis martiusii Benth essential oil in β-cyclodextrin. *Biomed Pharmacother*. 2017. doi:10.1016/j.biopha.2017.01.158
- 124. Yim WT, Bhandari B, Jackson L, James P. Repellent effects of Melaleuca alternifolia (tea tree) oil against cattle tick larvae (Rhipicephalus australis) when formulated as emulsions and in β-cyclodextrin inclusion complexes. *Vet Parasitol*. 2016. doi:10.1016/j.vetpar.2016.06.007
- 125. da Silva FV, de Barros Fernandes H, Oliveira IS, et al. Beta-cyclodextrin enhanced gastroprotective effect of (–)-linalool, a monoterpene present in rosewood essential oil, in gastric lesion models. *Naunyn Schmiedebergs Arch Pharmacol*. 2016. doi:10.1007/s00210-016-1298-3
- 126. Celebioglu A, Kayaci-Senirmak F, Ipek S, Durgun E, Uyar T. Polymer-free nanofibers from vanillin/cyclodextrin inclusion complexes: High thermal stability, enhanced solubility and antioxidant property. *Food Funct*. 2016. doi:10.1039/c6fo00569a

- 127. Effect of β-cyclodextrin inclusion complex on transport of major components of Xiangfu Siwu decoction essential oil in Caco-2 cell monolayer model. *China J Chinese Mater Medica*. 2016. doi:10.4268/cjcmm20151510
- 128. Abarca RL, Rodríguez FJ, Guarda A, Galotto MJ, Bruna JE. Characterization of beta-cyclodextrin inclusion complexes containing an essential oil component. *Food Chem*. 2016. doi:10.1016/j.foodchem.2015.10.023
- 129. Santos PL, Araujo AAS, Quintans JSS, et al. Preparation, Characterization, and Pharmacological Activity of Cymbopogon winterianus Jowitt ex Bor (Poaceae) Leaf Essential Oil of β-Cyclodextrin Inclusion Complexes. *Evidence-based Complement Altern Med.* 2015. doi:10.1155/2015/502454
- 130. Guimarães AG, Oliveira MA, Alves RDS, et al. Encapsulation of carvacrol, a monoterpene present in the essential oil of oregano, with β-cyclodextrin, improves the pharmacological response on cancer pain experimental protocols. *Chem Biol Interact*. 2015. doi:10.1016/j.cbi.2014.12.020
- 131. Ciobanu A, Mallard I, Landy D, Brabie G, Nistor D, Fourmentin S. Retention of aroma compounds from Mentha piperita essential oil by cyclodextrins and crosslinked cyclodextrin polymers. *Food Chem.* 2013. doi:10.1016/j.foodchem.2012.10.106
- 132. Rakmai J, Cheirsilp B, Mejuto JC, Torrado-Agrasar A, Simal-Gándara J. Physicochemical characterization and evaluation of bio-efficacies of black pepper essential oil encapsulated in hydroxypropyl-beta-cyclodextrin. *Food Hydrocoll*. 2017. doi:10.1016/j.foodhyd.2016.11.014
- 133. Songkro S, Hayook N, Jaisawang J, Maneenuan D, Chuchome T, Kaewnopparat N. Investigation of inclusion complexes of citronella oil, citronellal and citronellol with b-cyclodextrin for mosquito repellent. *J Incl Phenom Macrocycl Chem.* 2012. doi:10.1007/s10847-011-9985-7
- 134. Anaya-Castro MA, Ayala-Zavala JF, Muñoz-Castellanos L, Hernández-Ochoa L, Peydecastaing J, Durrieu V. β-Cyclodextrin inclusion complexes containing clove (Eugenia caryophyllata) and Mexican oregano (Lippia berlandieri) essential oils: Preparation, physicochemical and antimicrobial characterization. *Food Packag Shelf Life*. 2017. doi:10.1016/j.fpsl.2017.09.002
- 135. Rakmai J, Cheirsilp B, Mejuto JC, Simal-Gándara J, Torrado-Agrasar A. Antioxidant

- and antimicrobial properties of encapsulated guava leaf oil in hydroxypropyl-beta-cyclodextrin. *Ind Crops Prod.* 2018. doi:10.1016/j.indcrop.2017.10.027
- 136. Wang Y, Yuan C, Liu Y, Cui B. Fabrication of kappa–carrageenan hydrogels with cinnamon essential oil/hydroxypropyl–β–cyclodextrin composite: Evaluation of physicochemical properties, release kinetics and antimicrobial activity. *Int J Biol Macromol.* 2021. doi:10.1016/j.ijbiomac.2020.12.176
- 137. Xu Y, Hou K, Gao C, et al. Characterization of chitosan film with cinnamon essential oil emulsion co-stabilized by ethyl-Nα-lauroyl-L-arginate hydrochloride and hydroxypropyl-β-cyclodextrin. *Int J Biol Macromol*. 2021. doi:10.1016/j.ijbiomac.2021.08.007
- 138. Wen P, Zhu DH, Feng K, et al. Fabrication of electrospun polylactic acid nanofilm incorporating cinnamon essential oil/β-cyclodextrin inclusion complex for antimicrobial packaging. *Food Chem.* 2016. doi:10.1016/j.foodchem.2015.10.043
- 139. Kim J, Yoon CS, Lee S eun, Na JH, Han J. Development of insect-proof starch adhesive containing encapsulated cinnamon oil for paper box adhesion to inhibit Plodia interpunctella larvae infestation. *J Food Sci.* 2020. doi:10.1111/1750-3841.15425
- 140. Matshetshe KI, Parani S, Manki SM, Oluwafemi OS. Preparation, characterization and in vitro release study of β-cyclodextrin/chitosan nanoparticles loaded Cinnamomum zeylanicum essential oil. *Int J Biol Macromol*. 2018. doi:10.1016/j.ijbiomac.2018.06.125
- 141. Pan J, Ai F, Shao P, Chen H, Gao H. Development of polyvinyl alcohol/β-cyclodextrin antimicrobial nanofibers for fresh mushroom packaging. *Food Chem.* 2019. doi:10.1016/j.foodchem.2019.125249
- 142. Pandiyan GN, Mathew N, Munusamy S. Larvicidal activity of selected essential oil in synergized combinations against Aedes aegypti. *Ecotoxicol Environ Saf.* 2019. doi:10.1016/j.ecoenv.2019.03.019
- 143. Celebioglu A, Yildiz ZI, Uyar T. Fabrication of Electrospun Eugenol/Cyclodextrin Inclusion Complex Nanofibrous Webs for Enhanced Antioxidant Property, Water Solubility, and High Temperature Stability. *J Agric Food Chem*. 2018. doi:10.1021/acs.jafc.7b04312
- 144. Sebaaly C, Charcosset C, Stainmesse S, Fessi H, Greige-Gerges H. Clove essential oil-

- in-cyclodextrin-in-liposomes in the aqueous and lyophilized states: From laboratory to large scale using a membrane contactor. *Carbohydr Polym*. 2016. doi:10.1016/j.carbpol.2015.11.053
- 145. Hill LE, Gomes C, Taylor TM. Characterization of beta-cyclodextrin inclusion complexes containing essential oils (trans-cinnamaldehyde, eugenol, cinnamon bark, and clove bud extracts) for antimicrobial delivery applications. *LWT Food Sci Technol*. 2013. doi:10.1016/j.lwt.2012.11.011
- 146. Torres-Alvarez C, Castillo S, Sánchez-García E, et al. Inclusion Complexes of Concentrated Orange Oils and β-Cyclodextrin: Physicochemical and Biological Characterizations. *Molecules*. 2020. doi:10.3390/molecules25215109
- 147. Semcheddine F, Guissi NEI, Liu X, Wu Z, Wang B. Effects of the Preparation Method on the Formation of True Nimodipine SBE-β-CD/HP-β-CD Inclusion Complexes and Their Dissolution Rates Enhancement. *AAPS PharmSciTech*. 2015. doi:10.1208/s12249-014-0257-x
- 148. Silva IS, Feitosa EL, Santos MEP, et al. Theoretical and Experimental Investigations on Inclusion Complex β-Cyclodextrin and Sulcatone: A Cardiovascular Activity Evaluation. J Braz Chem Soc. 2020. doi:10.21577/0103-5053.20190273
- 149. Li D, Wu H, Huang W, Guo L, Dou H. Microcapsule of Sweet Orange Essential Oil Encapsulated in Beta-Cyclodextrin Improves the Release Behaviors In Vitro and In Vivo. *Eur J Lipid Sci Technol*. 2018. doi:10.1002/ejlt.201700521
- Cokol-Cakmak M, Cokol M. Miniaturized checkerboard assays to measure antibiotic interactions. In: *Methods in Molecular Biology*.; 2019. doi:10.1007/978-1-4939-9089-4\_1
- 151. Cokol-Cakmak M, Bakan F, Cetiner S, Cokol M. Diagonal Method to Measure Synergy Among Any Number of Drugs. *J Vis Exp.* 2018;(136):1-10. doi:10.3791/57713
- 152. Siva S, Li C, Cui H, Meenatchi V, Lin L. Encapsulation of essential oil components with methyl-β-cyclodextrin using ultrasonication: Solubility, characterization, DPPH and antibacterial assay. *Ultrason Sonochem*. 2020. doi:10.1016/j.ultsonch.2020.104997
- 153. Mohammed KAK, Abdulkadhim HM, Noori SI. Chemical Composition and Antibacterial Effects of Clove (Syzygium aromaticum) Flowers. *Int J Curr Microbiol Appl*

- Sci. 2016. doi:10.20546/ijcmas.2016.502.054
- 154. Piletti R, Bugiereck AM, Pereira AT, et al. Microencapsulation of eugenol molecules by β-cyclodextrine as a thermal protection method of antibacterial action. *Mater Sci Eng C*. 2017. doi:10.1016/j.msec.2017.02.075
- 155. Shankarrao KA, Mahadeo GD, Balavantrao KP. Formulation and in-vitro evaluation of orally disintegrating tablets of olanzapine-2-hydroxypropyl-β-cyclodextrin inclusion complex. *Iran J Pharm Res.* 2010. doi:10.22037/ijpr.2010.899
- 156. Sogali BS, Vikram BN, Ramana Murthy K V. Comparative studies with different cyclodextrin derivatives in improving the solubility and dissolution of saquinavir. *Asian J Pharm Clin Res.* 2018. doi:10.22159/ajpcr.2018.v11i6.24836
- 157. Evageliou V, Saliari D. Limonene encapsulation in freeze dried gellan systems. *Food Chem.* 2017. doi:10.1016/j.foodchem.2016.12.030
- 158. Kaushik V, Roos YH. Limonene encapsulation in freeze-drying of gum Arabic-sucrose-gelatin systems. *LWT Food Sci Technol*. 2007. doi:10.1016/j.lwt.2006.10.008
- 159. Darekar T, Aithal KS, Shirodkar R, Kumar L, Attari Z, Lewis S. Characterization and in vivo evaluation of lacidipine inclusion complexes with β-cyclodextrin and its derivatives. *J Incl Phenom Macrocycl Chem*. 2016. doi:10.1007/s10847-016-0600-9
- 160. Seo EJ, Min SG, Choi MJ. Release characteristics of freeze-dried eugenol encapsulated with β-cyclodextrin by molecular inclusion method. *J Microencapsul*. 2010. doi:10.3109/02652041003681398
- 161. Rakmai J, Cheirsilp B, Torrado-Agrasar A, Simal-Gándara J, Mejuto JC. Encapsulation of yarrow essential oil in hydroxypropyl-beta-cyclodextrin: physiochemical characterization and evaluation of bio-efficacies. *CyTA J Food*. 2017. doi:10.1080/19476337.2017.1286523
- 162. Kotronia M, Kavetsou E, Loupassaki S, Kikionis S, Vouyiouka S, Detsi A. Encapsulation of oregano (Origanum onites l.) essential oil in β-cyclodextrin (β-CD): Synthesis and characterization of the inclusion complexes. *Bioengineering*. 2017. doi:10.3390/bioengineering4030074
- 163. Menezes PP, Serafini MR, Quintans-Júnior LJ, et al. Inclusion complex of (-)-linalool and β-cyclodextrin. *J Therm Anal Calorim*. 2014. doi:10.1007/s10973-013-3367-x

- 164. Dou S, Ouyang Q, You K, Qian J, Tao N. An inclusion complex of thymol into β-cyclodextrin and its antifungal activity against Geotrichum citri-aurantii. *Postharvest Biol Technol.* 2018. doi:10.1016/j.postharvbio.2017.12.011
- 165. Kulkarni AD, Belgamwar VS. Inclusion complex of chrysin with sulfobutyl ether-β-cyclodextrin (Captisol®): Preparation, characterization, molecular modelling and in vitro anticancer activity. *J Mol Struct*. 2017. doi:10.1016/j.molstruc.2016.09.025
- 166. Gaumet M, Vargas A, Gurny R, Delie F. Nanoparticles for drug delivery: The need for precision in reporting particle size parameters. *Eur J Pharm Biopharm*. 2008. doi:10.1016/j.ejpb.2007.08.001
- 167. Singh R, Lillard JW. Nanoparticle-based targeted drug delivery. *Exp Mol Pathol*. 2009. doi:10.1016/j.yexmp.2008.12.004
- 168. Durak S, Arasoglu T, Ates SC, Derman S. Enhanced antibacterial and antiparasitic activity of multifunctional polymeric nanoparticles. *Nanotechnology*. 2020. doi:10.1088/1361-6528/ab6ab9
- 169. Çelik SE, Özyürek M, Güçlü K, Apak R. CUPRAC total antioxidant capacity assay of lipophilic antioxidants in combination with hydrophilic antioxidants using the macrocyclic oligosaccharide methyl β-cyclodextrin as the solubility enhancer. *React Funct Polym.* 2007. doi:10.1016/j.reactfunctpolym.2007.07.045
- 170. Yuen CWM, Ku SKA, Choi PSR, Kan CW, Tsang SY. Determining Functional Groups of Commercially Available Ink-Jet Printing Reactive Dyes Using Infrared Spectroscopy. *Res J Text Appar*. 2005. doi:10.1108/RJTA-09-02-2005-B004
- 171. Cannavà C, Crupi V, Guardo M, et al. Phase solubility and FTIR-ATR studies of idebenone/sulfobutyl ether β-cyclodextrin inclusion complex. In: *Journal of Inclusion Phenomena and Macrocyclic Chemistry*.; 2013. doi:10.1007/s10847-012-0110-3
- 172. Yallapu MM, Jaggi M, Chauhan SC. β-Cyclodextrin-curcumin self-assembly enhances curcumin delivery in prostate cancer cells. *Colloids Surfaces B Biointerfaces*. 2010. doi:10.1016/j.colsurfb.2010.03.039
- 173. Sambasevam KP, Mohamad S, Sarih NM, Ismail NA. Synthesis and characterization of the inclusion complex of β-cyclodextrin and azomethine. *Int J Mol Sci.* 2013. doi:10.3390/ijms14023671

- 174. Qu Q, Tucker E, Christian SD. Sulfoalkyl ether β-cyclodextrin derivatives: Synthesis and characterizations. *J Incl Phenom*. 2002. doi:10.1023/A:1021255314835
- 175. Ja'Far MH, Kamal NNSNM, Hui BY, et al. Inclusion of curcumin in β-cyclodextrins as potential drug delivery system: Preparation, characterization and its preliminary cytotoxicity approaches. *Sains Malaysiana*. 2018. doi:10.17576/jsm-2018-4705-13
- 176. Takahashi K, Andou K, Fujiwara S. Characterization and structural determination of 3A-amino-3A-deoxy-(2AS, 3AS)-cyclodextrins by NMR spectroscopy. In: *Polymer Journal*.; 2012. doi:10.1038/pj.2012.122
- 177. Ulanowska M, Olas B. Biological properties and prospects for the application of eugenol—a review. *Int J Mol Sci.* 2021. doi:10.3390/ijms22073671
- 178. Eckhardt S, Brunetto PS, Gagnon J, Priebe M, Giese B, Fromm KM. Nanobio silver: Its interactions with peptides and bacteria, and its uses in medicine. *Chem Rev.* 2013. doi:10.1021/cr300288v
- 179. Cui ZH, He HL, Wu S Bin, et al. Rapid screening of essential oils as substances which enhance antibiotic activity using a modifiedwell diffusion method. *Antibiotics*. 2021. doi:10.3390/antibiotics10040463
- 180. Halahlah A, Kavetsou E, Pitterou I, et al. Synthesis and characterization of inclusion complexes of rosemary essential oil with various β-cyclodextrins and evaluation of their antibacterial activity against Staphylococcus aureus. *J Drug Deliv Sci Technol*. 2021. doi:10.1016/j.jddst.2021.102660
- 181. de Almeida Magalhães TSS, de Oliveira Macedo PC, Pacheco SYK, et al. Development and evaluation of antimicrobial and modulatory activity of inclusion complex of euterpe oleracea mart oil and β-cyclodextrin or HP-β-cyclodextrin. *Int J Mol Sci.* 2020. doi:10.3390/ijms21030942
- 182. Theoret C. Physiology of Wound Healing. In: *Equine Wound Management: Third Edition*.; 2016. doi:10.1002/9781118999219.ch1
- 183. Editors W. The Four Stages of Wound Healing. WoundSource.
- 184. Chen L, Deng H, Cui H, et al. Inflammatory responses and inflammation-associated diseases in organs. *Oncotarget*. 2018. doi:10.18632/oncotarget.23208

- 185. El Ghalbzouri A, Hensbergen P, Gibbs S, Kempenaar J, Van Der Schors R, Ponec M. Fibroblasts facilitate re-epithelialization in wounded human skin equivalents. *Lab Investig.* 2004. doi:10.1038/labinvest.3700014
- 186. Schultz GS, Chin GA, Moldawer L, Diegelmann RF. Principles of wound healing. In: Mechanisms of Vascular Disease: A Reference Book for Vascular Specialists.; 2011. doi:10.1017/UPO9781922064004.024
- 187. Rolfe C, Daryaei H. Intrinsic and Extrinsic Factors Affecting Microbial Growth in Food Systems. In: *Food Engineering Series*.; 2020. doi:10.1007/978-3-030-42660-6\_1
- 188. Rumbaugh K, Watters C, Yuan T. Beneficial and deleterious bacterial–host interactions in chronic wound pathophysiology. *Chronic Wound Care Manag Res.* 2015. doi:10.2147/cwcmr.s60317
- 189. Maver T, Gradišnik L, Smrke DM, Stana Kleinschek K, Maver U. Systematic Evaluation of a Diclofenac-Loaded Carboxymethyl Cellulose-Based Wound Dressing and Its Release Performance with Changing pH and Temperature. AAPS PharmSciTech. 2019. doi:10.1208/s12249-018-1236-4
- 190. Ge Y, MacDonald D, Hait H, Lipsky B, Zasloff M, Holroyd K. Microbiological profile of infected diabetic foot ulcers [1]. *Diabet Med.* 2002. doi:10.1046/j.1464-5491.2002.00696\_1.x
- 191. Jneid J, Lavigne JP, La Scola B, Cassir N. The diabetic foot microbiota: A review. *Hum Microbiome J*. 2017. doi:10.1016/j.humic.2017.09.002
- 192. Ninan N, Forget A, Shastri VP, Voelcker NH, Blencowe A. Antibacterial and Anti-Inflammatory pH-Responsive Tannic Acid-Carboxylated Agarose Composite Hydrogels for Wound Healing. *ACS Appl Mater Interfaces*. 2016. doi:10.1021/acsami.6b10491
- 193. Andrady AL. Science and Technology of Polymer Nanofibers.; 2007. doi:10.1002/9780470229842
- 194. Blanco-Fernandez B, Castaño O, Mateos-Timoneda MÁ, Engel E, Pérez-Amodio S. Nanotechnology Approaches in Chronic Wound Healing. Adv Wound Care. 2021. doi:10.1089/wound.2019.1094
- 195. Ramakrishna S, Fujihara K, Teo WE, Yong T, Ma Z, Ramaseshan R. Electrospun nanofibers: Solving global issues. *Mater Today*. 2006. doi:10.1016/S1369-

- 7021(06)71389-X
- 196. Kenry, Lim CT. Nanofiber technology: current status and emerging developments. *Prog Polym Sci.* 2017. doi:10.1016/j.progpolymsci.2017.03.002
- 197. Hatiboglu B. Mechanical properties of individual polymeric micro and nano fibers using atomic force microscopy (AFM). *Thesis*. 2006.
- 198. Huang ZM, Zhang YZ, Kotaki M, Ramakrishna S. A review on polymer nanofibers by electrospinning and their applications in nanocomposites. *Compos Sci Technol.* 2003. doi:10.1016/S0266-3538(03)00178-7
- 199. Gaysinsky S, Davidson PM, McClements DJ, Weiss J. Formulation and characterization of phytophenol-carrying antimicrobial microemulsions. *Food Biophys.* 2008. doi:10.1007/s11483-007-9048-1
- 200. Zhang Y, Chwee TL, Ramakrishna S, Huang ZM. Recent development of polymer nanofibers for biomedical and biotechnological applications. *J Mater Sci Mater Med*. 2005. doi:10.1007/s10856-005-4428-x
- 201. Miguel SP, Figueira DR, Simões D, et al. Electrospun polymeric nanofibres as wound dressings: A review. *Colloids Surfaces B Biointerfaces*. 2018. doi:10.1016/j.colsurfb.2018.05.011
- 202. Liu M, Duan XP, Li YM, Yang DP, Long YZ. Electrospun nanofibers for wound healing. *Mater Sci Eng C*. 2017. doi:10.1016/j.msec.2017.03.034
- 203. Zhang C, Yuan X, Wu L, Han Y, Sheng J. Study on morphology of electrospun poly(vinyl alcohol) mats. *Eur Polym J.* 2005. doi:10.1016/j.eurpolymj.2004.10.027
- 204. dos Santos DM, Leite IS, Bukzem A de L, et al. Nanostructured electrospun nonwovens of poly(ε-caprolactone)/quaternized chitosan for potential biomedical applications. *Carbohydr Polym.* 2018. doi:10.1016/j.carbpol.2018.01.045
- 205. Zhou Y, Yang H, Liu X, Mao J, Gu S, Xu W. Electrospinning of carboxyethyl chitosan/poly(vinyl alcohol)/silk fibroin nanoparticles for wound dressings. *Int J Biol Macromol*. 2013. doi:10.1016/j.ijbiomac.2012.11.013
- 206. Khil MS, Cha D II, Kim HY, Kim IS, Bhattarai N. Electrospun Nanofibrous Polyurethane Membrane as Wound Dressing. *J Biomed Mater Res Part B Appl*

- Biomater. 2003. doi:10.1002/jbm.b.10058
- 207. Saeed SM, Mirzadeh H, Zandi M, Barzin J. Designing and fabrication of curcumin loaded PCL/PVA multi-layer nanofibrous electrospun structures as active wound dressing. *Prog Biomater*. 2017. doi:10.1007/s40204-017-0062-1
- 208. Kohsari I, Shariatinia Z, Pourmortazavi SM. Antibacterial electrospun chitosan-polyethylene oxide nanocomposite mats containing bioactive silver nanoparticles. *Carbohydr Polym.* 2016. doi:10.1016/j.carbpol.2015.12.075
- 209. Fu R, Li C, Yu C, et al. A novel electrospun membrane based on moxifloxacin hydrochloride/poly(vinyl alcohol)/sodium alginate for antibacterial wound dressings in practical application. *Drug Deliv.* 2016. doi:10.3109/10717544.2014.918676
- 210. Ignatova M, Manolova N, Rashkov I. Electrospinning of poly(vinyl pyrrolidone)-iodine complex and poly(ethylene oxide)/poly(vinyl pyrrolidone)-iodine complex a prospective route to antimicrobial wound dressing materials. *Eur Polym J.* 2007. doi:10.1016/j.eurpolymj.2007.02.020
- 211. Shalumon KT, Anulekha KH, Nair S V., Nair S V., Chennazhi KP, Jayakumar R. Sodium alginate/poly(vinyl alcohol)/nano ZnO composite nanofibers for antibacterial wound dressings. *Int J Biol Macromol*. 2011. doi:10.1016/j.ijbiomac.2011.04.005
- 212. Tsekova PB, Spasova MG, Manolova NE, Markova ND, Rashkov IB. Electrospun curcumin-loaded cellulose acetate/polyvinylpyrrolidone fibrous materials with complex architecture and antibacterial activity. *Mater Sci Eng C*. 2017. doi:10.1016/j.msec.2016.12.086
- 213. Uppal R, Ramaswamy GN, Arnold C, Goodband R, Wang Y. Hyaluronic acid nanofiber wound dressing-production, characterization, and in vivo behavior. *J Biomed Mater Res Part B Appl Biomater*. 2011. doi:10.1002/jbm.b.31776
- 214. Chen JP, Chang GY, Chen JK. Electrospun collagen/chitosan nanofibrous membrane as wound dressing. *Colloids Surfaces A Physicochem Eng Asp.* 2008. doi:10.1016/j.colsurfa.2007.04.129
- 215. Huang ZM, Zhang YZ, Ramakrishna S, Lim CT. Electrospinning and mechanical characterization of gelatin nanofibers. *Polymer (Guildf)*. 2004. doi:10.1016/j.polymer.2004.04.005

- 216. Perena Gouma PI. Nanomaterials for Chemical Sensors and Biotechnology.; 2009. doi:10.4032/9789814267618
- 217. Haghi AK. Multilayer laminated nanofibers. In: *Nanofibers and Nanotechnology Research Advances*.; 2011.
- 218. Athira KS, Sanpui P, Chatterjee K. Fabrication of Poly(Caprolactone) Nanofibers by Electrospinning. *J Polym Biopolym Phys Chem.* 2014.
- 219. Li Z, Wang C. One dimensional Nanostructures Electrospinning Technique and Unique Nanofibers. *One-Dimensional Nanostructures*. 2013.
- 220. Mirjalili M, Zohoori S. Review for application of electrospinning and electrospun nanofibers technology in textile industry. *J Nanostructure Chem.* 2016. doi:10.1007/s40097-016-0189-y
- 221. Wannatong L, Sirivat A, Supaphol P. Effects of solvents on electrospun polymeric fibers: Preliminary study on polystyrene. *Polym Int.* 2004. doi:10.1002/pi.1599
- 222. Patiño Vidal C, López de Dicastillo C, Rodríguez-Mercado F, Guarda A, Galotto MJ, Muñoz-Shugulí C. Electrospinning and cyclodextrin inclusion complexes: An emerging technological combination for developing novel active food packaging materials. *Crit Rev Food Sci Nutr.* 2021. doi:10.1080/10408398.2021.1886038
- 223. Celebioglu A, Uyar T. Metronidazole/Hydroxypropyl-β-Cyclodextrin inclusion complex nanofibrous webs as fast-dissolving oral drug delivery system. *Int J Pharm*. 2019. doi:10.1016/j.ijpharm.2019.118828
- 224. Celebioglu A, Uyar T. Fast Dissolving Oral Drug Delivery System Based on Electrospun Nanofibrous Webs of Cyclodextrin/Ibuprofen Inclusion Complex Nanofibers. *Mol Pharm*. 2019. doi:10.1021/acs.molpharmaceut.9b00798
- 225. Celebioglu A, Uyar T. Hydrocortisone/cyclodextrin complex electrospun nanofibers for a fast-dissolving oral drug delivery system. *RSC Med Chem.* 2020. doi:10.1039/c9md00390h
- 226. Li C, Chen C, Zhao J, et al. Electrospun Fibrous Membrane Containing a Cyclodextrin Covalent Organic Framework with Antibacterial Properties for Accelerating Wound Healing. *ACS Biomater Sci Eng.* 2021. doi:10.1021/acsbiomaterials.1c00648

- 227. Martínez-De Jesús FR, Ramos-De La Medina A, Remes-Troche JM, et al. Efficacy and safety of neutral pH superoxidised solution in severe diabetic foot infections. *Int Wound J.* 2007. doi:10.1111/j.1742-481X.2007.00363.x
- 228. Salvo P, Calisi N, Melai B, et al. Temperature-and pH-sensitive wearable materials for monitoring foot ulcers. *Int J Nanomedicine*. 2017. doi:10.2147/IJN.S121726
- 229. Kost B, Svyntkivska M, Brzeziński M, et al. PLA/β-CD-based fibres loaded with quercetin as potential antibacterial dressing materials. *Colloids Surfaces B Biointerfaces*. 2020. doi:10.1016/j.colsurfb.2020.110949
- 230. Balamurali V, Pramodkuma TM, Srujana N, et al. pH Sensitive Drug Delivery Systems: A Review. *Am J Drug Discov Dev.* 2010. doi:10.3923/ajdd.2011.24.48
- 231. Raza H, Javeria S, Rashid Z. Sustained released Metformin microparticles for better management of type II diabetes mellitus: In-vitro studies. *Mater Res Express*. 2020. doi:10.1088/2053-1591/ab6c0f
- 232. Roy I, Gupta MN. Smart Polymeric Materials: Emerging Biochemical Applications. *Chem Biol.* 2003. doi:10.1016/j.chembiol.2003.12.004
- 233. Sester C, Ofridam F, Lebaz N, Gagnière E, Mangin D, Elaissari A. pH-Sensitive methacrylic acid-methyl methacrylate copolymer Eudragit L100 and dimethylaminoethyl methacrylate, butyl methacrylate, and methyl methacrylate tricopolymer Eudragit E100. *Polym Adv Technol.* 2020. doi:10.1002/pat.4780
- 234. Coban O, Aytac Z, Yildiz ZI, Uyar T. Colon targeted delivery of niclosamide from β-cyclodextrin inclusion complex incorporated electrospun Eudragit® L100 nanofibers. *Colloids Surfaces B Biointerfaces*. 2021. doi:10.1016/j.colsurfb.2020.111391
- 235. Daghrery A, Aytac Z, Dubey N, Mei L, Schwendeman A, Bottino MC. Electrospinning of dexamethasone/cyclodextrin inclusion complex polymer fibers for dental pulp therapy. *Colloids Surfaces B Biointerfaces*. 2020. doi:10.1016/j.colsurfb.2020.111011
- 236. Celebioglu A, Uyar T. Fast-dissolving antioxidant curcumin/cyclodextrin inclusion complex electrospun nanofibrous webs. *Food Chem.* 2020. doi:10.1016/j.foodchem.2020.126397
- 237. Moyers-Montoya E, García-Casillas P, Vargas-Requena C, Escobedo-González R, Martel-Estrada SA, Martínez-Pérez CA. Polycaprolactone/amino-β-cyclodextrin

- inclusion complex prepared by an electrospinning technique. *Polymers (Basel)*. 2016. doi:10.3390/polym8110395
- 238. Aytac Z, Yildiz ZI, Kayaci-Senirmak F, Tekinay T, Uyar T. Electrospinning of cyclodextrin/linalool-inclusion complex nanofibers: Fast-dissolving nanofibrous web with prolonged release and antibacterial activity. *Food Chem.* 2017. doi:10.1016/j.foodchem.2017.03.113
- 239. Aytac Z, Kusku SI, Durgun E, Uyar T. Quercetin/β-cyclodextrin inclusion complex embedded nanofibres: Slow release and high solubility. *Food Chem.* 2016. doi:10.1016/j.foodchem.2015.11.051
- 240. Gao S, Liu Y, Jiang J, et al. Encapsulation of thiabendazole in hydroxypropyl-β-cyclodextrin nanofibers via polymer-free electrospinning and its characterization. *Pest Manag Sci.* 2020. doi:10.1002/ps.5885
- 241. Aytac Z, Yildiz ZI, Kayaci-Senirmak F, et al. Fast-Dissolving, Prolonged Release, and Antibacterial Cyclodextrin/Limonene-Inclusion Complex Nanofibrous Webs via Polymer-Free Electrospinning. *J Agric Food Chem.* 2016. doi:10.1021/acs.jafc.6b02632
- 242. Yildiz ZI, Kilic ME, Durgun E, Uyar T. Molecular Encapsulation of Cinnamaldehyde within Cyclodextrin Inclusion Complex Electrospun Nanofibers: Fast-Dissolution, Enhanced Water Solubility, High Temperature Stability, and Antibacterial Activity of Cinnamaldehyde. *J Agric Food Chem.* 2019. doi:10.1021/acs.jafc.9b02789
- 243. Celebioglu A, Uyar T. Antioxidant Vitamin E/Cyclodextrin Inclusion Complex Electrospun Nanofibers: Enhanced Water Solubility, Prolonged Shelf Life, and Photostability of Vitamin E. *J Agric Food Chem.* 2017. doi:10.1021/acs.jafc.7b01562
- 244. Celebioglu A, Uyar T. Encapsulation and Stabilization of α-Lipoic Acid in Cyclodextrin Inclusion Complex Electrospun Nanofibers: Antioxidant and Fast-Dissolving α-Lipoic Acid/Cyclodextrin Nanofibrous Webs. *J Agric Food Chem.* 2019. doi:10.1021/acs.jafc.9b05580
- 245. dos Santos JP, Zavareze E da R, Dias ARG, Vanier NL. Immobilization of xylanase and xylanase–β-cyclodextrin complex in polyvinyl alcohol via electrospinning improves enzyme activity at a wide pH and temperature range. *Int J Biol Macromol*. 2018. doi:10.1016/j.ijbiomac.2018.07.014

- 246. Aytac Z, Ipek S, Erol I, Durgun E, Uyar T. Fast-dissolving electrospun gelatin nanofibers encapsulating ciprofloxacin/cyclodextrin inclusion complex. *Colloids Surfaces B Biointerfaces*. 2019. doi:10.1016/j.colsurfb.2019.02.059
- 247. Yildiz ZI, Celebioglu A, Uyar T. Polymer-free electrospun nanofibers from sulfobutyl ether7-beta-cyclodextrin (SBE7-β-CD) inclusion complex with sulfisoxazole: Fast-dissolving and enhanced water-solubility of sulfisoxazole. *Int J Pharm.* 2017. doi:10.1016/j.ijpharm.2017.04.047
- 248. Aytac Z, Uyar T. Core-shell nanofibers of curcumin/cyclodextrin inclusion complex and polylactic acid: Enhanced water solubility and slow release of curcumin. *Int J Pharm*. 2017. doi:10.1016/j.ijpharm.2016.12.061
- 249. Aytac Z, Kusku SI, Durgun E, Uyar T. Encapsulation of gallic acid/cyclodextrin inclusion complex in electrospun polylactic acid nanofibers: Release behavior and antioxidant activity of gallic acid. *Mater Sci Eng C*. 2016. doi:10.1016/j.msec.2016.02.063
- 250. Aytac Z, Sen HS, Durgun E, Uyar T. Sulfisoxazole/cyclodextrin inclusion complex incorporated in electrospun hydroxypropyl cellulose nanofibers as drug delivery system. *Colloids Surfaces B Biointerfaces*. 2015. doi:10.1016/j.colsurfb.2015.02.019
- 251. Li N, Qian Y, Zhang Z, Wang Y, Lve L, Wei C. New Patent on Electrospinning for Increasing Rutin Loading in Nanofibers. Recent Pat Nanotechnol. 2019. doi:10.2174/1872210513666191107101326
- 252. Aytac Z, Ipek S, Durgun E, Tekinay T, Uyar T. Antibacterial electrospun zein nanofibrous web encapsulating thymol/cyclodextrin-inclusion complex for food packaging. *Food Chem.* 2017. doi:10.1016/j.foodchem.2017.04.095
- 253. Wang Y, Deng Z, Wang X, et al. Formononetin/methyl-β-cyclodextrin inclusion complex incorporated into electrospun polyvinyl-alcohol nanofibers: Enhanced water solubility and oral fast-dissolving property. *Int J Pharm.* 2021. doi:10.1016/j.ijpharm.2021.120696
- 254. Uyar T, Nur Y, Hacaloglu J, Besenbacher F. Electrospinning of functional poly(methyl methacrylate) nanofibers containing cyclodextrin-menthol inclusion complexes. *Nanotechnology*. 2009. doi:10.1088/0957-4484/20/12/125703

- 255. Kayaci F, Ertas Y, Uyar T. Enhanced thermal stability of eugenol by cyclodextrin inclusion complex encapsulated in electrospun polymeric nanofibers. *J Agric Food Chem.* 2013. doi:10.1021/jf402923c
- 256. Reda RI, Wen MM, El-Kamel AH. Ketoprofen-loaded Eudragit electrospun nanofibers for the treatment of oral mucositis. *Int J Nanomedicine*. 2017. doi:10.2147/IJN.S131253
- 257. Hassan MI, Sultana N, Hamdan S. Bioactivity assessment of poly(ε caprolactone)/hydroxyapatite electrospun fibers for bone tissue engineering application. *J Nanomater*, 2014, doi:10.1155/2014/573238
- 258. Unalan I, Slavik B, Buettner A, Goldmann WH, Frank G, Boccaccini AR. Physical and Antibacterial Properties of Peppermint Essential Oil Loaded Poly (ε-caprolactone) (PCL) Electrospun Fiber Mats for Wound Healing. *Front Bioeng Biotechnol*. 2019. doi:10.3389/fbioe.2019.00346
- 259. Napavichayanun S, Yamdech R, Aramwit P. The safety and efficacy of bacterial nanocellulose wound dressing incorporating sericin and polyhexamethylene biguanide: in vitro, in vivo and clinical studies. *Arch Dermatol Res.* 2016. doi:10.1007/s00403-016-1621-3
- 260. Unalan I, Endlein SJ, Slavik B, et al. Evaluation of electrospun poly(ε-caprolactone)/gelatin nanofiber mats containing clove essential oil for antibacterial wound dressing. *Pharmaceutics*. 2019. doi:10.3390/pharmaceutics11110570
- 261. Moghe AK, Gupta BS. Co-axial electrospinning for nanofiber structures: Preparation and applications. *Polym Rev.* 2008. doi:10.1080/15583720802022257
- 262. Akhgari A, Heshmati Z, Makhmalzadeh BS. Indomethacin electrospun nanofibers for colonic drug delivery: Preparation and characterization. *Adv Pharm Bull*. 2013. doi:10.5681/apb.2013.014
- 263. Shen XX, Yu DG, Zhu LM, Branford-White C. Preparation and characterization of ultrafine Eudragit L100 fibers via electrospinning. In: *3rd International Conference on Bioinformatics and Biomedical Engineering, ICBBE* 2009. ; 2009. doi:10.1109/ICBBE.2009.5163230
- 264. Ao F, Shen W, Ge X, et al. Effects of the crystallinity on quercetin loaded the Eudragit L-100 electrospun nanofibers. *Colloids Surfaces B Biointerfaces*. 2020.

- doi:10.1016/j.colsurfb.2020.111264
- 265. Uyar T, Besenbacher F. Electrospinning of uniform polystyrene fibers: The effect of solvent conductivity. *Polymer (Guildf)*. 2008. doi:10.1016/j.polymer.2008.09.025
- 266. Samprasit W, Akkaramongkolporn P, Ngawhirunpat T, Rojanarata T, Kaomongkolgit R, Opanasopit P. Fast releasing oral electrospun PVP/CD nanofiber mats of taste-masked meloxicam. *Int J Pharm.* 2015. doi:10.1016/j.ijpharm.2015.04.044
- 267. Bhardwaj N, Kundu SC. Electrospinning: A fascinating fiber fabrication technique. *Biotechnol Adv.* 2010. doi:10.1016/j.biotechadv.2010.01.004
- 268. Celebioglu A, Uyar T. Electrohydrodynamic encapsulation of eugenol-cyclodextrin complexes in pullulan nanofibers. *Food Hydrocoll*. 2021. doi:10.1016/j.foodhyd.2020.106264
- 269. Yildiz ZI, Celebioglu A, Kilic ME, Durgun E, Uyar T. Menthol/cyclodextrin inclusion complex nanofibers: Enhanced water-solubility and high-temperature stability of menthol. *J Food Eng.* 2018. doi:10.1016/j.jfoodeng.2017.12.020
- 270. Illangakoon UE, Yu DG, Ahmad BS, Chatterton NP, Williams GR. 5-Fluorouracil loaded Eudragit fibers prepared by electrospinning. *Int J Pharm*. 2015. doi:10.1016/j.ijpharm.2015.09.044
- 271. Aytac Z, Ipek S, Durgun E, Uyar T. Antioxidant electrospun zein nanofibrous web encapsulating quercetin/cyclodextrin inclusion complex. *J Mater Sci.* 2018. doi:10.1007/s10853-017-1580-x
- 272. Abrigo M, McArthur SL, Kingshott P. Electrospun nanofibers as dressings for chronic wound care: Advances, challenges, and future prospects. *Macromol Biosci*. 2014. doi:10.1002/mabi.201300561
- 273. Bonn D, Eggers J, Indekeu J, Meunier J. Wetting and spreading. *Rev Mod Phys*. 2009. doi:10.1103/RevModPhys.81.739
- 274. Pan Z, Cheng F, Zhao B. Bio-Inspired polymeric structures with special wettability and their applications: An overview. *Polymers (Basel)*. 2017. doi:10.3390/polym9120725
- 275. Eğri Ö, Erdemir N. Production of Hypericum perforatum oil-loaded membranes for wound dressing material and in vitro tests. *Artif Cells, Nanomedicine Biotechnol.* 2019.

- doi:10.1080/21691401.2019.1596933
- 276. Siafaka PI, Okur NÜ, Mone M, et al. Two different approaches for oral administration of voriconazole loaded formulations: Electrospun fibers versus β-cyclodextrin complexes. *Int J Mol Sci.* 2016. doi:10.3390/ijms17030282
- 277. Syafiq R, Sapuan SM, Zuhri MRM. Antimicrobial activity, physical, mechanical and barrier properties of sugar palm based nanocellulose/starch biocomposite films incorporated with cinnamon essential oil. *J Mater Res Technol*. 2021. doi:10.1016/j.jmrt.2020.12.091
- 278. Cui W, Li X, Zhu X, Yu G, Zhou S, Weng J. Investigation of drug release and matrix degradation of electrospun poly(DL-lactide) fibers with paracetanol inoculation. *Biomacromolecules*. 2006. doi:10.1021/bm060057z
- 279. Zhang R, Jiang G, Gao Q, et al. Sprayed copper peroxide nanodots for accelerating wound healing in a multidrug-resistant bacteria infected diabetic ulcer. *Nanoscale*. 2021. doi:10.1039/d1nr04687j
- 280. Rozman NAS, Tong WY, Leong CR, et al. Homalomena pineodora essential oil nanoparticle inhibits diabetic wound pathogens. *Sci Rep.* 2020. doi:10.1038/s41598-020-60364-0
- 281. Hosseini F, Miri MA, Najafi M, Soleimanifard S, Aran M. Encapsulation of rosemary essential oil in zein by electrospinning technique. *J Food Sci.* 2021. doi:10.1111/1750-3841.15876